Lanthanide complexes as OLED emitters

Valentina V. Utochnikova*
Lomonosov Moscow State University, Moscow, Russia
Corresponding author: e-mail: valentina.utochnikova@gmail.com

Chapter Outline

List of symbols and acronyms

α-NPD	or α-NPB, {*N*,*N*′-bis(naphtalen-2-yl)-*N*,*N*′-bis(phenyl) benzidine}
μ	mobility of electric charges in $cm^2\ V^{-1}\ s^{-1}$
2-TNATA	4,4′,4″-tris[2-naphthyl(phenyl)amino]triphenylamine
5NO$_2$phen	5-nitro-1,10-phenanthroline
9-hpo	9-hydroxyphenalen-1-one
acac	acetylacetonate

Handbook on the Physics and Chemistry of Rare Earths. https://doi.org/10.1016/bs.hpcre.2021.05.001

Alq_3	aluminum tris(8-hydroxyquinolinate)
AMOLED	active-matrix OLED
ant	9-anthracenate
α-NPB	or α-NPD, {*N*,*N*′-bis(naphtalen-2-yl)-*N*,*N*′-bis(phenyl) benzidine}
BCP	2,9-dimethyl-4,7-diphenyl-1,10-phenanthroline
BGA	benzoguanamine
bipy	2,2′-bipyridine
o-BBA	2-benzoylbenzoic acid
Bphen	bathophenanthroline
BSA	benzoyl salicylic acid
btz	benzothiazole-2-carboxylate
bz	benzoate
CB	chlorobenzene
CBP	4,4′-bis(*N*-carbazolyl)-1,1′-biphenyl
CC	coordination compound
cd	candela, unit of luminous intensity (= 1 lumen per unit of solid angle, 1 lm/sr)
CE	current efficiency in cd/A
cptfbd	1-(4-(9H-carbazol-9-yl)phenyl)-4,4,4-trifluorobutane-1,3-dione
CuPc	copper(II) phthalocyaninate
dbm	dibenzoylmethanate
DBR	distributed Bragg reflector
DBSO	dibenzyl sulfoxide
DC-18C6	dicyclohexyl-18-crown-6
DCPPO	di(9H-carbazol-9-yl)(phenyl)phosphine oxide
dcq	5,7-dichloro-8-hydroxyquinolinate
dfpp	2-(2,4-difluorophenyl)pyridine
dpab	4-diphenylamino-benzoate
DPAVBi	4,4′-bis[4-(di-*p*-tolylamino)styryl]biphenyl
dpbq	2,3-bis(2-pyridin)benzoquinoxaline
dpdbm	1-[4-(diphenylamino)phenyl]-3-phenylpropane-1,3-dione
DPEPO	bis(2-(diphenylphosphino)phenyl)ether oxide
DPM	2,2,6,6-tetramethyl-3,5-heptanedione
dpp	2,3-bis(2-pyridyl)pyrazine
DPPOC	9-(4-*tert*-butylphenyl)-3,6-bis(diphenylphosphineoxide)-carbazole
DPPZ	4,5,9,14-tetraazabenzotriphenylene
dpq	2,3-bis(2-pyridyl)quinoxaline
DPSO	diphenyl sulfoxide
EBL	electron blocking layer
EDFA	erbium-doped fiber amplifier
EIL	electron injection layer

EL	electroluminescence
EML	emission layer
EPBM	1-ethyl-2-(2-pyridyl)benzimidazole
EPI	exciton–polaron interaction
EQE	external quantum efficiency
ETL	electron transport layer
fb	fluorobenzoate
fpbim	5-fluoro-2-(pyrimidin-2-yl)-3-benzimidazole
FWHM	full width at half height
η	efficiency of recombination of charge carriers in the emission layer
HBL	hole blocking layer
hfa	hexafluoroacetylacetonate
hfnh	4,4,5,5,6,6,6-heptafluoro-1-(2-thienyl)hexane-1,3-dione
hhqc	*N*-hexadecyl-8-hydroxyquinoline-2-carboxamide
HIL	hole injection layer
HMME	hematoporphyrin monomethyl ether
HOMO	highest occupied molecular orbital
η_{out}	efficiency of light outcoupling from the OLED
hpbo	2-(2-hydroxyphenyl)benzoxazole
hpbt	2-(2-hydroxyphenyl)benzothiazole
HPLC	high-performance liquid chromatography
γ_r	theoretical fraction of excitons participating in electroluminescence
η_{sens}	sensitization efficiency
HTL	hole transport layer
IC	internal conversion
ind	indazole
ISC	intersystem crossing
ITO	indium tin oxide
j	current density in mA/cm^2
L	luminance or brightness in cd/m^2
LMCT	ligand-to-metal charge transfer state
Ln	lanthanide
LOEt	Kläui's ligand {CoCp[OP(Oet)$_2$]$_3$}
LP-OVPD	low-pressure organic vapor phase deposition
LUMO	lowest unoccupied molecular orbital
mba	*o*-methoxybenzoate
mbt	2-mercaptobenzothiazolate
mCP	1-methyl cyclopropene
MeHq	2-methyl-8-hydroxyquinolinate
mfb	monofluorobenzoate
***m*-MTDATA**	4,4′,4″-tris[3-methylphenyl(phenyl)-amino]triphenyl-amine
MOLED	microcavity OLED

NaDAPO	(4-naphthalen-1-yl-phenylaminophenyl) diphenylphosphine oxide
NON	9-(pyridin-2-yl)-2-(9-(pyridin-2-yl)-9H-carbazol-2-yloxy)-9H-carbazole
Np5mbo	3-(5-methylbenzoxazol-2-yl)naphtholate
Np6mbo	3-(6-methylbenzoxazol-2-yl)naphtholate
NpOON	3-(2-benzoxazol-2-yl)naphtholate
NpSON	3-(2-benzothiazol-2-yl)naphtholate
oac	acetonate
OLED	organic light-emitting diode
OON	2-(2-benzoxyazol-2-yl)phenolate
OSN	2-(2′-mercaptophenyl)benzoxazolate
OSN	2-(2-benzothiazol-2-yl)phenolate
OVPD	organic vapor phase deposition
pam	*p*-(amino)tetrafluorobenzoate
PBIm	2-(2-pyridyl)benzimidazole
PE	luminous efficiency or photon efficiency or light output in lm/W
PEDOT	poly(3,4-ethylenedioxythiophene)
pfap	phenyl-3-trifluoromethyl-4-acyl-5-pyrazolonate
pfb	pentafluorobenzoate
Pfbim	5-fluoro-2-(pyrimidin-2-yl)-1l2-benzo[d]imidazole
phen	phenanthroline
phm	*p*-(hydroxymethyl)tetrafluorobenzoate
piv	pivaloate
PL	photoluminescence
PLQY	photoluminescence quantum yield
pm	1-phenyl-3-methyl-4-isobutyryl-5-pyrazolone
pmbp	1-phenyl-3-methyl-4-(4-tert-butylbenzacyl)-5-pyrazolone
pmip	1-phenyl-3-methyl-4-isobutyryl-5-pyrazolone
pnd	*N*,*N*,*O*-ligand 6-(pyridin-2-yl)-1,5-naphthyridin-4-ol
PO	phosphine oxide
pobz	phenoxybenzoate
PPV	poly(phenylenevinylene)
PSS	polystyrene sulfonate
PTC	(x'-phenoxazin-10-yl)-[1,1′:3′,1″-terphenyl]-2′-carbonitrile
PVK	polyvinylcarbazole
Pyphen	pyrazino[2,3-f][1,10]phenanthroline
q	8-hydroxyquinolinate
quinHA	quinaldichydroxamic acid
QY	quantum yield
rms	root mean square or quadratic mean
R-NTB	tri R-substituted (*N*-alkylbenzimidazol-2-ylmethyl)amine (R = *n*Pr)

SPPO13	2,7-Bis(diphenylphosphoryl)-9,9′-spirobifluorene
SSA	singlet–singlet annihilation
SSN	2-(2′-mercaptophenyl)benzothiazolate
STA	singlet–triplet annihilation
τ	lifetime of excited state
TADF	thermally activated delayed fluorescence
TAZ	3-(biphenyl-4-yl)-5-(4-*tert*-butylphenyl)-4-phenyl-4H-1,2,4-triazole
TBADN	2-*tert*-butyl-9,10-di(naphth-2-yl)anthracene
TBM	tribenzoylmethide
TBP	2,5,8,11-tetra-tbutylperylene
TcTa	tris(4-carbazoyl-9-ylphenyl)amine
TDZP	[1,2,5]thiadiazole[3,4-f][1,10]phenanthroline
tfb	tetrafluorobenzoate
tfnb	4,4,4-trifluoro-1-(2-naphthyl)-1,3-butanedione
Tmphen	3,4,7,8-Tetramethyl-1,10-phenanthroline
Tol	toluene
TPBi	2,2′,2″-(1,3,5-benzinetriyl)-tris(1-phenyl-1-*H*-benzimidazole)
TPD	*N*,*N*′-bis(3-methylphenyl)-*N*,*N*′-diphenylbenzidine
tph	terephthalate
tpm	1,1,1-trifluoro-5,5-dimethyl-2,4-hexanedione
TPP	tetraphenylporphyrin
TPPO	triphenylphosphine oxide
trif	trifluoromethylsulfonate
tta	thenoyltrifluoroacetonate
TTA	triplet–triplet annihilation
U	applied voltage in V
UDC	Universal Display Corporation
UGH-2	bis(triphenylsilyl)benzene
VR	virtual reality
VTE	vacuum thermal evaporation
YAG	yttrium aluminum garnet

1 Introduction

Organic light-emitting diode (OLED) technology is used nowadays to create displays as well as lighting devices. Its rapid development is a result of several advantages [1,2]:

(1) high brightness (radiation brightness from several cd/m^2 for night work up to very high brightness of over 100,000 cd/m^2);
(2) high contrast (>1,000,000:1);
(3) low power consumption;
(4) ability to create flexible screens;

(5) smaller size and weight compared to plasma and liquid crystal displays;
(6) the only technology that allows the creation of panels with a large illumination area, as opposed to spot or linear lighting provided by LED and fluorescent lamps.

Today, leading OLED device manufacturers are constantly striving to improve the performance of their devices and reduce manufacturing costs. The development of OLED technology in recent years has been limited to the optimization of the composition of iridium-based compounds since these compounds have proved to be irreplaceable as materials for the emission layers of OLEDs; recently thermally activated delayed fluorescence (TADF) compounds also attracted remarkable attention. At the same time, the use of iridium and TADF compounds is expensive, since they are covered by the umbrella patents of the Universal Display Corporation [3]. Among other drawbacks, the most crucial is their wide emission bands (>100 nm), which limits the color purity in OLEDs.

This disadvantage can be avoided by using lanthanide (Ln) coordination compounds (CCs) as emitters for OLEDs. They have narrow emission bands (down to 10 nm) and this class of compounds is still not covered by patents. However, the reason for that is that presently, OLEDs based on Ln CCs demonstrate incomparably low characteristics.

Understanding the features of Ln CCs as OLED emitters, their prospectives, and the reasons for moderate electroluminescence (EL) intensity together with the potential pathways toward the solution of the arising problems is the goal of the present review.

2 Organic light-emitting diodes fundamentals

2.1 History and basics

Electroluminescence is the luminescence of a medium that occurs when an electric current is passed through it. It is a direct conversion of electrical energy into light. The discovery of the electroluminescence of anthracene crystals in 1960 by Pope et al. can be considered as the beginning of the era of organic electroluminescence [4]. An important phase in the development of organic electroluminescence began in the 1980s with the introduction of an aluminum complex with 8-hydroxyquinoline (Alq_3) as an active layer in the OLED structure by Tang and Van Slyke; this device exhibited a brightness of over 1000 cd/m^2 at voltages below 10 V [5]. In 1990, Burrows et al. demonstrated the possibility of using π-conjugated polymers, in particular poly(phenylenevinylene) (PPV), as emitting layers in organic light-emitting diodes [6]. In 1991, Kido demonstrated the possibility of using Ln CCs as emission layers in OLEDs [7], in 1999 Forrest first created OLEDs based on iridium(III) phosphorescent complexes [8], and in 2009 the first revelation of the impact of thermally-activated delayed fluorescence materials in OLEDs was presented by Adachi [9].

2.1.1 OLED structure and emission of light

A modern electroluminescent device is a multilayer heterostructure consisting of several organic layers enclosed between the cathode and anode, in which electrical energy is converted into light energy as a result of the recombination of electrons and holes injected from electrodes into the emission layer [10,11]. Electrons are first injected from the cathode and are then transported through the conduction bands of organic layers included in the heterostructure. The holes are injected from the anode and are transported through the valence bands of organic materials. It is important to note that in the case of molecular materials, the position of the "bottom" of the conduction band roughly corresponds to the position of the lowest unoccupied molecular orbital of the material (LUMO), and the top of the valence band corresponds to the highest occupied molecular orbital (HOMO). In the case of conductive materials, this is not entirely true, but when describing the operation of organic light-emitting diodes, the terms HOMO and LUMO are almost always used, including for OLEDs based on luminescent polymers. However, despite differences between the energy of the orbitals and of then bands, this approximate description is generally accepted.

The general heterostructure of a modern multilayer OLED includes several additional organic layers, and can be represented as follows:

anode/HIL/HTL/EBL/EML/HBL/ETL/EIL/cathode,

where HIL and EIL are hole and electron injection layers, HTL and ETL are hole and electron transport layers, EBL and HBL are electron and hole blocking layers, EML is emission layer (Fig. 1A). It is important to note that the same material is often used for ETL and HBL, as well as HTL and EBL.

When voltage is applied, the following processes occur (Fig. 1B):

1. injection of charge carriers from the electrodes,
2. transport of charge carriers to the emission layer,
3. recombination of charge carriers—electrons and holes—with the formation of an excited state (exciton),
4. light emission.

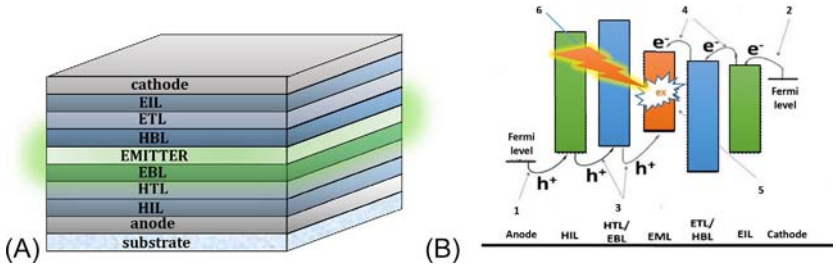

FIG. 1 (A) Schematic representation of an OLED heterostructure and (B) OLED energy diagram: (1) hole injection; (2) electron injection; (3) hole transport; (4) electron transport; (5) exciton formation; (6) light emission.

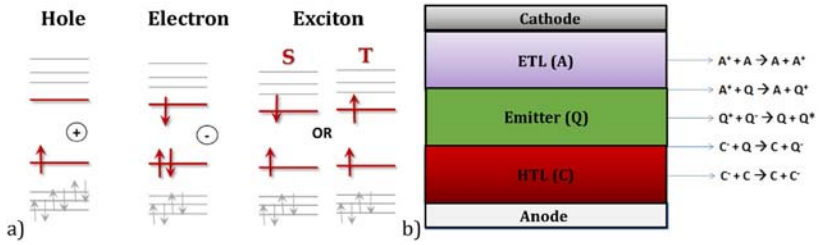

FIG. 2 (A) Electrons and holes in a molecular semiconductor and (B) transport of charge carriers in an OLED heterostructure.

First, electrons are injected from the cathode into the EIL and occupy the LUMO of the molecular semiconductor, while holes are injected from the anode into the HIL, which corresponds to the loss of an electron located in the HOMO of the HIL molecule (Fig. 2A). The subsequent transport of electrons and holes toward the emission layer is carried out over the LUMOs and HOMOs of the corresponding organic layers (Fig. 1B). To be able to transport charge carriers, EIL and ETL materials must possess high electron mobility, while HIL and HTL must possess high hole mobility; "high" corresponds to values of ca. 10^{-6}–10^{-3} $cm^2\,V^{-1}\,s^{-1}$. For efficient injection and transport of charge carriers in the OLED heterostructure, small (<0.5 eV) energy gaps are required between the anode Fermi level and HOMO levels of HIL–HTL–EML, as well as the cathode Fermi levels and LUMO levels of EIL–ETL–EML. To ensure the balance of charge carriers in the emission layer, it is necessary to balance the electron and hole currents, which can be achieved by varying the mobility of the transport layers, as well as by introducing blocking layers, which requires large (>0.5 eV) energy gaps between the HOMO energies of HBL and EML materials and the LUMO energies of EBL and EML materials, so that charge carriers do not leave the emission layer.

Upon reaching the emission layer (material Q, Fig. 2B), electrons and holes end up at its different boundaries. Subsequent transport and recombination of charge carriers occur inside the emission layer, for which noticeable mobility of charge carriers of at least one sign is necessary. Simplified transport within the emission layer can be represented by the following mechanism, where Q is the emitter material:

$Q + Q^+ \rightarrow Q^+ + Q$ (process 1: transport of holes)

$Q + Q^- \rightarrow Q^- + Q$ (process 2: transport of electrons)

$Q^+ + Q^- \rightarrow Q + Q^*$ (process 3: charge carrier recombination)

Often, the transport of charge carriers of the same sign is observed (i.e., process 1 or 2), and the subsequent recombination (process 3) occurs at the boundary of the EML/ETL layers (in the case of process 1) or HTL/EML (in the case of process 2).

During the recombination of charge carriers, an electron is transferred from the LUMO of Q^- to the LUMO of Q^+, which is accompanied by the

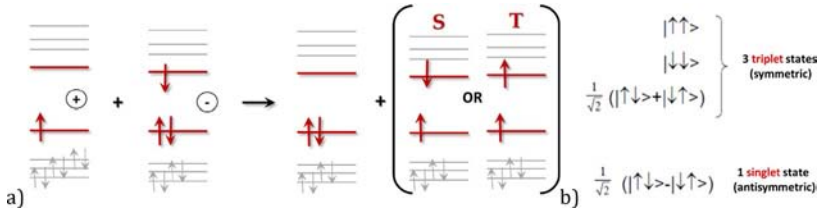

FIG. 3 (A) Formation of an excited state and (B) the ratio of singlet and triplet excitons.

formation of one molecule in the ground state and one molecule in an excited state. According to spin statistics (Fig. 3), upon electroexcitation, 25% of the formed excitons have a singlet nature (S1), and 75% have a triplet nature (T1) [5]. Subsequent radiative relaxation of excitons leads to the emission of light.

Thus, to achieve high efficiency of electroluminescence, it is necessary to ensure not only efficient luminescence, but, firstly, efficient electron and hole transport, including inside the emission layer, and, secondly, radiative relaxation of both singlet and triplet excitons, for which the emission material must involve the triplet level in the luminescence process. Besides, the energies of the boundary orbitals and charge mobilities should be taken into account when choosing materials for additional layers.

2.1.2 OLED characteristics and efficiency

The main characteristic of an OLED is its electroluminescence spectrum, which is recorded during device operation, as well as various efficiency parameters: current density j [mA/cm^2] and luminance (or brightness) L [cd/m^2] are measured in function of the applied voltage U [V], as well as luminous efficiency (or light output) PE [lm/W], current efficiency CE [cd/A] and external quantum efficiency of electroluminescence EQE [%] (Eqs. (1)–(3)):

$$PE = \frac{L \times \pi}{j \times U} \tag{1}$$

$$CE = \frac{L}{j} \tag{2}$$

$$EQE = \frac{N_{photon}}{N_{electron}} \times 100\% = \frac{\int\int \frac{2\pi\, E(\lambda,\theta)}{hc/\lambda} \sin\theta d\theta\, d\lambda}{I/e} \times 100\% \tag{3}$$

where λ is the wavelength (in nm), θ is the solid angle, h is Planks' constant ($6.626\ldots \times 10^{-34}$ kg m^2 s^{-1}), c is the speed of light in vacuo ($2.997\ldots \times 10^8$ m s^{-1}), I is the current (in A), and e is the electron charge ($1.602\ldots \times 10^{-19}$ C).

The switch-on voltage is also determined, that is, the voltage at which the brightness exceeds 1 cd/m^2. It is important to note that the theoretical minimum voltage at which the current can flow through the diode is $U_{on} = {}^{[E(LUMO)-E(HOMO)]}/_{e}$, where E(LUMO) and E(HOMO) correspond to the

energies of the boundary orbitals of the emission layer material. Therefore, the minimum possible OLED switch-on voltage cannot be lower than this value.

The energy efficiency of an OLED heterostructure is reflected by the EQE value, which can be represented by the expression:

$$EQE = \gamma \times \eta_r \times PLQY \times \eta_{out} \quad (4)$$

where γ is the efficiency of recombination of charge carriers in the emission layer, which is determined by the electrical properties of the device; η_r is the theoretical fraction of excitons participating in electroluminescence (25% for fluorescent materials, if only the singlet state is involved, and 100% if both singlet and triplet excitons are involved); PLQY is the photoluminescence quantum yield; η_{out} is the efficiency of light outcoupling from the device (for the simplest OLEDs it is in the range of 20–30%). Taking into account the efficiency of light outcoupling, the limit of the quantum yield of electroluminescence for fluorophores is 7.5%, and for materials using triplet excitons is 30% [12].

2.1.2.1 Transport of charge carriers in organic materials

In contrast to inorganic semiconductors, which have a band structure and free charge carriers, intermolecular interactions in amorphous films of organic semiconductors are very weak, and charges are highly localized. The most famous model of charge carrier transport in organic materials is the hopping mechanism [13], which consists of hopping between localized states widely distributed in energy, and the energy difference is compensated by the birth of phonons. The main contribution to the transport of charge carriers comes from carriers injected from contacts or generated in the organic material. The basis for the theoretical description of transport in organic materials remains the Gaussian disorder model [14,15], according to which the localized states are distributed in energy according to the Gaussian law, and the hopping rates are determined according to the Miller-Abrahams model [16]. Other models are describing the transport of charge carriers in organic semiconductors: the polaron model [17], the percolation model [18], and the Marcus charge transfer theory [19]. However, regardless of the choice of the model for transport description, the most important characteristic of carrier transport is the mobility μ [$cm^2\ V^{-1}\ s^{-1}$], which is the proportionality coefficient between the drift velocity of charge carriers and the applied external electric field.

Due to the above-described features of the transport of charge carriers in amorphous films of organic semiconductors, the typical values of mobility in organic materials are low: for materials used as electron and hole transport materials in OLEDs, they amount to $\mu_e = 10^{-6}...10^{-4}\ cm^2\ V^{-1}\ s^{-1}$ [20] and $\mu_h = 10^{-5}...10^{-3}\ cm^2\ V^{-1}\ s^{-1}$ [21], respectively. It should be noted that the mobility of charge carriers depends on the temperature and the applied electric field; therefore, for the same material, depending on the experimental

conditions, different values can be obtained. There are several methods for determining the mobility of charge carriers in organic materials, such as the time-of-flight method, determining the mobility in an organic field-effect transistor, the method of charges extraction by a linearly increasing field, the method of current limited by the space charge, the method of transient electroluminescence, the method of double injection, etc. [22–24].

2.1.2.2 Methods for deposition of thin films

OLED characteristics are directly related to the quality of thin films of the organic layers included in its heterostructure. The crystallinity of the film, the presence of impurities, as well as a large roughness of the film can lead to local overheating and local surges of the electric current, which will lead to the instantaneous or gradual destruction of the device [25]. Moreover, the presence of impurities will lead to impurity energy levels, which can severely distort the energy structure of an OLED device. Therefore, to obtain efficient OLED, thin films of all layers must be (1) amorphous, (2) free of impurities, (3) uniform in thickness. Thus, the quality of the film will depend on the nature of the material, the degree of purification, and the method of the film deposition. The latter will be considered next.

2.1.2.2.1 Vapor phase deposition *Vacuum thermal evaporation* (VTE) is a widespread method of vacuum deposition [25,26]. The starting material is carefully heated in a chamber under a high vacuum (10^{-5}–10^{-7} mmHg), then evaporated and condensed on a cold substrate. At low pressures, molecules move rectilinearly from the source to the substrate, since the mean free path of vapor molecules is comparable to the dimensions of the vacuum chamber. Due to the absence of collisions, the particles of the evaporated material retain a high temperature, which ensures their necessary mobility to form a dense homogeneous layer on the substrate. Vacuum is also a protective medium that allows the evaporation of chemically active materials without destroying their chemical composition. To obtain films with uniform thickness (= low roughness), uniform evaporation of the material is necessary, which is only possible by heating a small area, so this process is usually used to make small OLED devices. This method is not applicable to non-volatile materials that decompose under heating. The disadvantages of this method include both the high complexity and cost of the technological process, as well as the complexity of obtaining homogeneous composite films since this requires a long-term optimization of the material sputtering mode.

Today, most commercially available OLEDs are manufactured using VTE, which is associated with the high purity of the resulting films, ensured by high vacuum and the possibility of preliminary effective cleaning of materials by gradient vacuum sublimation to semiconductor purity [27]. This technology is used by every well-known OLED manufacturer such as LG Display, Samsung, Beijing Oriental Electronics (BOE), etc.

Organic vapor phase deposition (OVPD) is a cheaper deposition method, in which, similarly to VTE, a substance is heated in a chamber, but the material is transferred to a cooled substrate using a carrier gas (usually N_2 or Ar). Unlike VTE, in this case, the deposition rate can be controlled by two parameters: temperature and flow rate of the carrier gas.

A variation of this method, a low-pressure organic vapor phase deposition (LP-OVPD), is implemented at a pressure slightly below atmospheric pressure (<10 Torr). This type of OVPD is most often used to create OLEDs.

The main advantage of the OVPD method is its low cost compared to the VTE technology since this process does not require high vacuum conditions. Also, thanks to the carrier gas, almost all of the evaporated material is transferred to the substrate, which results in less material consumption. At the same time, due to the use of carrier gas, the roughness of the resulting films is higher. For example, using the LP-OVPD technology, 90 and 20 nm thick Alq_3 and TPD (*N*,*N*′-bis(3-methylphenyl)-*N*,*N*′-diphenylbenzidine) films with root mean square (rms) roughness values of 1 and 0.7 nm, respectively, were obtained [28], which exceeds the roughness of the films deposited by VTE (<0.45 nm).

OVPD technology is not yet applied in the production of diodes on an industrial scale, but recently Aixtron has developed an industrial setup for creating OLEDs using the OVPD method [29].

2.1.2.2.2 Solution deposition methods Recently, solution deposition methods have been rapidly developing, since they require a simpler hardware design, which can significantly reduce the cost of manufactured OLEDs. At the same time, the matching selection of materials and solvents becomes very important, since the previously deposited layers must be absolutely resistant to the solvent used to deposit subsequent layers. There are several methods of solution deposition [25].

2.1.2.2.2.1 Spin-coating In this method, a drop of a material solution is deposited on a rotating substrate, or the substrate starts rotating immediately after deposition of the solution. During this process, the solvent quickly evaporates, leaving a uniform film on the substrate. The thickness of the resulting film depends on the concentration and viscosity of the solution, the rotation speed of the substrate, the duration of rotation, the volatility of the solvent, surface wetting of the substrate, and temperature. This method is mainly used in laboratory conditions to create small samples; it is distinguished by its low cost due to the simplicity of the hardware design and allows the deposition of uniform films with a thickness of 10–200 nm.

2.1.2.2.2.2 Inkjet printing The principle of this deposition method is similar to the operation of an inkjet printer: a thin film is formed from microscopic drops of a solution of the printed material, sprayed by the print head.

2.1.2.2.2.3 Screen printing In this method, ink is forced through a well-defined stencil mask onto a substrate. This method is good for producing

irregularly shaped thin films. It is simple and cheap to implement and is also more rapid than inkjet printing since the ink is pressed simultaneously over the entire area of the stencil.

2.1.2.2.2.4 Gravure printing Gravure printing technology is a roll-to-roll method that uses a system of rollers to transfer the solution onto a moving substrate. There are several types of gravure printing (rotogravure, flexographic, offset), which differ from each other in the number of rolls and hardware design.

2.1.2.2.3 Comparison of solution methods Spin-coating is a laboratory only method, while gravure, screen, and inkjet printing can be used in the industry. Comparative characteristics of printing methods are shown in Table 1.

It is important to note that printing on traditional glass substrates is only possible by screen printing and inkjet printing. Gravure printing is only possible on flexible plastic substrates (polyethylene terephthalate, polyethylene naphthalate) that can be rolled between rolls. Gravure and screen printing have requirements for the minimum viscosity of the solutions used, so they can only deposit layers of polymers. Also, too thick films and their low quality in gravure and screen printing methods do not meet the modern requirements of OLED technology, therefore, despite the promising high speeds and volumes of production, these methods are not used in the industry. At the same time, inkjet technology is beginning to be introduced into production: in 2019, the first plant was opened by Joled (Japan) to produce TV screens and flexible phone displays using inkjet printing [30].

2.1.2.2.4 Comparison of the solution and vapor phase deposition methods On an industrial scale, almost all the OLEDs are manufactured using the VTE method, since the content of impurities in the film is minimal due to the high vacuum. However, bulky and expensive equipment is used in

TABLE 1 Comparative characteristics of printing methods.

	Engraving	Stencil	Inkjet
Solution viscosity	Medium/high (0.05–150 Pa·s)	High (1–100 Pa·s)	Low (<0.02 Pa·s)
Substrate type	Only flexible	Any	Any
Layer thickness	0.1–5 μm	0.1–20 μm	<0.1 μm
Production speed	Very high (500 m/min)	Low (<100 m/min)	Very low (<10 m/min)

the process of creating diodes by VTE. Besides, layers of polymers and non-volatile low-molecular compounds cannot be deposited by this method. Other disadvantages of VTE include the impossibility of creating flexible devices (since polymer flexible substrates cannot withstand heating), huge costs for creating OLEDs of large areas, and low production speed. The use of solution methods allows getting rid of all these disadvantages.

However, to date, the characteristics of OLEDs in which the layers are deposited by solution methods, are, as a rule, lower than those of OLEDs, in which the layers are deposited from the gas phase [31,32]. One of the main reasons is the different degrees of purification of the deposited material, as materials deposited from the gas phase are volatile, and therefore can be purified by gradient vacuum sublimation to semiconductor purity level before the deposition process. Non-volatile materials deposited by solution methods are purified using recrystallization and HPLC, which do not always allow achieving the desired degree of purity. HPLC is particularly difficult to use when it comes to the purification of complexes with neutral ligands. It is important to realize that in addition to the high purity of the deposited material, the use of solution methods also requires an extremely high purity of the solvent.

There are few studies devoted to the comparison of the deposition methods. Among them is the work of Ma and Duong [33], who compared OLEDs based on an iridium complex and with identical heterostructures, in which the emission layer was deposited by VTE and spin-coating. Both the maximum brightness and the efficiency of the diode, in which the emitter is deposited by the VTE method, are at least two times higher than the solution-processed analog (Table 2).

The poor performance of OLED devices in which the layers are deposited by solution methods, is primarily associated with the rapid degradation of the device. It was shown that the brightness of an OLED with TBADN:DPAVBi (Fig. 4A) as an emission layer obtained from the gas phase decreases threefold after 100 h of operation under constant current, while the brightness of an OLED with the same heterostructure but for which the emission layer is

TABLE 2 Comparison of OLED characteristics depending on the method of emitter film deposition [33].

Deposition method	U_{on} [V]	CE [cd/A]	PE [lm/W]	EQE [%]	L_{max} [cd/m^2]
Spin-coating	7,0	13,63	4,27	5,56	12,940
VTE	2,5	27,91	27,73	10,48	25,340

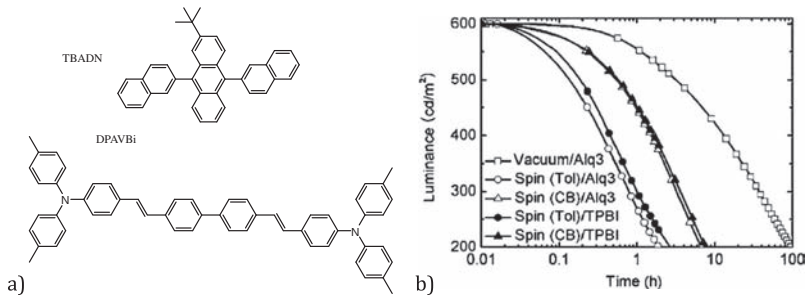

FIG. 4 (A) Structures of TBADN (2-*tert*-butyl-9,10-di(naphth-2-yl)anthracene) and DPAVBi (4,4′-bis[4-(di-*p*-tolylamino)styryl]biphenyl) materials and (B) dependence of brightness on time for OLED with heterostructure ITO/PEDOT:PSS/TBADN:DPAVBi/ETL (Alq_3 or TPBi)/LiF/Al, in which TBADN:DPAVBi films were deposited from the gas phase and solution in toluene (Tol) or chlorobenzene (CB). ITO is indium tin oxide, PEDOT:PSS poly(3,4-ethylenedioxythiophene) polystyrene sulfonate. *Reproduced from T.-W. Lee, T. Noh, H.-W. Shin, O. Kwon, J.-J. Park, B.-K. Choi, M.-S. Kim, D.W. Shin, Y.-R. Kim, Characteristics of solution-processed small-molecule organic films and light-emitting diodes compared with their vacuum-deposited counterparts, Adv. Funct. Mater. 19 (2009) 1625–1630. https://doi.org/10.1002/adfm.200801045,*

deposited by the spin-coating method, decreases threefold after 75–120 min of operation (Fig. 4B) [32]. It has been shown that film morphology and packing density, which are determined by the deposition method, are the decisive factors controlling the device life span. Impurities of solvent molecules can remain inside the solution-deposited films, and oxygen can more easily diffuse into them. It is important to note that the degradation time depends on the solvent from which the films were deposited.

Nevertheless, due to further optimization of the film deposition process, for example, the choice of the optimal solvent, substrate rotation rate, and deposition temperature, for some materials deposited from a solution, it has already been possible to obtain OLEDs which are only slightly inferior to similar devices fabricated using thermal vacuum deposition. For example, an OLED, in which the emission layer was deposited by the spin-coating method, demonstrates efficiencies comparable to those of an OLED in which the film was deposited by thermal co-deposition in vacuum (Table 3) [34].

Even higher injected current density and higher luminance were obtained from an OLED with solution-processed TPD compared to VTE [35]. The authors found that the surface of the solution-processed TPD films was even smoother and more hydrophilic than that of the vacuum-deposited film, while its density was higher. This resulted in higher hole mobility of the solution-processed TPD films, and thus better OLED performances.

At the same time, the maximum brightness of the OLED for which the emission layer is deposited by the spin-coating method, is still inferior to the gas phase analog, which is associated with the rapid degradation of the device.

TABLE 3 Comparison of OLED characteristics depending on the method of emitter film deposition [34].

Deposition method	U_{on} [V]	CE [cd/A]	PE [lm/W]	EQE [%]	L_{max} [cd/m^2]
Spin-coating	4	22,5	14,5	8,7	3473
VTE	5	26,7	12,7	9,5	23,990

2.2 OLED applications

Currently, the main applications of OLED devices can be divided into: (1) display production, (2) lighting, and (3) sensor applications.

2.2.1 Displays

The first commercial OLED device was produced just a decade after the first OLED was obtained by Tang et al. at Eastman Kodak. In 1997, Pioneer applied it in car audio systems as a passive matrix-driven display screen [36]. After these first applications, OLED display development was heavily industry-driven. In 2002, Philips introduced polymer-based OLEDs, in 2002 SK Display Corporation released full-color active-matrix OLEDs (AMOLEDs), in 2007, Sony produced the first OLED TV, and in 2011, the first OLED lighting device was proposed by Lumiotec. Since then, OLED technology became commonly used and demonstrated its unique features: flexible OLEDs (curved 5.7″ AMOLED in Samsung Galaxy Round smartphone, 6″ HD curved polymer-based OLED in LG G-Flex smartphone), bendable TV (LG), rollable TV (LG), foldable devices (Samsung and Huawei), foldable notebook (Lenovo and Intel) are since recently new reality [36]. The leading AMOLED producer is presently Samsung Display.

Today OLED-based displays are used in mobile phones, digital cameras, virtual reality (VR) headsets, tablets, laptops, and TV sets. In 2018, over 500 million AMOLED screens were produced, most of them for mobile phones (both rigid and flexible). Various AMOLED displays were named the world's best smartphone displays, including the display of the iPhone XS Max (6.5″ 1242×2688 flexible AMOLED) in 2018 and the Samsung Galaxy S20 Ultra (6.9″ 3200×1400 Dynamic AMOLED) in 2020 [37].

OLEDs are used for TV production today because they offer the best image quality, the thinnest sets, and the possibility to make large rollable and transparent OLED TVs. For mobile devices, they are superior as thin, efficient, flexible, and bright. An OLED display has the following advantages over an LCD:

1. Improved image quality: better contrast, higher brightness, fuller viewing angle, a wider color range, and much faster refresh rates;
2. Lower power consumption;
3. Simpler design that enables ultra-thin, flexible, foldable, and transparent displays;
4. Better durability: OLEDs are very durable and can operate in a broader temperature range.

They offer a large viewing angle, high resolution, high speed, good color gamut with blazing fastest response rate time. Every pixel is lit independently, and the light can be seen from off-axis viewing angles to about 180° since OLED pixels emit light directly.

2.2.2 Lighting

OLED white lighting is another opportunity, as OLEDs can be used to create excellent light sources. The accelerating growth of the energy demand gives an opportunity for environmentally benevolent technologies, among which OLED-based lighting is intended to be a cost-effective, energy-efficient, and high-quality replacement for incandescent and fluorescent lamps. Unlike traditional incandescent light bulbs and fluorescent lamps, OLED lighting creates visible light with virtually no heat or energy dissipation and also provides great resistance to shock and vibrations. Besides, same as for displays, they are superior in being flexible, light, thin, transparent, color-tunable, and in allowing completely novel designs.

Companies all over the world are developing OLED lighting, and today low-volume panels, though still quite expensive, can be seen not only in showrooms but also as light sources, i.e., flexible and rigid LG OLED light panels installed in Seoul Baskin Robbins (Fig. 5) [38].

OLED lighting panels are self-emissive, making them energy-saving, as well as very thin and light. They offer a higher contrast ratio, i.e., the image quality attribute that affects our ability to perceive image brightness and image detail. As OLEDs can switch their pixels off, they effectively have an infinite contrast ratio, making them effective in this category. They can be operated effectively within the temperature range between 20 °C and 70 °C. They can be printed onto any medium, hence making lightweight designs and flexible screens. Besides, they are highly sustainable, as (i) they are thinner, lighter in weight, and flexible, (ii) they consume very little power, and (iii) they do not contain mercury and are easily disposable. Moreover, they do not emit any UV radiation.

Compared to LEDs, OLED lighting also has important advantages, despite their similar light-emitting mechanism [39]. The most important is that OLEDs produce a uniform diffuse lighting source. This also makes them able to achieve the same brightness as point LED lighting sources, if the surface is large enough, even though basically LEDs can produce higher intensity.

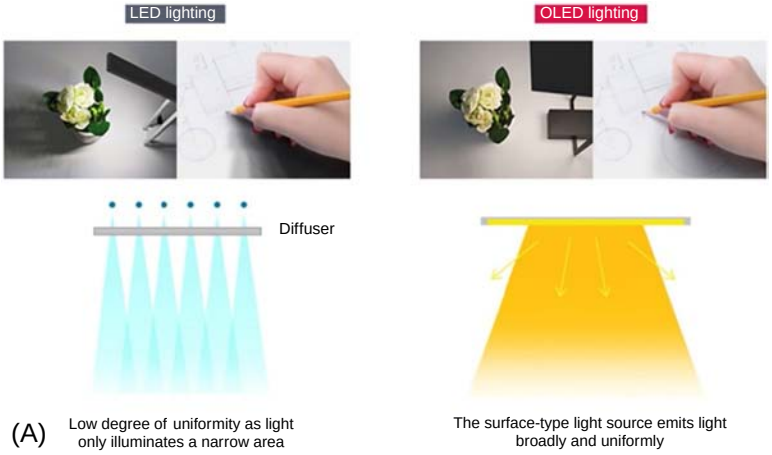

FIG. 5 (A) Comparison between LED and OLED lighting. (B) Flexible and rigid LG OLED light panels installed in Baskin Robbins commercial center (Seoul). Panel A: *Reproduced from OLED Light, (2014). http://www.lgdisplay.com/eng/product/oled_light.jsp (Accessed 22 November 2020), © 2014 LG Display Co. Ltd;* Panel B*: Reproduced from Flexible and Rigid LG OLED Light Panels Installed in Baskin Robbins Brown Store, (2021). https://www.linkedin.com/pulse/flexible-rigid-lg-oled-light-panels-installed-baskin-robbins-chung (Accessed 22 November 2020), © 2017 LG Display Co. Ltd.*

OLED disadvantages for displays and lighting include high costs of their production. This should change in the future, as OLEDs have the potential to be even cheaper than LCDs because of their simple design (some believe that future OLEDs will be printed using simple inkjet processes), but not yet. OLEDs have a short lifetime, and despite constant progress, this is still an issue today, even though OLEDs last long enough to be used in mobile devices and TVs.

2.2.3 *Photonic sensors*

OLEDs have been primarily applied to display and lighting technologies, and the reason for that, i.e., potential for large-area roll-to-roll manufacturing in large quantities, also makes them very attractive for medical sensors, where flexibility together with large areas can result in a remarkable improvement of the sensor performance [40]. Besides the stability issue - their main drawback - is not relevant for disposable medical sensors, which would be used for a few days instead of years.

Recently, the use of OLEDs as an excitation light source in a miniaturized PL-based sensor has been proposed for developing compact, low-cost, sensitive, and fast-response sensor arrays for a variety of analytes, i.e., oxygen, glucose, etc. [41,42]. A compact sensor where the OLED pixel array, the organic thin-film transistors, and the sensing films are structurally integrated on a single substrate was successfully operated (Fig. 6A) [43]. Pulse-oximetry

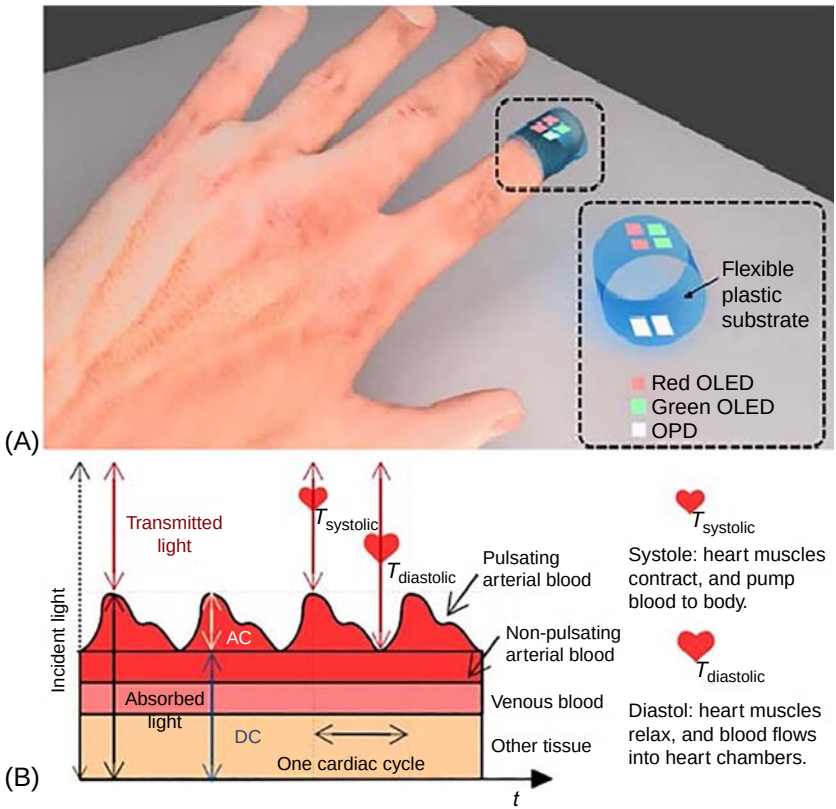

FIG. 6 (A) Pulse-oximetry sensor composed of two OLED arrays and two organic photodiodes (OPDs). (B) A schematic illustration of a model for the pulse oximeter light transmission path through pulsating arterial blood, non-pulsating arterial blood, venous blood, and other tissues over several cardiac cycles. *Reproduced with permission from C.M. Lochner, Y. Khan, A. Pierre, A.C. Arias, All-organic optoelectronic sensor for pulse oximetry, Nat. Commun. 5 (2014) 1–7. https://doi.org/10.1038/ncomms6745, © 2014 Springer Nature.*

can also be considered as a very promising and urgent application since the primary assessment of oxygen level becomes a challenging task in hospitals due to a large number of COVID-19 patients [44].

Such an oximeter contains two OLEDs, emitting at different wavelengths, and two organic photodiodes. Incident light from the OLEDs is attenuated by pulsating arterial blood, non-pulsating arterial blood, venous blood, and other tissues (Fig. 6B). When sampled with the OPD, light absorption in the finger peaks in systole (the heart's contraction phase) due to a large amount of fresh arterial blood. During diastole (the heart's relaxation phase), reverse flow of arterial blood to the heart chambers reduces blood volume in the sensing location, which results in minima in light absorption. This continuous change in arterial blood volume translates into a pulsating signal—the human pulse. The d.c. signal resulting from the non-pulsating arterial blood, venous blood, and tissue is subtracted from the pulsating signal to give the amount of light absorbed by oxy-hemoglobin (HbO_2) and deoxy-hemoglobin (Hb) in the pulsating arterial blood. HbO_2 and Hb have different absorptivities, resulting in the possibility of oxygenation determination.

3 Lanthanide luminescence

The basics of lanthanide luminescence, well-known to the readers [45], are given here to stress out the important features to be considered in the following discussion of electroluminescence. From the perspective of the luminescence mechanism, lanthanides can be roughly divided into f-f transition and d-f transition ions; however, some ions display both types of transitions, for instance Ce^{3+} (f-f transitions in the 2000–4000 cm^{-1} range and d-f emission in the visible) or Sm^{2+}.

3.1 Luminescence arising from f-f transitions

3.1.1 Electronic levels of $4f^N$ configurations

Trivalent Ln^{3+} ions are known for their unique luminescent properties due to the typical electronic configuration $[Xe]4f^n$, where $n = 0 \ldots 14$ from La^{3+} to Lu^{3+}. The presence of N electrons with different values of the spin quantum number in the 4f shell leads to the presence of 14!/N!(14-N)! states, transitions between which lead to intrinsic absorption and luminescence. Thus, most Ln^{3+} ions, except for La^{3+}, Ce^{3+}, and Lu^{3+}, exhibit luminescence due to intraconfigurational f-f transitions in the visible (for example, Eu^{3+} or Tb^{3+}) and near-infrared (for example, Yb^{3+}, Nd^{3+}, Er^{3+}, as well as Pr^{3+}, Ho^{3+}, and Tm^{3+}) range. Sm^{3+} and Dy^{3+} ions have transitions in both the visible and NIR ranges, while the Gd^{3+} ion exhibits luminescence in the ultraviolet range in the absence of organic ligands with low-lying singlet and triplet levels. The luminescence and absorption wavelength of the lanthanide ion depends on the value of the energy of its electronic levels between which the

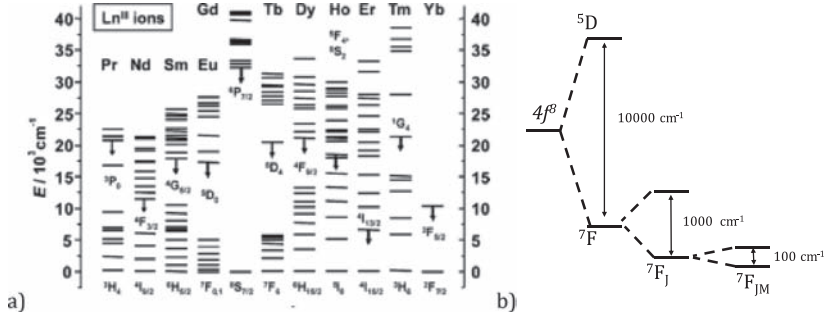

FIG. 7 (A) Diecke diagram for Ln^{3+} ions and (B) energy structure of the Tb^{3+} ion taking into account the electron-electron repulsion, spin-orbit interaction, and the crystal field generated by the ligands.

transitions occur. At the same time, the luminescence of the Ln^{3+} ion is possible only from certain levels, in view of selection rules.

Information about the ground and excited states of lanthanide ions and their energies can be extracted from the Diecke diagram (Fig. 7A). Each of these SLJ levels can be split by weak ligand field effects into the so-called Stark sublevels (Fig. 7B). Nevertheless, due to the screening of the partially filled 4f shell by the filled $5s^2$ and $5p^6$ shells, the ligands practically do not affect the electronic configuration of trivalent lanthanide ions, and the energy of this splitting is about 10^2 cm^{-1}.

Shielding also gives rise to specific luminescence properties of lanthanides, in particular, narrow luminescence bands, the position of which is practically constant. Electronic transitions between two levels are of different nature; the most intense being electric dipole transitions, while magnetic dipole and electric quadrupole transitions are much weaker. Since electric dipole f-f transitions are forbidden by Laporte's selection rule, lifetimes of the excited states are long ($\sim 10^{-6}$–10^{-2} s).

3.1.2 *Luminescence of lanthanide coordination compounds*

The forbidding of electric dipole f-f transitions leads to extremely low molar absorption coefficients ($<12.5\,M^{-1}$ cm^{-1}, but usually $<1\,M^{-1}$ cm^{-1}) and, as a consequence, to ineffective direct excitation of the lanthanide ions. To increase the luminescence intensity of lanthanide ions, an alternative pathway was developed, i.e., luminescence sensitization, or the "antenna effect." A luminescent ion is located in a matrix or organic medium that is capable of efficiently absorbing light, then energy is transferred to the ion, which eventually emits its characteristic light. Thus, designing lanthanide coordination compounds with various organic ligands will increase the intensity of luminescence if a high efficiency of sensitization is achieved.

In the case of coordination compounds, effective light absorption is mainly carried out by aromatic groups of unsaturated ligands with large one-photon absorption cross-sections. Due to the shielding of the 4f orbitals, the lanthanide-ligand bonds are mainly electrostatic, and only a slight admixture of the electronic wave functions of the ion and ligand promotes covalence. Therefore, it is justified to consider separately ligand-centered and metal-centered excited states in lanthanide complexes, and the Jablonski diagram is a convenient model for representing energy migration pathways (Fig. 8).

The organic ligand is excited, undergoing a transition from the ground state to one of the excited singlet states ($S_0 \rightarrow S_n$). After that, deactivation can occur along three paths: (1) a nonradiative transition to the ground state (internal conversion; IC), (2) a radiative transition to the ground state, i.e., fluorescence, (3) intersystem crossing (ISC), which occurs through the transition between the states of different multiplicity $S_n \rightarrow T_n$. Deactivation of the triplet state can also occur nonradiatively or due to phosphorescence, the radiative $T_1 \rightarrow S_0$ transition. The probability of such a spin-forbidden transition is low; nevertheless, in lanthanide CCs it may be higher due to the lanthanide magnetic moment, which makes the transition partially allowed. The role of the magnetic moment in this process is rather important; for instance for CCs with methyl salicylate, the rate constant of ISC is higher ($k_{isc} = 7.5 \times 10^8\ s^{-1}$) for gadolinium, which has the highest spin magnetic moment among lanthanides, than for lanthanum ($k_{isc} = 5.5 \times 10^7\ s^{-1}$), or for lutetium methyl salicylate ($k_{isc} = 7.9 \times 10^7\ s^{-1}$) [46]. It is very important to pay attention to the

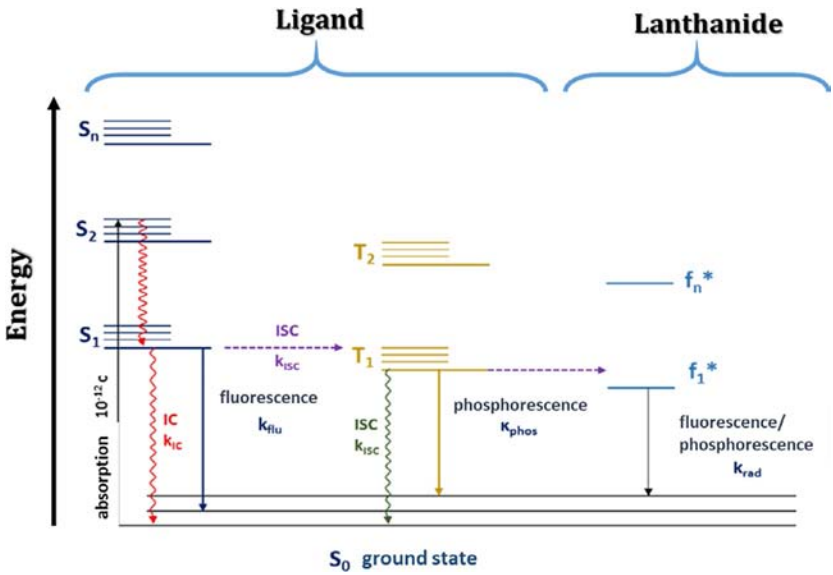

FIG. 8 Jablonski diagram for coordination compounds of lanthanides.

comparison between the lifetimes of complexes of La^{3+}, Lu^{3+}, and Gd^{3+}, given in this paper: it directly proves that it is the magnetic moment, and not heavy atom effect, that results in phosphorescence enhancement, though the opposite is usually claimed.

The sensitization of the lanthanide ion predominantly occurs from the triplet state due to its longer lifetime compared to the singlet state [46], although energy transfer from the singlet state to lanthanide is also possible, however, the contribution of this process to sensitization is often smaller [47,48]. Energy transfer $T_1 \rightarrow Ln^{3+}$ can be carried out by two main mechanisms: electron exchange (Dexter mechanism, Fig. 9A) and Coulomb dipole-dipole interaction (Förster mechanism, Fig. 9B) [49,50]. When the transfer occurs according to the Förster mechanism, the energy transfer rate is proportional to r^{-6}, where r is the distance between the ligand and lanthanide, and the transfer efficiency is determined by the overlap integral between the emission spectrum of the triplet state of the ligand and the adsorption spectrum of Ln^{3+}. The Dexter mechanism is a physical transfer of two electrons between a donor and an acceptor, which requires a sufficiently strong overlap of the ligand and metal orbitals; and the energy transfer rate, in this case, is proportional to e^{-r}.

In the case of lanthanide CCs, the total quantum yield ${QY_{Ln}}^{L}$ will be determined by the internal quantum yield of luminescence upon excitation through lanthanide ${QY_{Ln}}^{Ln}$ and the efficiency of L → Ln transfer (sensitization, η_{sens}):

$$QY_{Ln}^{L} = \eta_{sens} QY_{Ln}^{Ln} = \eta_{sens} \frac{\tau_{obs}}{\tau_{rad}} \tag{5}$$

3.2 Luminescence arising from d-f transitions

Different from the f-f transitions, the parity-allowed lanthanide d-f transitions imply relatively short excited lifetimes and broadband emission. Unlike 4f orbitals, whose interaction with their surrounding ions is weak, the 5d orbitals are not protected by the shielding effect, and therefore the $4f^n \leftrightarrow 4f^{n-1}5d^1$ transitions are strongly influenced by the chemical environment of Ce^{3+} or Ln^{2+} ions [51]. As a result, the emission color of d-f transition lanthanide compounds can

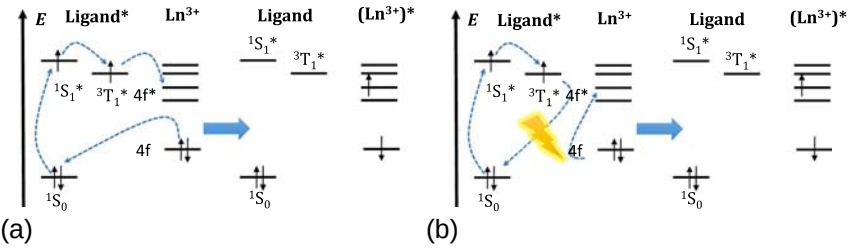

FIG. 9 Main mechanisms of energy transfer in the CC of lanthanides: (A) Dexter mechanism, (B) Förster mechanism.

be tuned in a very broad range: so, divalent europium can emit from ultraviolet to red, depending on the host [52–55]. The shift is attributed to differences in the covalency in the chemical bonds between Eu^{2+} and the anion ligands, resulting in a shift of the center of gravity (also called the barycenter) of the 5d-orbitals (centroid shift) and the crystal field splitting of the 5d orbitals [56].

Trivalent Ce^{3+} and divalent lanthanide ions, particularly Eu^{2+}, in inorganic matrices have been extensively investigated during the last three decades [53,55–61]. Nevertheless, the first attempts to record the PL of Ln^{2+} ions in solution were not successful. Thus, back in 1948, F.D.S. Butement noted that PL of europium, ytterbium, and samarium dichlorides in aqueous solutions is not observed due to their oxidation by water [62]. Later in 1973, R.G. Bulgakov succeeded to register the PL of divalent europium in acid-aqueous solutions with $\lambda_{max} = 450–470$ nm at the temperature of liquid nitrogen. It was found that when the frozen sample is heated, the brightness of this PL decreases, and at room temperature, the PL of Eu^{2+} disappears completely.

Currently, the research is mainly focused on Eu^{2+} complexes, though complexes of other divalent lanthanides are also investigated [63–67]. Among Eu^{2+} complexes, the most important are complexes with macrocyclic ligands [68,69] and cyclopentadienyl complexes [70]. However, complexes that can remain stable in air for a long time are very rare.

3.3 Concentration quenching

The phenomenon of concentration quenching relates to the decrease in the luminescence intensity with an increase in the number of emitting centers and is caused by the transfer of excited state energy between the luminescence centers until a defect is reached or nonradiative processes begin [71–73]. As a result, at small fractions of a luminescent ion, the luminescence intensity increases in proportion to its fraction, reaches a maximum, and then decreases (Fig. 10). An increase in the contribution of concentration quenching processes with an increase in the fraction of luminescent ions, as well as any processes of nonradiative relaxation of the excited state, leads to a decrease in the lifetime of the excited state.

Most of the research has focused on concentration quenching in inorganic systems, where this problem usually causes a significant decrease in luminescence efficiency at a high concentration of Ln^{3+}. A striking example is yttrium-aluminum garnet doped with neodymium ions Nd:YAG, for which the lifetime of the excited state increases by 90% with a decrease in the neodymium fraction down to 8% [75]. Partial substitution of a luminescent ion with an optically inactive one allows one to increase the quantum yield of even NIR luminescence up to 100%, as, for example, in the case of LaF_3:Er [76].

There are four possible mechanisms of concentration quenching: self-absorption, quenching by defects, cross-relaxation, and the phonon mechanism. Self-absorption (Fig. 11A) can be characteristic of any phosphor and consists in

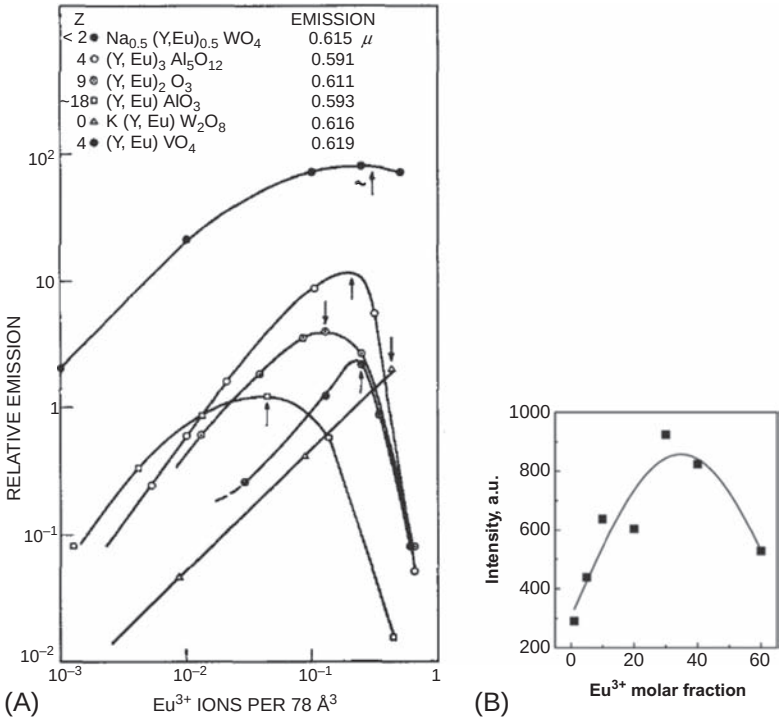

FIG. 10 Dependence of the Eu^{3+} luminescence intensity on its concentration in various yttrium inorganic matrices: (A) oxides [74]; (B) LaF_3 [73]. *Reproduced with permission from D. Pi, F. Wang, X. Fan, M. Wang, Y. Zhang, Luminescence behavior of Eu^{3+} doped LaF_3 nanoparticles., Spectrochim. Acta A Mol. Biomol. Spectrosc. 61 (2005) 2455–9. https://doi.org/10.1016/j.saa.2004.09.009, © 2005 2021 Elsevier B.V; L.G. Van Uitert, L.F. Johnson, Energy transfer between rare earth ions, J. Chem. Phys. 44 (1966) 3514–3522, © 1966 AIP Publishing LLC.*

the absorption of the photon emitted during luminescence by the same substance. Defect quenching (Fig. 11B) implies nonradiative energy transfer inside the crystal over significant distances to quenching defects. Cross-relaxation (Fig. 11C) is observed in the case of lanthanide ions with a large number of energy levels, when there is a redistribution of energy between ions. The energy from an excited level of one Ln^{3+} reaches an intermediate excited state of another Ln^{3+} with similar energy; then vibrational relaxation or further transfer can occur. Finally, phonon relaxation (Fig. 11D) is a process in which the donor energy is directly transferred to the phonon modes of the acceptor.

The mechanisms of concentration quenching occur because the increase in concentration results in a decrease in the average distance between the ions, causing an increase in the interaction strength between them. Due to the specific arrangement of their electronic levels, Eu^{3+} and Tb^{3+} compounds usually do not undergo cross-relaxation quenching; however, it was shown in [73] that the quenching of the $^5D_1$ excited Eu^{3+} level occurs precisely by this

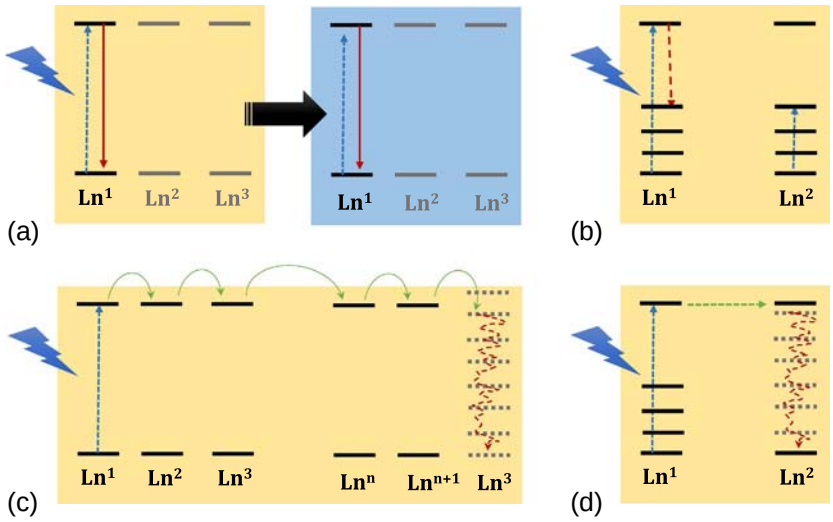

FIG. 11 Schemes of concentration quenching mechanisms: (A) self-absorption; (B) cross-relaxation; (C) quenching on defects; (D) phonon relaxation.

mechanism. Cross-relaxation is especially characteristic of ions with a large number of electronic levels, such as Nd^{3+}, Sm^{3+}, Dy^{3+}, Er^{3+}, or Tm^{3+} [77]. Due to their similar electronic structure, the optimal concentrations at which the maximum values of the luminescence intensity are observed for dysprosium and samarium are almost equal (4% and 5% for Sm^{3+} and Dy^{3+} in $Ln_xY_{1-x}Al_3B_4O_{12}$). Since the rest of the mechanisms are not associated with the electronic structure, they can be active for any lanthanide ion.

So, lanthanide luminescence undergoes concentration quenching, but the effect of this phenomenon is different for different classes of compounds. In inorganic matrices to avoid concentration quenching, Eu^{3+} is usually doped at 5% molar fraction [78–82], while optimal doping concentration of NIR-emitting ions is sometimes below 1% [76,83–90].

Concentration quenching is usually considered being less important for lanthanide complexes [91] due to the large separation of the emitting centers. Indeed, unlike organic compounds, whose boundary orbitals are localized on the neighboring organic species, or lanthanide inorganic salts, where emitting ions are separated by a few atoms, in coordination compounds with organic ligands, the emitting lanthanide ions are usually separated by bulky organic ligands. Nonetheless, examples of concentration quenching in lanthanide complexes are well-known. NIR-emitting ions mostly suffer from concentration quenching: indeed, the highest quantum yields of ytterbium were obtained in solution [92–95]. Ytterbium luminescence quenching by resonant Yb-Yb energy transfer takes place in inorganic compounds if the concentration of the dopant ion is above a certain critical value. Knowing the parameters of the crystal lattice, one can transform these concentration values

into critical distances d(Yb-Yb), which reach 10 Å [96] and even 20 Å [97]. These values are easily encountered in coordination compounds, leading to pronounced concentration quenching. So, the ytterbium lifetime in 9-anthracenates [$Yb_xLu_{1-x}(ant)_3$] linearly decreases in the range of x = 0.1…1, which witnesses the concentration quenching; indeed, the highest quantum yield of 2.5% is reached at x = 0.2 (Fig. 12A).

Similarly, samarium and dysprosium complexes suffer from concentration quenching as observed for both dysprosium terephthalate and phenoxybenzoate [98]. This is manifested in the presence of maxima on the curves of the dependence of the luminescence intensity of Dy^{3+} on its molar fraction x in the CC. The maximum luminescence intensity falls for x = 0.20–0.25 (Fig. 12B). For dysprosium terephthalate, partial substitution of the emitting ion by yttrium resulted in a threefold increase of the quantum yield (from 0.8% up to 2.5%).

Regarding the highly emissive terbium and europium ions, no direct evidence of concentration quenching was published. Nevertheless, in [99,100] the possibility of this effect was studied. It was considered that the probability of concentration quenching increases when (1) the distance between the emitting ions decreases, and (2) the lifetime of the excited state increases, which allows more room for the radiationless relaxation, including quenching. It turned out that among the studied complexes the dependence of the lifetime on the metal fraction was only observed in the dehydrated terephthalates, which, taking into account the small size and dianionic nature of the ligands, correspond to the complexes with organic ligands with the smallest intralanthanide distance. Plotting lifetimes *vs* volume concentration of the emitting

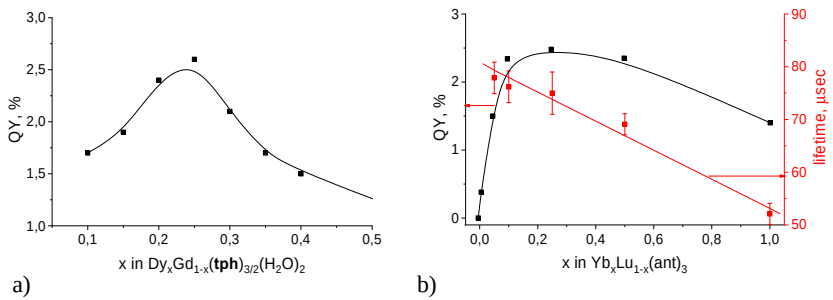

FIG. 12 (A) The quantum yields of the luminescence of powders of [$Dy_xGd_{1-x}(tph)_{3/2}(H_2O)_2$]. (B) The lifetime of the excited state and quantum yields of the luminescence of powders of [$Yb_xLu_{1-x}(ant)_3$]; tph is terephthalate and ant 9-anthracenate. Panel A: *Redrawn from data A. V. Orlova, V.Y. Kozhevnikova, L.S. Lepnev, A.S. Goloveshkin, I.M. Le-Deigen, V. V. Utochnikova, NIR emitting terephthalates (SmxDyyGd1-x-y)2(tph)3(H2O)4 for luminescence thermometry in the physiological range, J. Rare Earths 38 (2020) 492–497. https://doi.org/10.1016/j.jre.2020.01.010;* Panel B*: Redrawn from data V. V. Utochnikova, A.S. Kalyakina, I.S. Bushmarinov, A.A. Vashchenko, L. Marciniak, A.M. Kaczmarek, R. Van Deun, S. Bräse, N.P. Kuzmina, Lanthanide 9-anthracenate: solution processable emitters for efficient purely NIR emitting host-free OLED, J. Mater. Chem. C 4 (2016) 9848–9855.*

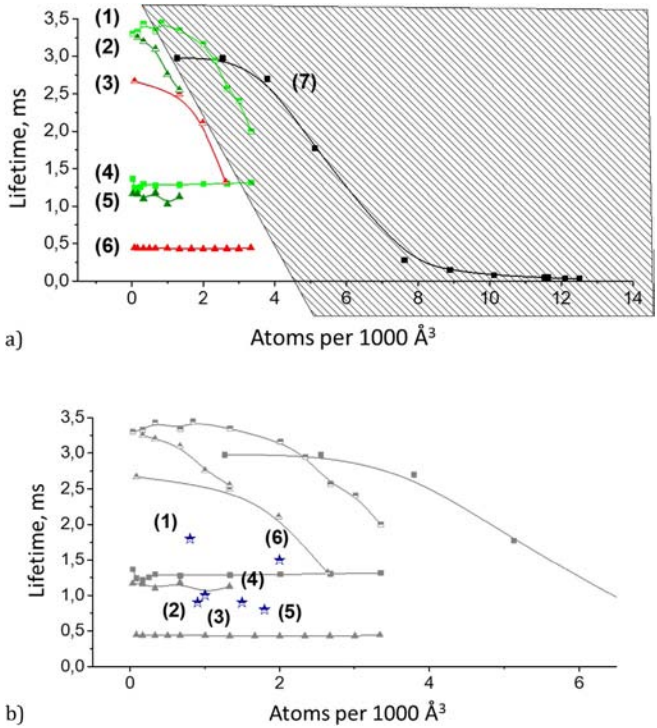

FIG. 13 Lifetimes of the excited states of Eu^{3+} and Tb^{3+} powders (ms) (A) (1) $[Tb_xY_{1-x}(tph)_3]$, (2) $[Tb_xGd_{1-x}(tph)_3]$, (3) $[Eu_xY_{1-x}(tph)_3]$, (4) $[Tb_xY_{1-x}(tph)_3(H_2O)_4]$, (5) $[Tb_xGd_{1-x}(tph)_3(H_2O)_4]$, (6) $[Eu_xY_{1-x}(tph)_3(H_2O)_4]$, (7) $[(Tb_xY_{1-x})Al_5O_{12}]$; (B) (1) $[Eu(tfb)_3(H_2O)_2]$, (2) $[Tb(pam)_3(H_2O)_4]$, (3) $[Eu(tfb)_3(phen)_2]$, (4) $[Tb(phm)_3(H_2O)_2]$, (5) $[Eu(pfb)_3(H_2O)]$, (6) $[Tb(pfb)_3(H_2O)]$. *tph*: terephthalate; *tfb*: tetrafluorobenzoate; *pam*: *p*(amino)tetrafluorobenzoate; *phm*: *p*(hydroxymethyl) tetrafluorobenzoate; *pfb*: pentafluorobenzoate. *Plotted according to data reported in A.Y. Grishko, V. V. Utochnikova, A.A. Averin, A. V. Mironov, N.P. Kuzmina, Unusual luminescence properties of heterometallic REE terephthalates, Eur. J. Inorg. Chem. 2015 (2015) 1660–1664. https://doi.org/10.1002/ejic.201403071; V. V. Utochnikova, N.N. Solodukhin, A.N.A.N. Aslandukov, L. Marciniak, I.S. Bushmarinov, A.A. Vashchenko, N.P. Kuzmina, Lanthanide tetrafluorobenzoates as emitters for OLEDs: new approach for host selection, Org. Electron. 44 (2017) 85–93. https://doi.org/10.1016/j.orgel.2017.01.026; V. V. Utochnikova, N.N. Solodukhin, A.A. Aslandukov, K. V. Zaitsev, A.S. Kalyakina, A.A. Averin, I.A. Ananyev, A. V. Churakov, N.P. Kuzmina, Highly luminescent, water-soluble lanthanide fluorobenzoates: syntheses, structures and photophysics. Part II: luminescence enhancement by p-substituent variation, Eur. J. Inorg. Chem. 2017 (2016) 107–114; A.S. Kalyakina, V. V. Utochnikova, I.S. Bushmarinov, I. V. Ananyev, I.L. Eremenko, D. Volz, F. Rönicke, U. Schepers, R. Van Deun, A.L. Trigub, Y. V. Zubavichus, N.P. Kuzmina, S. Bräse, Highly luminescent, water-soluble lanthanide fluorobenzoates: syntheses, structures and photophysics, part I: lanthanide pentafluorobenzoates, Chem. A Eur. J. 21 (2016) 17921–17932. https://doi.org/10.1002/chem.201501816.*

ion for some complexes together with those of inorganic $(Tb_xY_{1-x})Al_5O_{12}$ allowed to determine an area where concentration quenching is possible (shaded in Fig. 13A). It is clear that most typical complexes are far from this area (Fig. 13B).

In conclusion, concentration quenching is possible for lanthanide complexes, including those of Tb^{3+} and Eu^{3+}, but is rarely observed for the latter two ions.

4 Lanthanide OLEDs

After presenting the fundamental aspects of OLED performances and lanthanide luminescence, we now discuss the peculiarities of lanthanide compounds as emitters in OLEDs. It is very important to note that the mechanism of the luminescence of lanthanide complexes differs significantly from that of typical fluorescent and phosphorescent emitters, and even TADF emitters differ less from them than lanthanide complexes. Therefore, despite the possibility to utilize the wide experience gathered during the years of OLED investigation, almost every stage of OLED heterostructure selection and optimization should be thought out separately, taking in mind the peculiarities of lanthanide photophysics.

Since trivalent lanthanide ions are mostly utilized in lanthanide-based OLEDs nowadays, we will be referring to them unless other is stated.

4.1 Cost

Price may not be the most important factor but has to be also considered when discussing various emitter materials. Both iridium complexes and TADF materials have the high-cost drawback, which originates from expensive organic synthesis, high iridium price, but mainly the cost of the portfolio of patents owned by Universal Display Corporation (UDC) [101]. UDC holds over 4000 issued and pending patents. All the major OLED makers (including Samsung and LG) are using UDC's materials to achieve higher display efficiencies, beyond what is available from fluorescent emitters.

This is not the case for lanthanide complexes; while their own cost is also relatively reasonable: despite lanthanides belong to "rare earths," they are not rare. Their availability is primarily limited because their concentration levels are quite low (<5% w/w). However, collectively, they rank as the 22nd most abundant (at the 68th percentile mark) elements [102]. The most abundant Ce ranks 28th, and the least abundant Tm is 63rd; even traces of Pm ($t_{½} = 17.7$ years) are found in radioactive ores. Lanthanum and the lighter lanthanides (Ce-Eu) are more abundant than the heavier ones (Gd-Lu), and thus are generally less expensive as individual elements. The atoms with an even atomic number are more abundant due to the Oddo-Harkins rule.

Each known lanthanide mineral contains most of the rare earth metals, but at very different concentrations: monazite mostly contains the lighter lanthanides, xenotime—the heavier lanthanides, etc. (Table 4). Therefore to obtain these elements and in view of their similar chemical properties, the minerals must go through a lengthy and costly separation process, which also affects their prices (Table 5).

TABLE 4 Rare-earth content in selected minerals [102].

R	Bastnasite (USA)	Bastnasite (China)	Monazite (Australia)	Xenotime (Malaysia)	High-Y laterite (China)	Low-Y laterite (China)	Loparite (Russia)
La	33.8	23.0	25.5	1.2	1.8	43.4	25.0
Ce	49.6	50.0	46.7	3.1	0.4	2.4	50.5
Pr	4.1	6.2	5.3	0.5	0.7	9.0	5.0
Nd	11.2	18.5	18.5	1.6	3.0	31.7	15.0
Sm	0.9	0.8	2.3	1.1	2.8	3.9	0.7
Eu	0.1	0.2	0.4	Trace	0.1	0.5	0.1
Gd	0.2	0.7	<0.1	3.5	6.9	3.0	0.6
Tb	0.0	0.1	<0.1	0.9	1.3	Trace	Trace
Dy	0.0	0.1	0.1	8.3	6.7	Trace	0.6
Ho	0.0	Trace	Trace	2.0	1.6	Trace	0.7
Er	0.0	Trace	Trace	6.4	4.9	Trace	0.8
Tm	0.0	Trace	None	1.1	0.7	Trace	0.1
Yb	0.0	Trace	None	6.8	2.5	0.3	0.2
Lu	Trace	Trace	None	1.0	0.4	0.1	0.2
Y	0.1	Trace	<0.1	61.0	65.0	8.0	1.3

TABLE 5 Chinese domestic prices for rare earth oxides 2018 (renminbi per metric ton) [105].

Praseodymium oxide	440,000	Gadolinium oxide	100,000	Samarium oxide	14,000
Neodymium oxide	360,000	Yttrium oxide	21,500	Terbium oxide	3075
Didymium oxide	350,000	Cerium oxide	14,000	Dysprosium oxide	1180
Erbium oxide	170,000	Lanthanum oxide	14,000	Europium oxide	420

Rare-earth ore deposits are found all over the world. The major ores are in China, the United States, Australia, Vietnam, and Russia. In 2020, China had a mine production of some 140,000 metric tons of rare-earth oxides representing a 58% share of the world production, down from 98% in 2011. China's monopoly allowed it to raise prices by hundreds of percent for various rare-earth materials from 2009 to 2011 (Fig. 14), so lanthanide price relates to their localization, not general abundance. As a result, in 2012 mining of bastnasite resumed in the USA, while mining of monazite began a year before in Australia. At the same time, loparite was being mined in Russia, while monazite was mined in India, Vietnam, Thailand, and Malaysia. Those and other mining operations brought a new equilibrium between demand and supply in which China is still the major supplier of rare-earth minerals, but the price significantly decreased and is forecasted to remain more or less on the same level unless unforeseen geopolitical factors occur.

As of 2019, estimated world reserves of rare-earth minerals amounted to some 120 million metric tons of oxides (Fig. 15). Platinum metal reserve, for example, is thousands of times less (69,000 metric tons)!

4.2 Chemical and thermal stability

When considering divalent lanthanide complexes, stability is the main issue [108], while, on the other hand, complexes of trivalent lanthanides have usually much higher stability in air relative to emitters of other classes, particularly d-metal metallocycled compounds [109,110]. The stability under electric current is a separate issue, making it impossible to operate lanthanide-based OLEDs without encapsulation, particularly since other materials are also utilized. Despite this, air-stability significantly facilitates manipulations with lanthanide complexes.

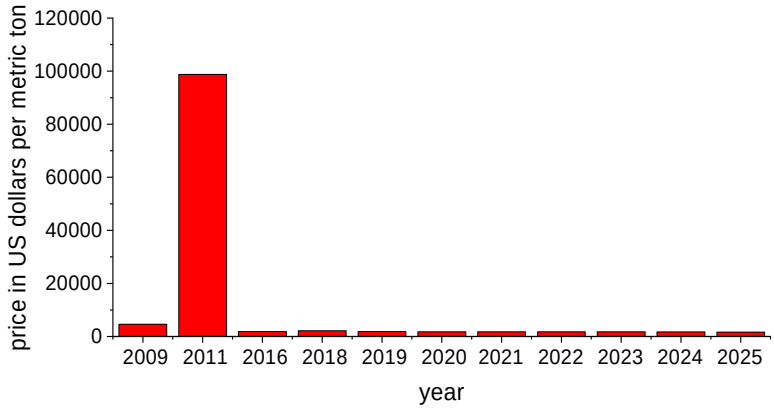

a)

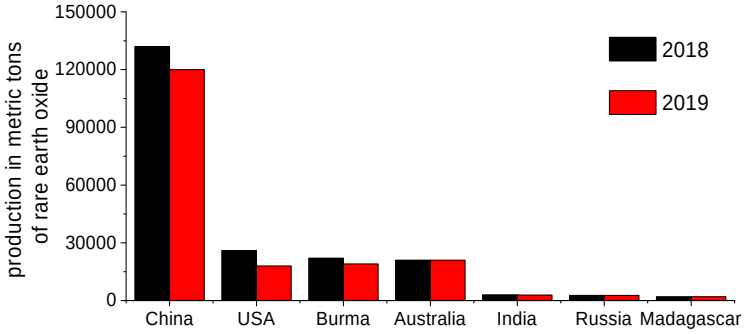

b)

FIG. 14 (A) Lanthanum oxide price worldwide [103] and (B) major countries in rare earth mine production worldwide in 2018 (black) and 2019 (red) [104].

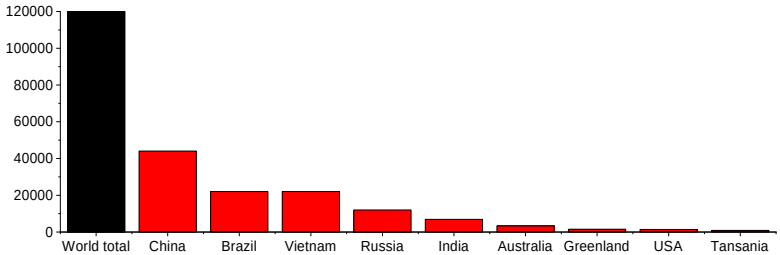

a)

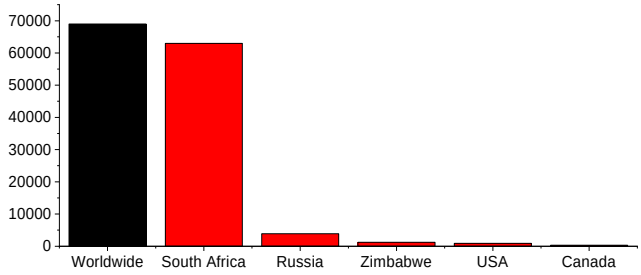

b)

FIG. 15 (A) Rare-earth [106] (in 1000 metric tons) vs (B) platinum metal total reserves [107] (in metric tons) worldwide as of 2019, by country.

The thermal stability of lanthanide complexes significantly varies depending on the organic ligands. For instance, the thermal stability of β-diketonates, even solvent-free, usually not exceeds ca. 200–250 °C [111–113], while for aromatic carboxylates thermal stability up to 400 °C [114–117] and even higher [118–120] can be easily obtained after dehydration. This can be matched by d-metal compounds, but barely by organic molecules.

Altogether, lanthanide complexes are more stable than emitters of any other class.

4.3 Triplet state and quantum yield

The formation of the excitons under electroexcitation obeys the spin-statistics rule and results in 75% of triplet and 25% of singlet excitons. Therefore, the involvement of triplet excitons in the luminescence process is among the basic requirements for prospective electroluminescent materials. The emission of lanthanide complexes answers this requirement: though the direct singlet-to-lanthanide sensitization process is often discussed and even directly evidenced in several publications [121–124], the through-triplet sensitization process remains a preferred pathway leading to lanthanide luminescence.

The photoluminescence quantum yield, which shows the efficiency of radiative relaxation, is directly proportional to the luminance within the same class of material, and it definitely affects the final OLED performance. The achievable quantum yields of lanthanide complexes depend primarily on the central ion, but for each ion, the ligand nature affects considerably the quantum yield value.

The highest quantum yields are obtained for terbium and europium complexes, the main reason for which is the largest gap between the emitting state and the nearest lower-lying state. This results in more difficult quenching of their luminescence: indeed, the smaller this gap is, the smaller the number of phonons is required to fill the energy gap. So, europium with the ($^5D_0$-$^7F_6$) gap of ca. 12,000 cm^{-1} can be quenched by the 3rd harmonics of the OH-vibration, while terbium only by the 4th. Similarly, concentration quenching is less effective when the gap is larger and the density of states is lower: i.e., resonance energy transfer requires the presence of an intermediate state, equally distant from the ground and excited states, and in the case of distance inequality the energy difference must be compensated by phonons. The highest intermediate state of Eu^{3+} lies at ca. 5000 cm^{-1}, which is quite far from equidistant (½E($^5D_0$) = 8600 cm^{-1}), while in the case of samarium with a similar excited state energy, but higher state density, there is a state at exactly halfway (9000 cm^{-1}). This results in incomparably smaller PLQYs of Sm^{3+} compounds with respect to Eu^{3+}; the same is true for Dy^{3+} and Tb^{3+} pair with similar excited state energies: while for terbium complexes PLQYs close to 100% are readily achievable, the highest PLQYs of Dy^{3+} complexes are in the range of 5–10% [125].

For europium complexes, the quantum yields are lower, and the typical values lie below 50%. At the same time, several examples exist in the literature, where PLQYs as high as 90% are reported, and the values of 70–80% are suitable to satisfy the demands of material design for OLED applications.

In the NIR range, the PLQYs are expectedly lower, which is connected with the ease of quenching due to the fundamentally low energy gaps between the states (Fig. 16). In addition, in the case of lanthanides, the PLQY decrease is also connected with difficulties in sensitization: the selection of the proper ligands for low-energy NIR luminescence sensitization is a specific problem. As NIR-emitting ions the following are considered:

- Yb^{3+}, which demonstrates the highest quantum yields in view of its only excited state with an energy of 10,000 cm^{-1}. The absence of other middle states complicates its luminescence quenching, which, however, remains more efficient, than in the case of Tb^{3+} and Eu^{3+}, but much lower than for other NIR-emitting lanthanides. So, in solution, where concentration quenching is completely absent, quantum yields of ytterbium complexes as high as 63% were obtained (β-fluorinated ytterbium porphyrinate in CD_2Cl_2) [126], which in the present case was also a consequence of the proper fluorinated ligand selection to avoid CH-vibrations, also known to effectively quench NIR luminescence. In the solid state the quantum yields are significantly lower: PLQYs of ca. 1–4% are considered as high values, and can be reached for complexes with ligands of various classes, i.e., Schiff bases (1.4% in [127]), aromatic carboxylates (1.5% in [128]), metallacrown complexes {Yb^{3+}[Zn(II)MCquinHA]} (2.4% in [94]), or benzoxazole-substituted 8-hydroxyquinolinate (3.7% in [129]); as said above, higher quantum yields may be obtained in solution. A decrease in the concentration quenching efficiency in the solid state is also possible due to the partial substitution of the luminescent metal with a non-emitting one. This allowed increasing the PLQY of 1.5% for ytterbium 9-anthracenate up to 2.5% for bimetallic $[Yb_{0.3}Lu_{0.7}(ant)_3]$ [128] (Table 6).
- Nd^{3+}, for which one of the highest quantum yields in the solid state was also obtained for the metallacrown complex Nd^{3+}[Zn(II)MCquinHA] (1.13%) [94], but values much below 1% are considered as high quantum yields of Nd^{3+} complexes [136], and for most of them these values are below measurement.
- Er^{3+} is important in view of its 1.5 μm emission, ideal for optical fiber amplification. Nonetheless, despite it is widely used within inorganic matrices, the unprecedented ease of its luminescence quenching still makes it difficult to obtain coordination compounds with organic ligands with measurable quantum yields.
- Dy^{3+} and Sm^{3+} are considered as NIR-emitting metals due to two reasons: (1) the possibility to obtain dual emission in visible and NIR range and (2) the high excited state energy, easy to be sensitized. However, they were shown to be inferior to ytterbium NIR emitters [83].

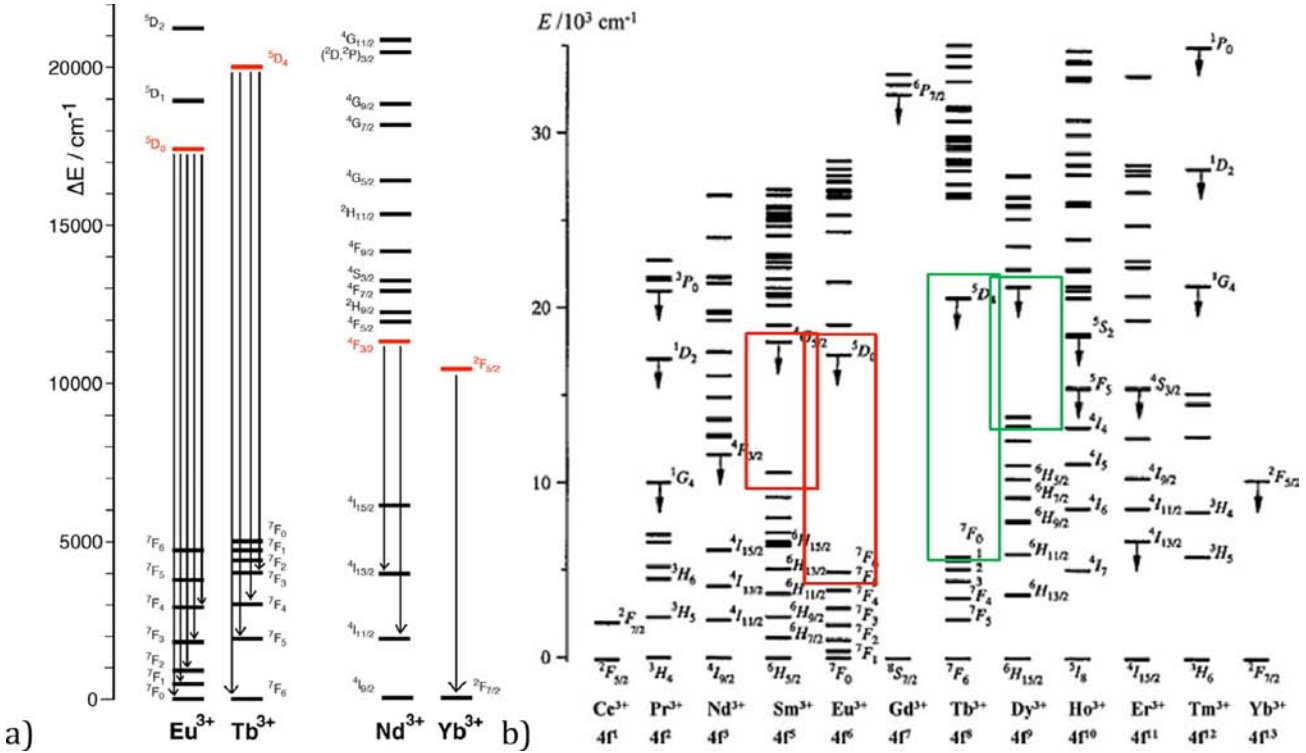

FIG. 16 (A) Emitting states of Eu^{3+}, Tb^{3+}, Nd^{3+}, Yb^{3+}. (B) The gap between the emitting state and the nearest lower-lying state of red-emitting Sm^{3+} and Eu^{3+} and green-emitting Tb^{3+} and Dy^{3+}.

TABLE 6 Quantum yields of some highly emissive Tb^{3+}, Eu^{3+}, and Yb^{3+} complexes.

Terbium complex	PLQY, %	References	Terbium complex	PLQY, %	References
$[Tb(bz)_3(H_2O)_2]$	100	[115]	$[Tb(pobz)_3(PO1)]$	100	[130]
$[Tb(pobz)_3(H_2O)_{2]}$	96	[131]	$[Tb(pobz)_3(PO2)]$	100	[130]
$[Tb(PA)_3(H_2O)_2]$	100	[132]	$[Tb(pobz)_3(PO3)]$	90	[130]
			$[Tb(pobz)_3(PO4)]$	100	[130]
Europium complex	**PLQY, %**	**References**	**Europium complex**	**PLQY, %**	**References**
$[Eu(fb1)_3phen]$	90	[133]	$[Eu(mfb)_3Bphen]$	90	[134]
$[Eu(fb2)_3phen]$	82	[133]	$[Eu(oac)_3Bphen]$	85	[134]
$[Eu(hfa)_3(DPEPO)]$	85[a]	[135]	$[Eu(piv)_3Bphen]$	85	[134]
			$[Eu(tta)_3Bphen]$	90	[134]
Ytterbium complex	**PLQY, %**	**References**	**Ytterbium complex**	**PLQY, %**	**References**
Yb^{3+}[Zn(II)MCquinHA]	2.44	[94]	$[Yb(HL)_2Cl]$	1.4	[127]
$[Yb(ant)_3]$	1.5	[128]	Yb1	63[b]	[126]
$[Yb_{0.3}Lu_{0.7}(ant)_3]$	2.5	[128]			

Key: *bz*, benzoate; *pobz*, phenoxybenzoate; *PA*, pyrazolecarboxylate; *PO1–4*, di(phosphine oxides); *fb1–2*, fluorobenzoates; *phen*, phenanthroline; *tta*, thenoyltrifluoroacetylacetonate; *Bphen*, bathophenanthroline; *mfb*, monofluorobenzoate; *oac*, acetate; *piv*, pivaloate; *hfa*, hexafluoroacetylacetonate; *DPEPO*, bis(2-(diphenylphosphino)phenyl)ether oxide; *quinHA*, quinaldichydroxamic acid; *ant*, anthracenate; *HL*, 2-(tosylamino)benzylidene-N-benzoylhydrazone; *Yb1*, Yb octafluorinated porphyrinate with fully deuterated Kläui's ligand.
[a] *In PMMA.*
[b] *In CD_2Cl_2.*

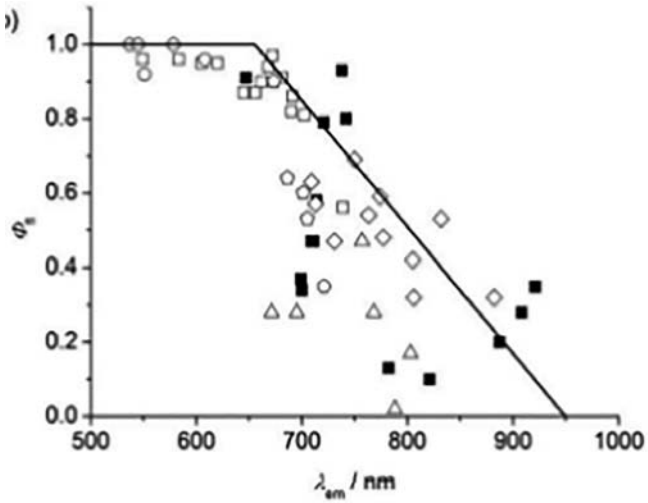

FIG. 17 Dependence of quantum yields on the wavelength (λ_{em}) of emission for several classes of organic NIR dyes. *Reproduced from A. Zampetti, A. Minotto, F. Cacialli, Near-infrared (NIR) organic light-emitting diodes (OLEDs): challenges and opportunities, Adv. Funct. Mater. 29 (2019) 1807623. https://doi.org/10.1002/adfm.201807623, © 2019 John Wiley & Sons, Inc.*

For organic dyes of various classes, a noticeable decrease in quantum yields is also observed as the luminescence wavelength increases (Fig. 17). Therefore the PLQY values obtained for lanthanide complexes not only in green (Tb^{3+}, up to 100%) and red ranges (Eu^{3+}, up to 90%) but also in the NIR range (Yb^{3+}, up to 3.7% in solid state) are remarkably high, which makes lanthanide complexes potentially prospective for OLED applications from this point of view as well.

4.4 Emission bandwidth

The ideal *light source* should resemble the sun in its spectrum, which is almost uniform within the visible range. The use of typical LEDs, whose spectra consist of a wide yellow band of Ce:YAG, excited by a narrow blue band of InGaN, also present in the spectrum, are now gradually substituted by other sources, which do not emit narrow bands at all.

Lanthanide luminescence features narrow f-f emission bands, which is not suitable for lighting. As an exception gadolinium complexes can be considered: gadolinium with its half-filled f-shell has its lowest excited state above 30,000 cm^{-1} and its ionic luminescence, observed in ca. 300 nm range, is hardly sensitized by typical organic ligands; therefore luminescence of the organic part is observed after excitation of the gadolinium complexes. However, unlike complexes of lanthanum and lutetium, which do not possess any f-states due to empty or filled f-shell, ligand phosphorescence of gadolinium complexes can be observed, originating from the T_1 state and suitable for OLEDs (Fig. 18). This is due to efficient intersystem crossing favored by

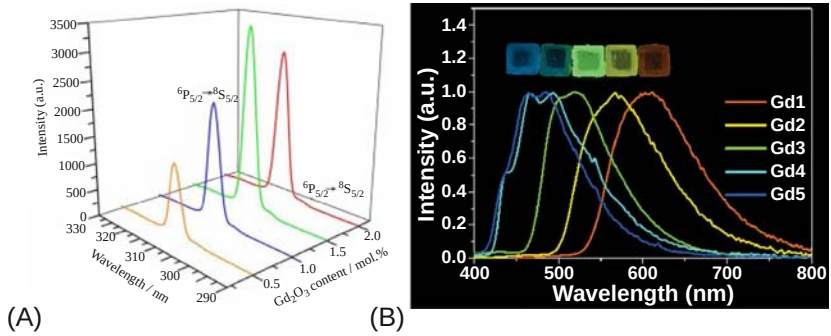

FIG. 18 (A) Luminescence spectra of Gd_2O_3 doped lithium borate glasses. (B) Room temperature phosphorescence of gadolinium complexes. Panel A: *Reproduced from D.D. Ramteke, R.S. Gedam, Luminescence properties of Gd3+ containing glasses for ultra-violet (UV) light, J. Rare Earths 32 (2014) 389–393. https://doi.org/10.1016/S1002-0721(14)60082-X, © 2014 Elsevier B.V;* Panel B*: Reproduced from B. Sun, C. Wei, H. Wei, Z. Cai, H. Liu, Z. Zang, W. Yan, Z. Liu, Z. Bian, C. Huang, Highly efficient roomerature phosphorescence achieved by gadolinium complexes, Dalton Trans. 48 (2019) 14958–14961. https://doi.org/10.1039/c9dt03050f, © 2019 Royal Society of Chemistry*.

the high magnetic moment of Gd^{3+}. However, phosphorescence is usually observed only at low temperatures, and even though the examples of room temperature phosphorescent gadolinium complexes are known, e.g., in [137–139], their phosphorescence efficiency is still low. No special attention was paid to obtaining highly emissive phosphorescent gadolinium complexes yet, except for some rare works [140–143]. For instance, room temperature phosphorescent gadolinium complexes with emission color from blue to orange have been obtained with a maximum photoluminescence quantum yield of 66% and emission lifetimes in the microsecond range [140]. In [142] a quantum yield of 28% was obtained from the gadolinium labeled hematoporphyrin monomethyl ether (Gd-HMME) by the titration of free Gd^{3+}. The effect of the free Gd^{3+} was proved by the sevenfold lifetime increase, which was attributed by the author to the decrease of the nonradiative relaxation efficiency from 2.2×10^5 to $2.8 \times 10^4\ s^{-1}$. Important is that in the absence of free Gd^{3+} the PLQY of Gd-HMME is only equal to 4%.

OLEDs, based on Gd complexes, are not numerous, but a few examples exist [144–146] (see Section 5.2) with emission wavelength in the range 500–650 nm and brightness up to 1350 cd/m^2 (2 cd/A at 100 cd/m^2).

Another exception is the use of divalent lanthanide complexes, mainly of Eu^{2+}. Theoretically, d-f transition Eu^{2+} complexes are prospective for OLEDs due to high exciton utilization efficiency up to 100% and tunable emission as the 5d orbitals are sensitive to the ligand field, not typical for Ln^{3+} ions; besides, since the transitions within Ln^{2+} complexes are allowed, short decay lifetimes are typical for them (ns vs ms for Ln^{3+}) [51]. However, the instability of Eu^{2+} complexes in ambient conditions hampers their EL study: until

recently, the highest EQE obtained for Eu^{2+} complexes reached only 0.01% (maximum luminance 10 cd/m^2) for bis[hydrotris(3,5-dimethylpyrazolyl)-borate]europium(II) [147]. Important to note is that the PLQY of this complex reached 85%, but its low stability resulted in low OLED performance. Recently, another work appeared, reporting OLED based on bis[hydrotris (3-trifluoromethylpyrazolyl)borate]europium(II) (**Eu-1**) and bis[hydrotris (3-methylpyrazolyl)borate]europium(II) (**Eu-2**) [148]. While **Eu-1** did not lead to good OLED performance, **Eu-2** did with the corresponding OLED having a maximum luminance of 30,620 cd/m^2, and a maximum EQE of 6.5% (Fig. 19); this corresponds to an exciton utilization efficiency around 100%, which the authors attributed to the increased air-stability of the complex. Though it is the only example of such a high value, and though high air-stability was demonstrated for **Eu-1**, and not for **Eu-2**, it is a very promising work, which may open a new field of OLED development.

In summary, narrow bandwidth makes lanthanide-based OLEDs basically not suitable for lighting applications with the potential exception of phosphorescent gadolinium complexes and d-f emitting trivalent cerium (Section 5.6.4) and divalent europium complexes.

Unlike lighting, *display applications* demand exactly the opposite: narrow emission bands are required to increase color purity, which is currently one of the most important goals, as demonstrated, i.e., by the efforts, spent by the LG Displays in production of their TVs (Fig. 20B) [149]. The use of Ir compounds and TADF materials with wide emission bands as OLED emitters does not allow to solve it. This is particularly problematic in the case of TADF emitters, as unlike phosphorescent Ir compounds, they exhibit fluorescence, even though delayed, which, corresponding to an allowed transition, is fundamentally broader. Various approaches are explored to increase OLED color purity. To improve the color purity of TADF emitters, two isomeric compounds, (x'-phenoxazin-10-yl)-[1,1′:3′,1″-terphenyl]-2′-carbonitrile, with x' = 2′ (mPTC) and 5′ (oPTC) were synthesized with the same skeleton but different molecular restrictions [150]. With the increased molecular space restriction induced by the phenyl substitutions at meta-position of the cyano group, a much weaker positive solvatochromic effect is observed for mPTC. And the color purity of emission from mPTC (full width at half-maximum—FWHM—of 86 nm) is also somewhat larger with respect to that of oPTC (FWHM of 97 nm) in the devices. The authors claim that these results prove that increased restriction of the molecular structure is a simple and effective method to improve the color purity of the TADF emitters.

Another approach, consisting in inserting nanoscale periodic structures composed of low-refractive-index material in OLEDs, has advantages, such as high efficiency and increased color purity matched with the emission wavelength of the OLED [151]. A microcavity OLED (MOLED) with ITO distributed Bragg reflector (DBR) electrode was proposed [152]. A FWHM of the 6.5-period MOLED as narrow as 7 nm was achieved.

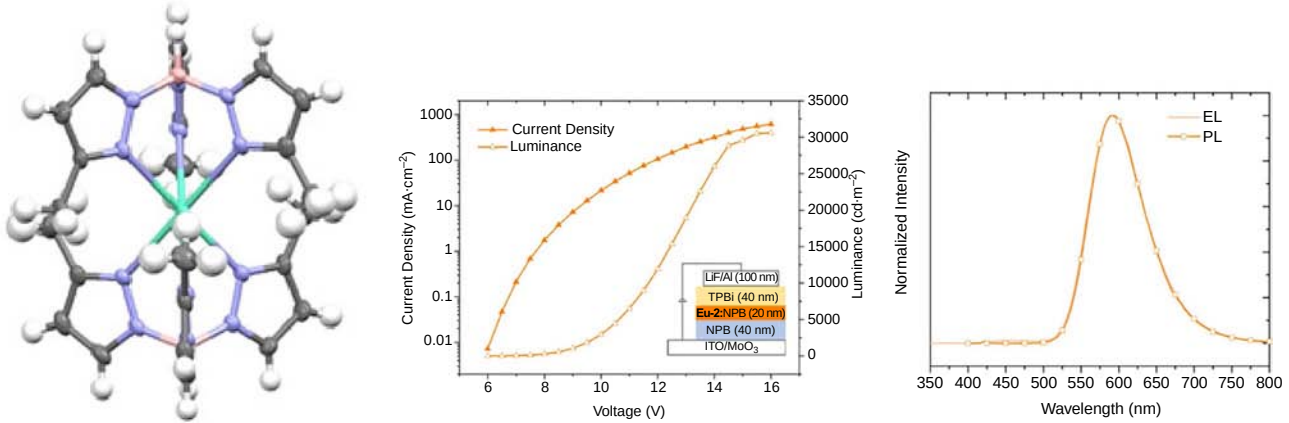

FIG. 19 Molecule in the crystal structure, current-density–voltage–luminance curves of the Eu-2 based OLED, inset: device structure; EL spectrum of the Eu-2 based OLED at a luminance of 10,000 cd/m^2 and the PL spectrum of Eu-2 in dichloromethane (10 − 4 M). *Reproduced with the permission of G. Zhan, L. Wang, Z. Zhao, P. Fang, Z. Bian, Z. Liu, Highly efficient and air-stable lanthanide EuII complex: new emitter in organic light emitting diodes, Angew. Chem. Int. Ed. 59 (2020) 19011–19015. https://doi.org/10.1002/anie.202008423, © 2020 John Wiley & Sons, Inc.*

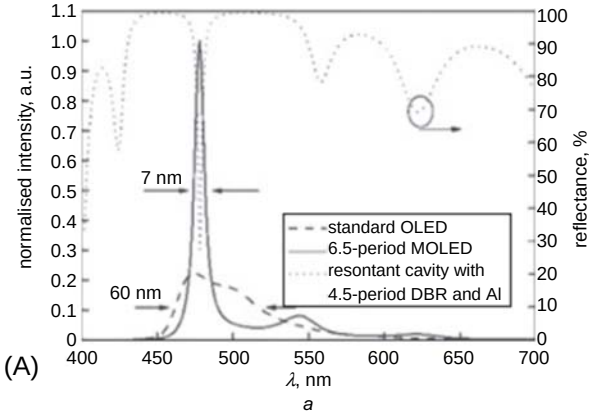

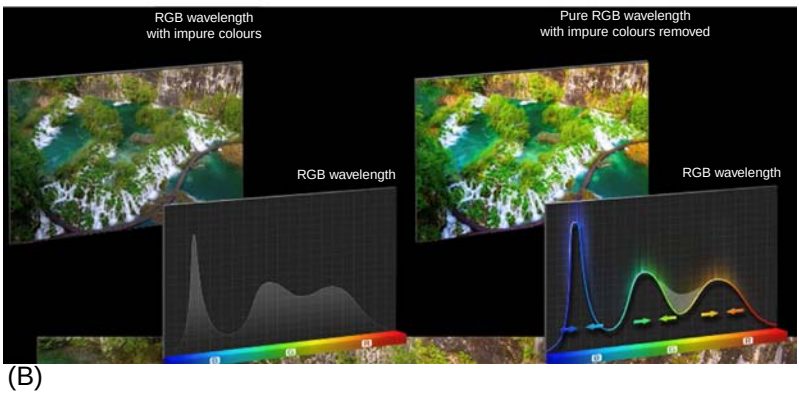

FIG. 20 (A) Luminescence band narrowing by resonant cavity. (B) Increase of color purity with a slight decrease of the band width by LG Nanocell: conventional RGB wavelength with impure colors (display and emission spectrum) vs LG NanoCell TV, where impure colors are removed using nanoparticles that work as color purifiers. Panel A: *Reproduced with permission from W.C. Tien, L.Y. Chen, Y.W. Zeng, K.W. Chang, A.K. Chu, Narrow-band emitting microcavity OLED with ITO DBR electrode for sensing applications, Electron. Lett. 51 (2015) 2034–2035. https://doi.org/10.1049/el.2015.2464, © 2015 The Institution of Engineering and Technology.* Panel B*: Adapted with permission from LG NanoCell, (2021). https://www.lg.com/uk/lgnanocell/color.jsp, © 2009–2021 LG Electronics.*

Careful management of polaron and exciton density inside the EML can also help improving the performances of OLEDs. This has been tested with a platinum complex with 9-(pyridin-2-yl)-2-(9-(pyridin-2-yl)-9*H*-carbazol-2-yloxy)-9*H*-carbazole (PtNON) as "triplet sensitizer" introduced in an alternating donor–acceptor doped emissive layer. The device emission color purity can be improved by carefully managing the efficient Förster resonant energy transfer from PtNON to 2,5,8,11-tetra-tert-butylperylene as a selected acceptor material [153].

These efforts demonstrate the importance of the problem of narrowing the emission bands, though neither of them allows a perfect solution. Unlike in the presented examples, the "wideband" disadvantage can be easily avoided by using lanthanide complexes. Due to the screening of f-orbitals, the geometry of the excited state does not practically differ from the geometry of the ground state, which leads to narrow emission bands (<10 nm), which in turn allows achieving high contrast values in OLED displays.

Narrow bandwidth is particularly important for *detection applications*. So, high bandwidth is a crucial drawback for modern pulse-oximetry. The spectral linewidth of OLED EL is relatively large, often larger than 60 nm, making it difficult to be used as an excitation light source because the mixing of the EL of OLED with PL of sensing films cannot be completely eliminated even when a longpass optical filter is used. For the design of a compact and efficient sensor, optical filters should be totally excluded; therefore, alternative OLEDs with preferred EL spectra are necessary for increasing the absorption of the sensing films and reducing EL contribution to the measured signals.

Sharp and well-defined emission bands of lanthanides, long considered ideal for chemical sensing [154–156], inherit their benefits as ideal electroluminescence source for detection.

4.5 Band position

With the exceptions of Ce^{3+} and divalent lanthanide complexes, as well as complexes exhibiting ligand-centered emission, lanthanide complexes are characterized by almost constant emission bands. Indeed, due to the screening of f-orbitals from the external field of the ligands, the energy of the lanthanide SLJ levels is hardly affected by the crystal field; therefore, each ion has its own constant characteristic set of luminescence bands. In the visible range, Eu^{3+} and Tb^{3+} ions emit most efficiently in the red (maximum ~612 nm, transition $^5D_0 \rightarrow {}^7F_2$) and green (maximum ~545 nm, transition $^5D_4 \rightarrow {}^7F_5$), respectively; in the NIR range, ytterbium emits at ~977 nm (transition $^2F_{7/2} \rightarrow {}^2F_{5/2}$).

The impossibility of band shifting is usually considered as a drawback of lanthanide luminescence, unlike other classes of emitters, where fine tuning of the emission wavelength is easy.

Nonetheless, for practical applications, these wavelengths fit very well the needs of some applications. So, for *display applications*, the set of basic colors required, called a gamut, can cover as many colors, detected by the human eye, as possible. As a quantitative link between distributions of wavelengths in the electromagnetic visible spectrum and physiologically perceived colors in human color vision, the CIE 1931 color space was defined, where CIE corresponds to the "Commission internationale de l'éclairage," known in English as the International Commission on Illumination, by which the system was designed.

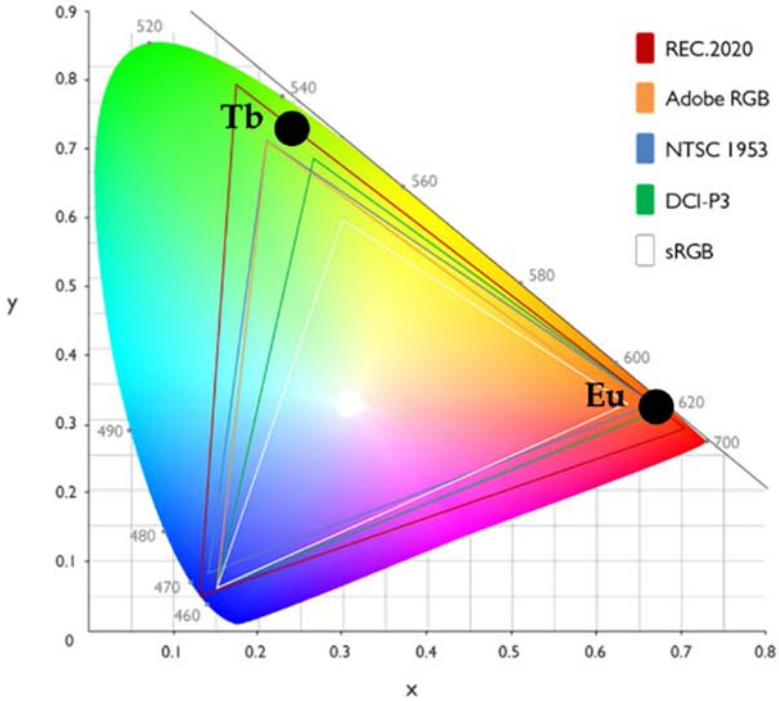

FIG. 21 CIE diagram, representing color gamuts utilized in various displays, as well as the CIE coordinates of Tb^{3+} and Eu^{3+} luminescence.

This diagram represents all of the chromaticities visible to the average person (Fig. 21). These are shown in color and this region is called the gamut of human vision. The curved edge of the gamut is called the spectral locus and corresponds to monochromatic light (each point representing a pure hue of a single wavelength), with wavelengths listed in nanometers. The straight edge on the lower part of the gamut is called the line of purples. These colors, although they are on the border of the gamut, have no counterpart in monochromatic light. Less saturated colors appear in the interior of the diagram with white at the center.

It can be seen that the whole gamut of human vision can be covered with three monochromatic sources. Production of a display aims at the creation of the best possible gamut, which covers as much of the CIE diagram as possible. Various gamut standards are represented in Fig. 21, together with the CIE coordinates of Eu^{3+} and Tb^{3+} luminescence.

It can be seen that the Eu^{3+} luminescence corresponds to the so-called "ideal red color," which, together with its narrow bandwidth, makes Eu^{3+}-based OLEDs ideal for display application from the color point of view. Tb^{3+}

luminescence does not exactly match the top of the CIE diagram, however, it coincides with one of the points of modern gamut triangles, making its luminescence also suitable for display applications.

Lanthanide luminescence wavelengths match *sensing applications* requirements as well. As shown before, for pulse-oximetry, typically selected wavelengths for excitation/detection usually do not correspond to the most effective ones, i.e., to those for which the difference in Hb and HbO2 absorption is the largest. Careful evaluation of the full plot of the absorptivity of oxygenated (orange solid line) and deoxygenated (blue dashed line) hemoglobin in arterial blood (Fig. 22) demonstrates that the optimal wavelengths correspond to ca. 600 and 1000 nm, which matches the maximum of europium and ytterbium luminescence, respectively.

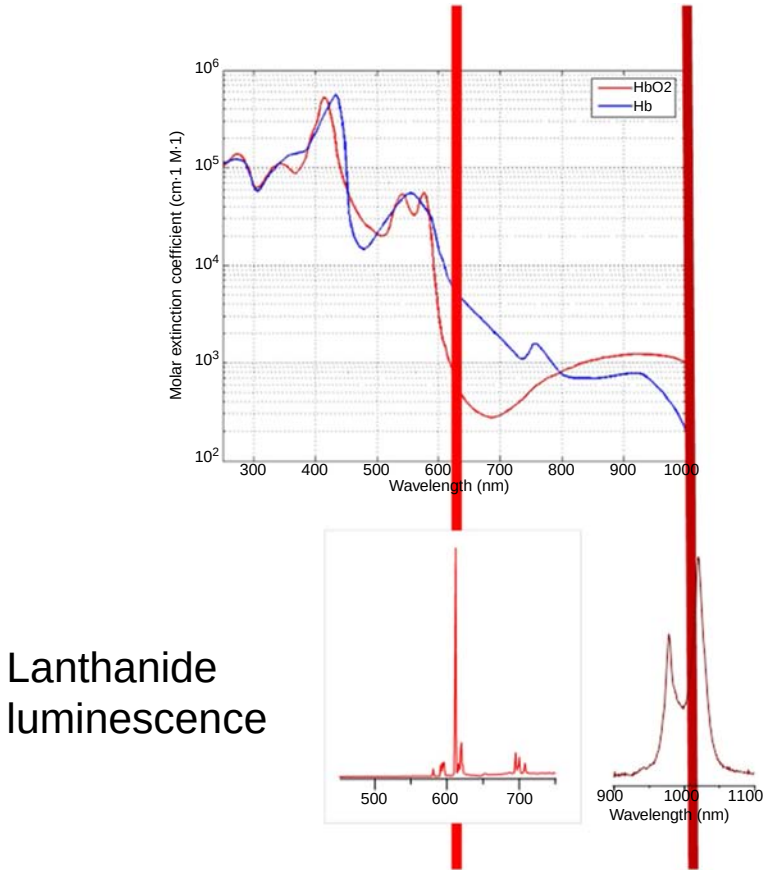

FIG. 22 Absorptivity of HbO2 (red line) and Hb (blue line) with the spectra of Eu^{3+} and Yb^{3+} luminescence plotted below.

4.6 Concentration quenching and host selection

Concentration quenching is an important issue in the discussion of OLED production, since its presence in the case of organic and metal-organic compounds rather not limits their applications but opens new horizons. Indeed, emission layers in classical OLEDs are made of composite films, which consist of the emitter material doped into the host material to avoid concentration quenching. The host material must be selected to ensure efficient energy transfer to the emitter material, i.e., its excited state energy must be higher than that of the emitter. Moreover, it should be kept in mind that the current flow occurs primarily through the host materials boundary orbitals, and not those of the emitter, doped at a small concentration (typically 5% w/w) [10,11,157].

The role of the host material is primarily in avoiding concentration quenching, thus increasing the overall emission layer quantum yield; however, its design can answer other demands as well, among which is the possibility to tune the charge carrier mobility of the composite emission layer by manipulating both host and emitter.

The selection process of the host materials itself differs for the lanthanides from the one for other emissive compounds; despite this, it is almost never discussed in scientific papers. The reason is the large ligand-induced Stokes shift of lanthanide complexes, which results in the necessity of using very wide-bandgap hosts. Moreover, unlike low-energy ligands for NIR luminescence sensitization, ligands efficiently sensitizing europium and terbium possess so high excited state energy, that sometimes the selection of the host for such a system is complicated or just impossible. Indeed, the excited state energy of the host must exceed the one of the ligand to ensure efficient energy transfer, as the direct energy transfer to the emitting center—lanthanide ion—is usually impossible due to the large distance between Ln ions and the host, resulting from the presence of bulky organic ligands in the lanthanide coordination environment.

The host selection for terbium complexes is very difficult due to its high excited state energy, which results in the high-energy ligand excited states, needed for efficient sensitization (Fig. 23). So, host selection for non-volatile terbium *o*-phenoxybenzoate with its PLQY($Tb(pobz)_3$) = 96% literally failed due to the high ligand excited state energy [131]. As a pure host-free layer it demonstrated a switch-on voltage of 18 V due to the low charge carrier mobility. To increase it, the well-known host TPD (*N*,*N*′-bis(3-methylphenyl)-*N*,*N*′-diphenylbenzidine) was used together with wide-bandgap host UGH-2 (1,4-bis(triphenylsilyl)benzene), as well as triphenylphosphine oxide (TPPO), which was also expected to increase charge mobility. While the latter two turned out to be unsuitable for solution deposition, electroluminescence was only recorded for OLEDs with TPD host; however, the band of TPD dominated in the EL spectra. PL studies revealed that expectedly when excited into the

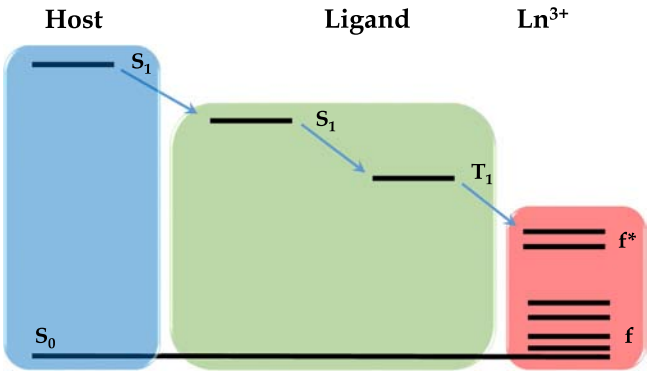

FIG. 23 Scheme of the host-emitter energy transfer for Ln CCs as emitters.

TPD absorption band, the composite film demonstrated almost only TPD luminescence. CBP (4,4′-bis(*N*-carbazolyl)-1,1′-biphenyl) was also used as a host for terbium luminescence, but the analysis of the absorption spectrum of the {tris(acetylacetonate) [1,2,5]thiadiazolo [3,4-f][1,10]phenanthroline}terbium (III) ($Tb(acac)_3TDZP$) complex clearly demonstrated no overlap with the emission spectrum of CBP, which is a strict requirement for efficient Förster energy transfer [158]. This resulted in low efficiency and high switch-on voltage (10 V). This shows that host selection is a yet-to-solve challenge for terbium complexes.

The selection of the host for Eu-based emitters is easier, as its lower-energy excited state (17,200 vs 20,400 cm^{-1} for terbium) results in typically lower excited state energies of sensitizing ligands, and thus hosts can be selected among well-known ones, which are able to transfer energy to the ligands. Usually, these are, however, rather wide-bandgap hosts, such as PVK and CBP, and even for europium complexes, the possibility of such an energy transfer should be studied prior to the use of the host, which is not always the case. So, in [159] novel volatile europium pyrazolates were used within the CBP host, and no overlap of complex absorption and CBP was again observed.

Even the use of the properly selected host, ensuring energy transfer to the emitting complex, is complicated due to the much less pronounced concentration quenching. This results in a different effect of host molecules within the emission layer based on lanthanide complexes as emitters. Unlike typical emitters of other classes, lanthanide complexes with high PLQYs suffer from the doping into the host (Fig. 24): so, europium mixed-ligand complexes with bathophenanthroline demonstrated the highest quantum yields in the form of pure, host-free films, while doping into the typical hosts resulted in a significant PLQY decrease, at least twofold for those with the highest PLQYs (ca. 90%). However, and most importantly, the OLED efficiency still increased by the use of the host due to the increased charge mobility.

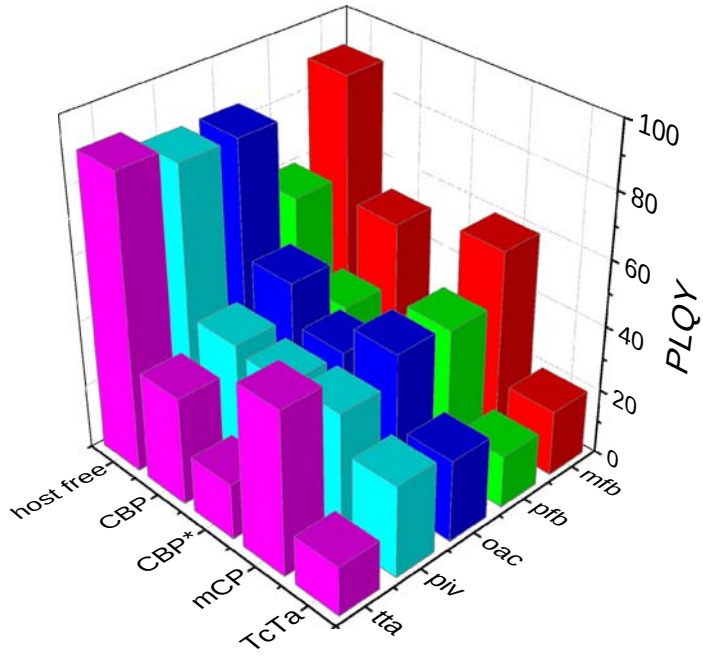

FIG. 24 PLQYs of several europium complexes, doped into typical hosts and as pure films.

Therefore, based on the high excited state energy and insignificant concentration quenching, it is preferable to design terbium and europium complexes that can be utilized without a host. It is important to stress out that neither of these problems applies to ytterbium compounds. Even though the use of the host increases the already large ligand-induced Stokes shift, which results in a decrease in energy efficiency, its selection is not complicated, and its use is usually not harmful.

4.7 Charge carrier mobility

The charge carrier mobility (μ) can be considered as the speed ($cm\,s^{-1}$) at which the charge carriers move in the material in a given direction and under a given applied electric field ($V\,cm^{-1}$). Increasing charge carrier mobility and the balance of the mobility of charges of different signs are two of the problems which can be most easily solved using a host material. Indeed, CBP, for example, known as a bipolar host [160], ensures the transport of both charges through the emitter film. This results in the preferable charge recombination in the volume rather than on the interlayer boundary.

Inexpediency, or even impossibility, of host exploitation in the most important cases of Eu- and Tb-based emitters rises another, not previously seen, question of the charge carrier mobility increase within the pure emitter

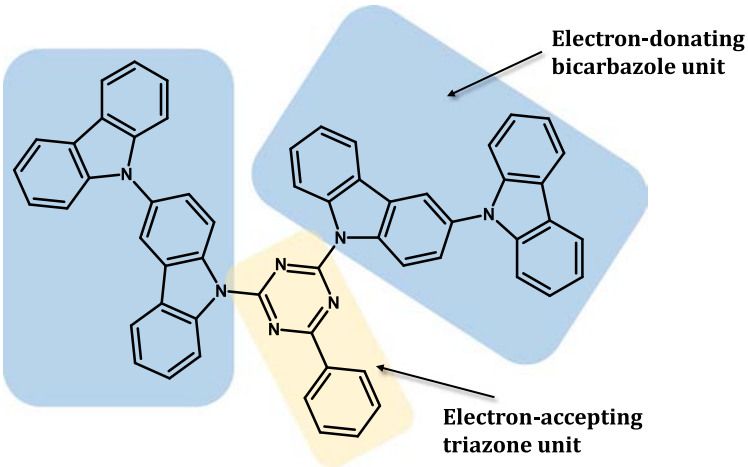

FIG. 25 An example of an organic TADF emitting molecule.

layer. The novelty of this question is connected not only to the possibility to use hosts for emitters of other classes. So, TADF emitters inevitably demonstrate perceptible mobility of both electrons and holes: to ensure HOMO and LUMO separation and, thus, small bandgap, they must contain electron-donating and electron-accepting groups (Fig. 25) [161–163]. For lanthanide complexes, providing charge mobility is a separate task, which can easily contradict the search for efficient luminescence.

Charge carrier mobility is a characteristics of the materials and strongly depends on the molecular packing, microstructure of the OLED, etc. Nonetheless, as the process of charge carrier includes charge acceptance prior to its transport to the neighboring species, the predominant requirement for inducing charge carrier mobility is the presence of electron-donating or electron-accepting fragments in the design of the hole and electron transport layers, respectively. The presence of an electron-donating group within the ligand coordinated by the europium ion, may readily result in the formation of ligand-to-metal charge transfer (LMCT) states [164], which usually act as quenchers, and thus the mobility is increased at the cost of PLQY.

Another, positive, point is that the features of lanthanide chemistry result, in particular, in high coordination numbers, which allow lanthanide ions to coordinate neutral ligands in addition to the anionic ones. The different nature of these ligands (charged or neutral) results in an the ease of the combination of electron-accepting and electron-donating ligands within one complex molecule.

The design of europium complexes, able to ensure charge carrier mobility, is perfectly discussed in a review [165] on the example of europium tris-β-diketonates with phenanthroline derivatives. It demonstrates that the hole mobility is most effectively increased by the gradual introduction of carbazole

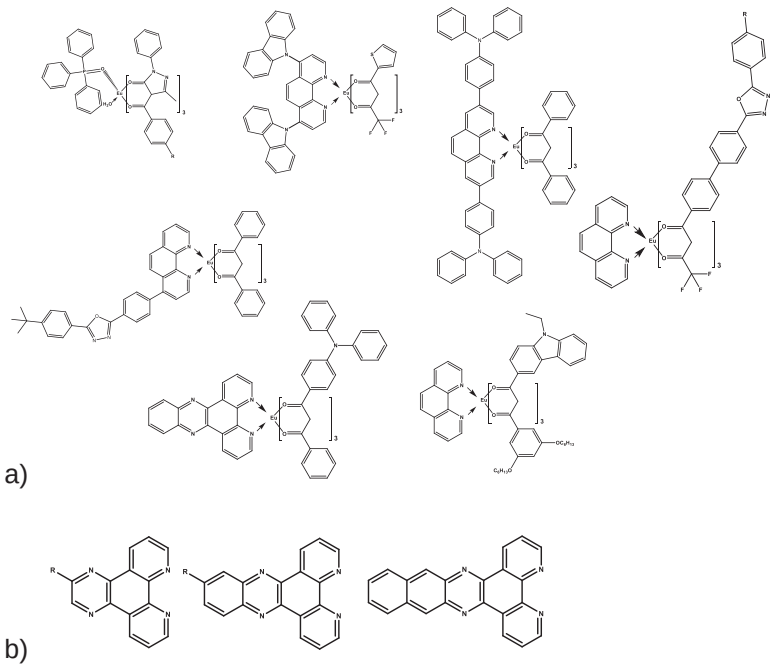

FIG. 26 (A) Europium ternary complexes and (B) neutral ligands with a design aimed at increasing the electron and hole mobility.

substituents, both in anionic ligands and neutral phenanthroline-based ligands; the triphenylamino group is also a prospective substituent for neutral ligands. As for electron affinity, the oxadiazole fragment proved itself to effectively increase electron mobility. Another approach was found in the extension of the aromatic chain by using the neutral ligands depicted in Fig. 26.

Similar approaches were utilized to increase charge carrier mobility of other types of europium complexes. For instance, heteroaromatic carboxylates were used as both sensitizers of europium luminescence and electron-accepting ligands, increasing electron mobility [166,167]. As a result, a solution-processed OLED with structure ITO/PEDOT-PSS/poly-TPD/**[Eu(btz)$_3$phen]**/TPBi/LiF/Al (btz = benzothiazole-2-carboxylate) featured pure metal-centered europium electroluminescence and rather low switch-on voltage (4 V). Important is that lanthanide aromatic carboxylates, usually suffering from low solubility, were readily solution-deposited in this work due to the heteroatom introduction which increased the solubility. Interestingly, an attempt to further increase the electron mobility by further extending the conjugation in the ligand failed. The triplet state energy decreased, leading to loss of the sensitization efficiency. As a result, poorly emitting complexes with quantum yields 0.25–5.4% were obtained with low EL intensity.

As a universal approach to better electron mobility in europium complexes, one can consider the use of bathophenanthroline (Bphen) as a neutral ligand. Indeed, as an individual compound, Bphen has high electron mobility (3.22×10^{-4} cm^2 V^{-1} s^{-1}), while numerous examples of highly emissive europium complexes with Bphen witness that it is an efficient sensitizer of europium luminescence [168–171], even if the anionic ligand, like pivaloate, does not participate in the luminescence sensitization. In an example [172] Bphen was used as a host for europium tetrafluorobenzoate, which did not demonstrate EL as a pure film. Doping into Bphen (1:1 up to 1:20) resulted in the prompt increase of the EL intensity.

In another work [133], a series of europium fluorobenzoates with phen and Bphen was synthesized for OLED applications, and [Eu(fb)$_3$(Bphen)] (fb = various fluorobenzoates) demonstrated pure europium electroluminescence with brightness up to 25 cd/m^2, which is high for solution-processed carboxylates. Important is that the highest PLQY among europium complexes (90%) was obtained in that work, but this was reached for phen-derivatives, while Bphen-containing complexes, though also highly emissive, only reached PLQY = 70%. At the same time, [Eu(fb)$_3$(phen)] demonstrated very poor EL intensity, which clearly indicates the importance of the electronic properties of Bphen-derivatives, i.e., electron mobility.

Mixed-ligand europium pentafluorobenzoates with Bphen and Pyphen were designed to combine high PLQY and large charge mobility [173]. The former was successfully tested in OLEDs. Charge carrier mobilities were directly measured for this complex by the photo-CELIV method, and electron mobility indeed was rather high (3.33×10^{-5} cm^2 V^{-1} s^{-1}); hole mobility was an order of magnitude lower (1.87×10^{-6} cm^2 V^{-1} s^{-1}). Important is that electron mobility of the complex was ten times lower compared to pure Bphen (3.22×10^{-4} cm^2 V^{-1} s^{-1}) [174]. This demonstrates that though the superior performance of Bphen ensures the increase of electron mobility of the Bphen-containing complex, it is not up to the same value, and emphasizes the importance of the direct measurements of charge mobility.

Host selection for ytterbium complexes is possible, however, the use of host results in the decrease of the energy efficiency of OLED. Therefore in several papers, attempts were made to design ytterbium complexes able to be used in OLEDs without transport hosts. In [175] an ytterbium complex, [Yb(L^2)(HL^2)] (H$_2$L^2 = 2-(tosylamino)-benzilidene-*N*-(pyridiloyl)hydrazone), featured EL efficiency of 50 μW/W, which is the highest value for solution-processed Yb-based OLEDs. Another example of Yb-based host-free OLEDs with an anionic ligand, ensuring charge carrier mobility, refers to ytterbium 9-anthracenate [128], which reached EQE = 0.21% in a solution-processed OLED. It is noteworthy that only pure metal-centered luminescence was observed, proving a well-balanced OLED structure together with high energy transfer efficiency from 9-anthracenate anion to ytterbium. In the same work a gadolinium phosphorescent complex was also successfully tested in OLED.

Other host-free OLEDs were obtained with ytterbium complexes containing an electron-accepting neutral ligand [173]. EL efficiency of 30 μW/W was reached for pure metal-centered ytterbium electroluminescence.

As already mentioned, it is particularly important to ensure charge mobility within terbium complexes, since host selection for these systems is highly challenging. So, TcTa was used as a host for the complex [$Tb(pmip)_3$], which resulted in high OLED efficiency, up to 1694 cd/m^2 [176]. This is, however, lower, than 12,000 cd/m^2, obtained by the same authors with the same [$Tb(pmip)_3$] complex, but inserted into TPPO as a host [177], which clearly served as a ligand.

An unprecedently high efficiency of a terbium-based OLED was obtained with an optimized device reaching a maximum efficiency of 52 lm/W, 57 cd/A, and EQE of 15% [178]. Host-free OLED containing Tb^{3+} complexes with neutral ligands were utilized. It is clear that they ensure both hole and electron mobility. It is noteworthy that this complex demonstrates moderate quantum yield: although PL data are not reported in [178], in the previous paper of the same authors investigating the same complexes [179] their PLQY only reaches 16.7%. Particularly interesting is that all the record terbium electroluminescence efficiencies [176–179] were obtained for $Tb(pmip)_3$-based compounds, which makes to consider the nature of this anionic ligand primarily to other factors.

To increase the electron mobility in the emitting layer containing a terbium complex, an approach using the coordinating host was implemented [130]. A series of phosphine oxides (POs) was investigated as hosts, and their ability to be coordinated by the central ion, as well as to sensitize its luminescence, was demonstrated. The coordination of the ligand makes it reasonable to refer to the emission layers as to [TbL_3(PO)]:PO, rather than just [TbL_3:PO] (L = Cl^- or *o*-phenoxybenzoate in the present paper). The PLQY of PO-containing terbium chlorides reached 70%, which proves efficient energy transfer from PO to the terbium ion. Interestingly, despite that the exciton is formed on the host molecule, the role of the anionic ligand remains important: the efficiency of the OLEDs based on [$TbCl_3$(PO)]:PO was lower, than the efficiency of those based on [$Tb(pobz)_3$(PO)]:PO, the PLQY of which is about 100%. The most efficient neutral ligand was PO4, represented in Fig. 27

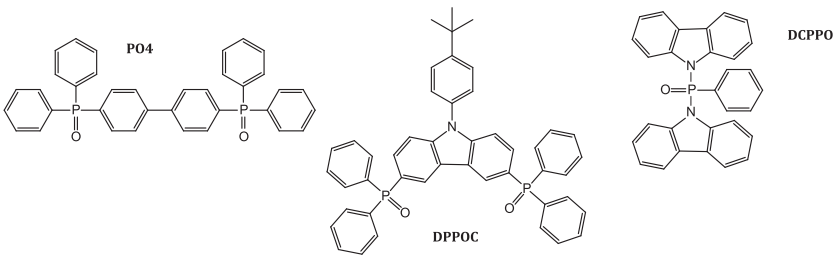

FIG. 27 PO4, DCPPO, and DPPOC ligands, able to sensitize terbium luminescence and ensure electron mobility.

together with two other ligands effectively combining the ability to sensitize terbium luminescence and ensure electron mobility, i.e., DCPPO and DPPOC [178].

4.8 Lifetime

Another issue affecting the OLED performance is the excited state lifetime. The correlation between the PLQY and the lifetime does not usually allow to consider it separately: the decrease of the lifetime is often associated with the presence of quenching processes, which inevitably result in the simultaneous decrease of the PLQY. However, some works in the field of OLEDs based on iridium consider separately the role of the lifetime [180,181], i.e., the shorter the lifetime is, the better is the OLED performance. The reason for that is the mechanistic difference between electroluminescence and photoluminescence.

Generally, the longer the lifetime of the excited state, the higher the exciton density. This usually allows considering that long lifetimes increase the probability of roll-off processes, decreasing the efficiency of the OLED. These problematics is discussed in ref. [180], in which the following mechanisms are considered:

(1) *Triplet–Triplet Annihilation (TTA)*, which is an energy transfer mechanism between two molecules in their triplet state. This mechanism is mostly relevant to the roll-off efficiency in phosphorescent OLEDs and it was suggested that the observed decrease in EQE at high currents is caused by a bimolecular quenching process [181].

(2) *Singlet–Singlet Annihilation (SSA)*, which is a bimolecular annihilation process between two excited singlet states. This process can contribute to experimentally observed roll-offs, especially for fluorescent OLEDs. SSA was first observed in anthracene crystals [182].

(3) *Singlet–Triplet Annihilation (STA)*, a bimolecular annihilation process that occurs when singlet and triplet excited states interact. STA is negligible in phosphorescent OLEDs, as singlets undergo rapid ISC to a triplet state, but was detected for fluorescent materials.

(4) *Exciton–Polaron Interaction (EPI)*, which, in contrast to the previous interactions, corresponds to the annihilation of excitons by charge carriers, or polarons.

(5) *Field-Induced Quenching*, which is a reduction in photoluminescence intensity when a high voltage is applied to electrodes surrounding the film. Field-induced quenching is also documented in OLEDs [183].

Despite they have never been deeply investigated, these mechanisms are hardly applicable to lanthanide complexes as emitters: indeed, both singlet and triplet excited states undergo rapid relaxation to lanthanide excited states, and lanthanide-centered excitons are well separated from each other being surrounded by bulky organic ligands. At the same time, there is another

simple reason for the lifetime influence on the OLED performance. Indeed, if the excited state is very long, exciton relaxation is slow, and the number of molecules in the ground state may be insufficient to ensure the formation of new excitons as a result of the electron-hole recombination. Orders of magnitude higher lifetime of the lanthanide excited states may result in their generally inferior performance as OLED emitters. Indeed, despite a report stating that europium complexes have low efficiency due to TTA at high current, caused by the long lifetime of the Eu^{3+} excited state (350 μs) [184], in the original paper the authors specify that TTA occurred between the CBP molecules, used as a host, and not between the europium complex molecules themselves [160].

Despite direct evidence of the roll-off mechanism in Ln complexes has yet to be obtained, existing data favor the simple "rare exciton formation" mechanism. Indeed, regardless of the efficiency of this mechanism and TTA increase with the increase of the lifetime, they should be differently affected by the concentration of the complex in the film: TTA decreases as the complex concentration decreases, because the intramolecular distance increases. At the same time, the lower the concentration is, the fewer molecules, able to be excited, remain in the film, and so if the "rare excitons formation" mechanism is dominating, complex concentration decrease should rather decrease the efficiency. In ref. [130], PO4 films (Fig. 26) doped with terbium phenoxybenzoate, $[Tb(pobz)_3]$:xPO4, were studied, for which the PLQY value reached 100% independently of x. Despite charge mobility could not be increased with a decrease in x, the best OLED performance was achieved for the lowest $x = 1$, which corresponded to the highest emitter fraction. Similarly, in [172], the best performance of OLEDs with $[Eu(tfb)_3]$:xBphen films ($tfb^- =$ tetrafluorobenzoate) was achieved for the lowest $x = 2$, corresponding to the pure mixed-ligand complex $[Eu(tfb)_3(Bphen)_2]$.

The limiting role of the lifetime, without the discussion of the exact mechanism, is widely witnessed in the literature. For instance, the introduction of a neutral ligand, 4,5,9,14-tetraazabenzotriphenylene (DPPZ), in a europium triphenylamine-derivatized β-diketonate resulted in a very short lifetime of 30 μs, which led to the OLED maximum luminance increasing to 2910 cd/m^2 [185]. The authors attributed this to the decrease of the roll-off processes, not specifying the mechanism. The DPPZ ligand ensures high OLED brightness (1000–3000 cd/m^2) in a number of cases [185–187], which follows, however, not only from its electronic properties but also from its non-sensitization due to its low-energy triplet state 18,500 cm^{-1}; in fact, this ligand **quenches** europium luminescence by favoring back-energy transfer [173] as exemplified by the PLQY of $[Eu(tta)_3(DPPZ)]$, which is only equal to 5%, and its lifetime is short, 80 μs. The comparison between $[Eu(dbm)_3phen]$ [188] and $[Eu(dbm)_3DPPZ]$ [187] demonstrates that the substitution of the sensitizing phen ligand with the quenching DPPZ increases the OLED maximum luminance from 460 to 2910 cd/m^2, despite the quantum yield decreasing from

81% down to <1%. This stops being contradictory taking in mind the simultaneous drop of the lifetime (from 130 to 30 μs).

The importance of the lifetime is confirmed by the comparison between complexes of terbium and europium. So, despite the quantum yields of ~100% can be reached [115,130,132] for terbium complexes, Tb-based OLEDs are much less numerous, and their brightnesses are much less than those of Eu-based OLEDs. This cannot be understood, since the maximum of the human eye sensitivity (~550 nm) matches exactly the terbium emission maximum, unlike the europium emission, if not the lifetime explanation. So, [Ln(DPM)$_3$]-based OLEDs (Ln = Eu, Tb), the emission layers of which differ only in PL characteristics, demonstrated remarkably different performance: [Eu(DPM)$_3$] reaches an EL brightness of 2123 cd/m^2, while electroluminescence of [Tb(DPM)$_3$] is hardly detectable despite its reasonably high PLQY = 33%. The only possible explanation for that is the ~10-fold difference in lifetimes (49 vs 440 μs). Furthermore, one of the brightest Tb-based OLEDs is based on [Tb(tpa)$_3$] [189]; its PLQY is dramatically small, <1%, but its lifetime is very short (80 μs), which explains its large luminance.

The long lifetime issue also explains the low stability of the lanthanide-based OLEDs: if the current flows through the diodes not forming the excitons, it results in degradation.

To conclude, despite the exact mechanism of the roll-off in lanthanide complexes is still unclear, it is undoubtedly evident that their long lifetimes result in a significant decrease in their EL performance. Thus, efforts should be devoted to decreasing the lifetime while maintaining a reasonable quantum yield. Important is that ytterbium complexes have significantly shorter lifetimes, with typical values within the 10–50 μs range [88,190,191], which is 1–2 orders of magnitude lower compared to europium and terbium complexes. As a result, ytterbium is the only lanthanide whose electroluminescence can compete in efficiency with other classes of EL compounds, and in the 1000 nm range, the highest NIR OLED efficiencies were obtained from ytterbium complexes [128,175,192].

5 Examples

In the present section, a few examples are described to illustrate the discussions presented in Section 4. The most studied complexes of lanthanides are β-diketonates and related acylpyrazolates, which is usually explained by their volatility. However, their short lifetimes related to ligand polarizability may be a better explanation. Among the most studied neutral ligands are various phenanthroline derivatives and arylphosphine oxide derivatives.

5.1 Europium: Red emission

The typical brightness of OLEDs based on europium CCs (Fig. 28) deposited from the gas phase varies in the range of 400–1500 cd/m^2, and the EQE efficiency reaches 1–3% [165]. Diodes based on mixed-ligand complexes of

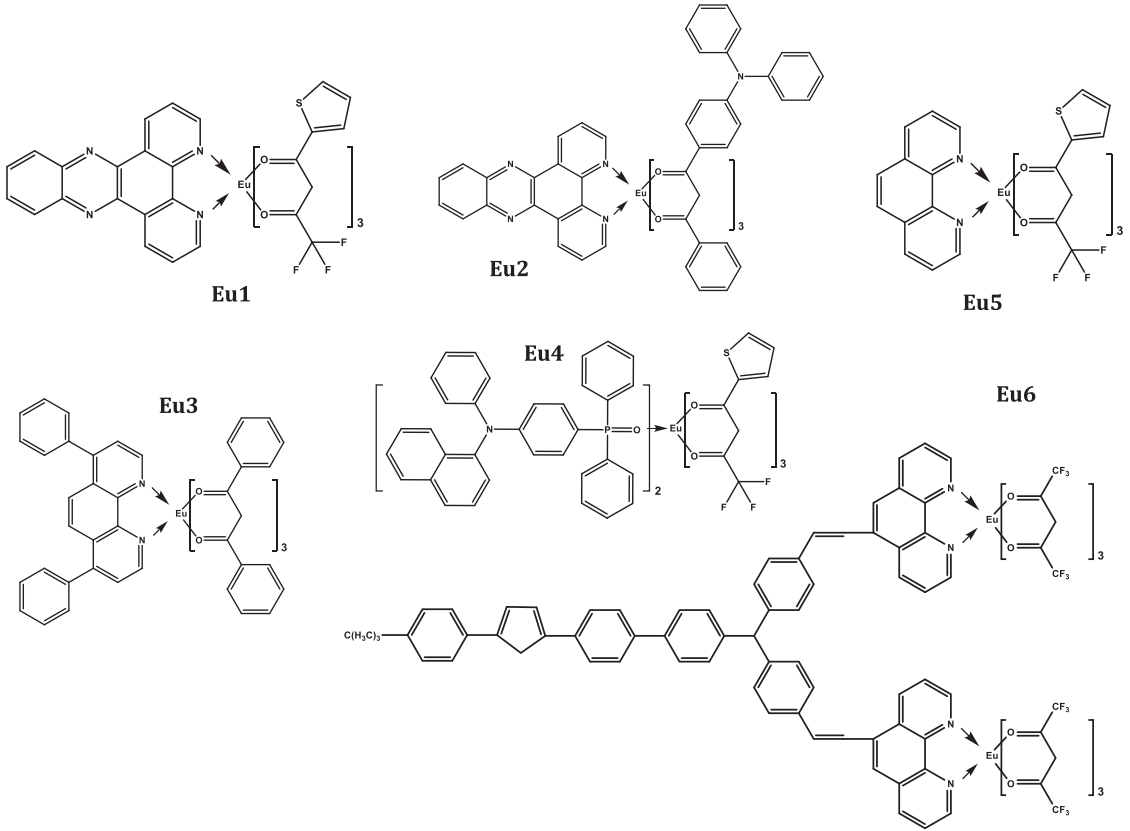

FIG. 28 Europium complexes *Eu1*: [Eu(tta)$_3$(DPPZ)]; *Eu2*: [Eu(dpdbm)$_3$(DPPZ)]; *Eu3*: [Eu(dbm)$_3$(Bphen)]; *Eu4*: [Eu(tta)$_3$(NaDAPO)$_2$]; *Eu5*: [Eu(tta)$_3$(phen)]; *Eu6*: [Eu$_2$(tta)$_6$(BuOXDTPA-phen)$_2$]; *Eu7*: [Eu(dbm)$_3$(BuOXD-phen)].

europium with the phenanthroline derivative DPPZ, namely [Eu(tta)$_3$(DPPZ)] [186] and [Eu(dpdbm)$_3$(DPPZ)] [185], have high brightness exceeding 2000 cd/m^2. The OLED based on [Eu(dbm)$_3$(Bphen)] has the maximum efficiency, known today, EQE = 7.8%; however, it should be noted that such a value was obtained at minimum currents of ~0.02 mA/cm^2, and that with further increase in voltage, the efficiency decreases: at a brightness of 100 cd/m^2, EQE drops down to 4.9% [193]. Among europium complexes, where a triphenylphosphine oxide derivative is used as a neutral ligand, the OLED based on [Eu(tta)$_3$(NaDAPO)$_2$] serving directly as emitting layer has interesting characteristics with a luminance of 59 cd/m^2 at 18.2 V [194].

Diodes in which the emission layer is deposited from a solution usually demonstrate lower brightness (1–300 cd/m^2), and the efficiency of such diodes is extremely low, so their values are usually not even published (Table 7). Among OLEDs based on europium CCs, obtained using solution technology, the OLED featuring [Eu(dbm)$_3$(BuOXD-phen)] as emitting layer has a record brightness of 568 cd/m^2 [206], while the OLED with [Eu(dpdbm)$_3$(DPPZ)] as emissive layer deposited by VTE reaches 2910 cd/m^2.

5.2 Terbium: Green emission

The brightness of terbium-based OLEDs is usually much lower than that of europium-based ones; however, some notable exceptions exist, which feature extremely high brightnesses. Efficient electroluminescence is exhibited, for example, by the mixed-ligand complex [Tb(acac)$_3$(TDZP)] [213], containing the electron-depleted phenanthroline derivative [1,2,5]thiadiazole[3,4-f] [1,10]phenanthroline (TDZP) leading to a diode brightness of 1673 cd/m^2. Even better, the diode based on [Tb(pmip)$_3$(DPPOC)] [179], which contains both electron-depleted and electron-rich fragments, has a record brightness of 3823 cd/m^2, as well as a high efficiency EQE = 2.6% (Fig. 29). Optimization of the OLED heterostructure and the simultaneous use of two complexes [Tb(pmip)$_3$(DPPOC)] and [Tb(pmip)$_3$(DCPPO)] made it possible to achieve the record efficiency values PE = 52 lm/W, CE = 57 cd/A, EQE = 14.8% [178] (Table 8).

With the transition to solution technology, again, the typical values of brightness and efficiency of OLEDs are reduced by orders of magnitude. So, for example, diodes obtained by the spin-coating method based on the non-volatile carboxylates [Tb(pobz)$_3$(PO)], [Tb(o-mba)$_3$(phen)] and [Tb(dpab)$_3$], exhibit maximum brightnesses of only 75, 180, and 230 cd/m^2, respectively [130,189,216]. However, in 2019, an article was published [215], in which the authors created a solution-based OLED with [Tb(pfap)$_3$(TDZP)] having a record high brightness of 6365 cd/m^2 and efficiency EQE = 7.15%, which is brighter than all known diodes, including those made by vacuum thermal evaporation. This suggests that the solution method is promising, but so far this is the only example of an efficient OLED deposited from the solution.

TABLE 7 Characteristics of some OLEDs based on europium CCs.

Emitter	Deposition method	Diode heterostructure	L_{max}, cd/m^2	References
Eu1	VTE	ITO/NPB/CBP:**Eu1**/BCP/Alq3/Mg:Ag	2046	[186]
Eu2	VTE	ITO/m-MTDATA/NPB/CBP:**Eu2**/Bphen/Alq3/LiF/Al	2910	[185]
Eu3	VTE	ITO/TPD/TPD:**Eu3**/**Eu3**/TAZ/LiF/Al	1000	[193]
Eu4	VTE	ITO/NPB/**Eu4**/BCP/Alq_3/Mg:Ag	1158	[194]
Eu5	Spin-coating	ITO/PVK:PBD:**Eu5**/Ca/Al	30	[195]
$Eu(tta)_3$	VTE	ITO/PMPS:**Eu1**/PBD/Mg:Ag	0.1	[7]
$Eu(tta)_3$phen	VTE	ITO/TPD/**Eu2**:CBP(1%)/BCP/Alq3/Mg:Ag	505	[196]
	Spin-coating	ITO/PVK:PBD:**Eu2**/Ca/Al	30	[195]
$Eu(tta)_3$SFXPO	Spin-coating	ITO/PEDOT:PSS/PVK/CBP:PBD:**Eu24**/TPBi/LiF/Al	620	[197]
$Eu(nta)_3$SFXPO	Spin-coating	ITO/PEDOT:PSS/PVK/CBP:PBD:**Eu26**/TPBi/LiF/Al	430	[197]
$EuZnL(tta)_2$(μ-tfa)	VTE	ITO/TPD/**Eu40**:CBP 10%/TPBI/LiF/Al	1982	[198]
Eu6	Spin-coating	ITO/PEDOT:PSS/PVK:PBD:**EuPP**/LiF/Al	296	[199]
$Eu(tta)_3(NADAPO)_2$	VTE	ITO/NPB/**Eu16**/BCP/Alq_3/Mg:Ag	1158	[194]
$Eu(tta)_3$(DPEPO)	VTE	ITO/NPB/CBP:**Eu-19**/BCP/Alq3/LiF/Al	632	[200]
$Eu(tta)_3$(Tmphen)	VTE	ITO/TPD/1%**Eu**:CBP/BCP/AlQ/LiF/Al	800	[201]
	VTE	ITO/TPD/1%**Eu**:CBP:FIrPic/BCP/AlQ/LiF/Al	1156	[202]
$Eu(tta)_3$DPPZ	VTE	ITO/NPB/CBP:**Eu1**/BCP/Alq3/Mg:Ag	2046	[186]
$Eu(DPDBM)_3$DPPZ	VTE	ITO/m-MTDATA/NPB/CBP:**Eu64**/Bphen/Alq3/LiF/Al	2910	[185]
$Eu(DBM)_3$phen	VTE	ITO/TPD/**Eu54**:PBD/Alq3/Mg:Ag	460	[188]
	VTE	ITO/MoO3/mCP/mCP:PO-T2T:**Eu54**/PO-T2T/LiF/Al	330	[203]
$Eu(DBM)_3$Bphen	VTE	ITO/TPD/**Eu67**/TAZ/LiF/Al	380	[193]
$Eu(DBM)_3$Bphen	VTE	ITO/TPD/TPD:**Eu67**/**Eu67**/TAZ/LiF/Al	1000	[193]

Continued

TABLE 7 Characteristics of some OLEDs based on europium CCs.—Cont'd

Emitter	Deposition method	Diode heterostructure	L_{max}, cd/m^2	References
$Eu(dbm)_3DPPZ$	VTE	ITO/PEDOT:PSS/PVK/PFO:PBD:**Eu-68**/Ba/Al	1381	[187]
$Eu(DBM)_3(DFPP)$	VTE	ITO/TPD/**Eu-79**:CBP:DCJTB/BCP/Alq3/LiF/Al	1200	[204]
$Eu(DBM)_3EPBM$	VTE	ITO/TPD/**Eu-85**/Alq3/Al	180	[205]
$Eu(DPM)_3(BuOXD\text{-}phen)$	Spin-coating	ITO/PEDOT:PSS/PVK/PFO:PBD:**EuP**/Ba/Al	568	[206]
$Eu(DPM)_3$	VTE	ITO/TAPC/**Eu-91**:BCP/BCP/Alq3/Mg:Ag/Ag	2123	[207]
$[Eu(hfa)_3(indazole)_3]$	VTE	ITO/CuPc/**Eu-92**:CBP/BCP/Alq3/LiF/Al	1750	[208]
$NBu_4[EuL_4]$	VTE	ITO/PEDOT:PSS/CBP:OXD-7:**Eu-95**/BCP/LiF/Al	1234	[209]
$Eu(L1)_3(TPPO)(H_2O)$	VTE	ITO/NPB/CBP:**Eu-88**/BCP/Alq3/Mg:Ag	247	[210]
$Eu(BSA)_3phen$	Spin-coating	ITO/PVK:**Eu97**/LiF/Al	55	[211]
$Eu(o\text{-}BBA)_3(phen)$	Spin-coating	ITO/PVK:**Eu96**/Al	n.a.	[212]
$Eu(tfb)_3(Bphen)_2$	Spin-coating	ITO/PEDOT:PSS/PVK/Eu(tfb)3:10Bphen/Bphen/Al	1	[172]
$Eu(fb\text{-}1)_3(phen)$	Spin-coating	ITO/PEDOT:PSS/PVK/**Eu**/TPBi/Al	<1	[133]
$Eu(fb\text{-}2)_3(phen)$	Spin-coating	ITO/PEDOT:PSS/PVK/**Eu**/TPBi/Al	<1	[133]
$Eu(fb\text{-}1)_3(Bphen)$	Spin-coating	ITO/PEDOT:PSS/PVK/**Eu**/TPBi/Al	10	[133]
$Eu(fb\text{-}2)_3(Bphen)$	Spin-coating	ITO/PEDOT:PSS/PVK/**Eu**/TPBi/Al	25	[133]
$Eu(pfb)_3(Bphen)$	Spin-coating	ITO/PEDOT:PSS/poly-TPD/CBP (60 wt%):OXD-7 (30 wt%): **Eu(pfb)3(Bphen)** (10 wt%)/OXD-7/LiF/Al	9	[173]
$Eu(btz)_3Bphen$	Spin-coating	ITO/PEDOT:PSS/poly-TPD/**Eu**/TPBi/Al	<1	[167]

Key: *tta*, 2-thenoyltrifluoroacetonate; *phen*, o-phenanthroline; *SFXPO*, spirofluorene-xanthene diphosphine oxide; *nta*, naphthoyltrifluoroacetonate; *tfa*, trifluoroacetate; *NADAPO*, (4-naphthalen-1-yl-phenylaminophenyl)diphenylphosphine oxide; *DPEPO*, bis(2-(diphenylphosphino)phenyl)ether oxide; *Tmphen*, 3,4,7,8-Tetramethyl-1, 10-phenanthroline; *DPPZ*, dipyridophenazine; *dpdbm*, 1-(4-diphenylamino-phenyl)-3-phenylpropane-1,3-dione; *dbm*, 1,3-diphenyl-propane-1,3-dione; *Bphen*, bathophenanthroline; *DFPP*, 2-(2,4-difluorophenyl)pyridine; *EPBM*, 1-ethyl-2-(2-pyridyl)benzimidazole; *DPM*, 2,2,6,6-tetramethyl-3,5-heptanedione; *BuOXD-Phen*, 5-(2-(4-tert-Butylbenzenyl)-5-benzenyl-1,3,4-oxadiazole-4′)-1,10-phenanthroline; *hfa*, hexafluoroacetylacetonate; *L*, 1-(4-(9*H*-carbazol-9-yl)phenyl)-4,4,4-trifluorobutane-1,3-dione; *L1*, 1-phenyl-3-methyl-4-(1-naphthoyl)-5-pyrazolone; *TPPO*, triphenylphosphine oxide; *BSA*, benzoyl salicylic acid; *o-BBA*, 2-benzoylbenzoic acid; *fb1–2*, fluorobenzoates; *pfb*, pentafluorobenzoate; *btz*, benzothiazole-2-carboxylate.

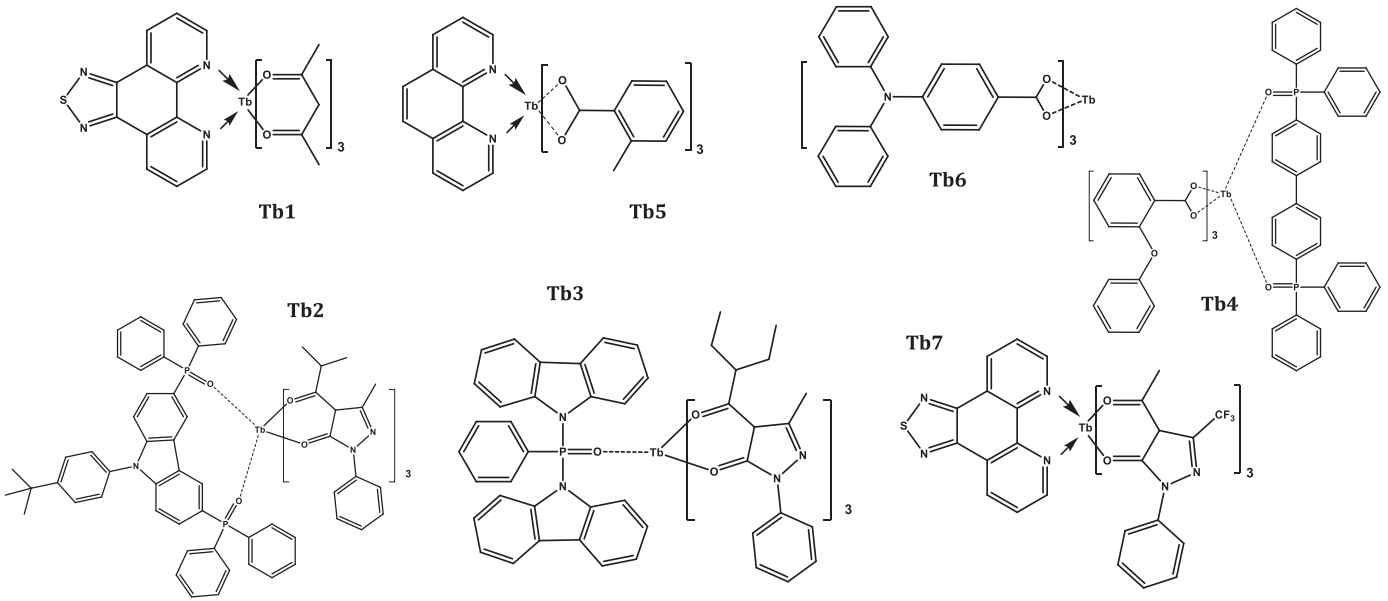

FIG. 29 Terbium complexes *Tb1*: [Tb(acac)$_3$(TDZP)] [213]; *Tb2*: [Tb(pmip)$_3$(DPPOC)] [179]; *Tb3*: [Tb(pmip)$_3$(DCPPO)] [178]; *Tb4*: [Tb(pobz)$_3$(PO)] [130]; *Tb5*: [Tb(o-mba)$_3$(phen)] [214]; *Tb6*: [Tb(dpab)$_3$] [189]; *Tb7*: [Tb(pfap)$_3$(TDZP)] [215].

TABLE 8 Characteristics of some OLEDs based on terbium CCs.

Emitter	Deposition method	Diode heterostructure	L_{max}, cd/m^2	References
Tb1	VTE	ITO/NPB/**Tb1**/Al	1673	[213]
Tb2	VTE	ITO/MoO_3/NPB/**Tb2**/Alq3/LiF/Al	3823	[179]
Tb2 and Tb3	VTE	ITO/MoO_3/TCTA:MoO_3/TcTa/**Tb3**/**Tb2**/3TPYMB/LiF/Al	2784	[178]
Tb4	Spin-coating	ITO/PEDOT:PSS/PVK/**Tb4**/TPBi/LiF/Al	75	[130]
Tb5	Spin-coating	ITO/BCP/PVK:**Tb5**/Alq_3/LiF/Al	180	[216]
Tb6	Spin-coating	ITO/PVK:**Tb6**/TPBi/Alq3/LiF/Al	230	[189]
Tb7	Spin-coating	ITO/PEDOT:PSS/Poly-TPD/TCTA:OXD-7:**Tb7**/Tm3PyPB/LiF/Al	6365	[215]
$Tb(DPM)_3$	VTE		Visible light	[217]
$Tb(pobz)_3(PO4)$	Spin-coating		75	[130]

Key: *DPM*, 2,2,6,6-tetramethyl-3,5-heptanedione; *pobz*, phenoxybenzoate; *PO4*, di(phosphine oxide).

5.3 Ytterbium: NIR emission

Near-infrared (NIR) luminescence has received considerable attention in biomedical research owing to its attractive features, such as excellent tissue penetration and low phototoxicity. In particular, the 1000–1700 nm spectral range (NIR-II biological window) is of wide interest [218]. Ytterbium luminescence (980–1100 nm) falls at the beginning of this spectral range, and since Yb^{3+} complexes have the highest quantum yields among the NIR-emitting lanthanides, they attract great attention as OLED emitters. Table 9 presents some data on ytterbium-based OLEDs as well as on a pair of efficient emitters of other classes emitting in the same range for comparison (Fig. 30). It can be seen that the EL performance of ytterbium complexes is often the best.

5.4 Erbium

Among the NIR-emitting lanthanide ions, Er^{3+} plays a special role in telecommunications technologies since it displays a reasonably sharp emission around 1.55 μm (0.8 eV), thus covering a spectroscopic window in which glass optical fibers show high transparency (so-called "third communication window"). Doped silica fibers such as erbium-doped fiber amplifiers (EDFAs) are at the heart of the optical amplification technology used in the communication systems operating in the 1.5-μm communication window. A disadvantage of this technology based on the low absorption of lanthanide ions, and their very low solubility in all-inorganic matrices, resulting in long and expensive amplifiers. To overcome these problems, metal complexes with organic ligands are considered as representing a new generation of low-cost optical amplifiers in the centimeter-length scale, suitable for the fabrication of photonic integrated circuits. Nonetheless, limited successes was achieved in sensitization of the luminescence of erbium, mostly subject to quenching, which in turn results in low OLED efficiency (Table 10).

5.5 Neodymium

Neodymium complexes are also important in optical amplifiers since they can strengthen the signal in the second communication window at 1.33 μm. However, they also suffer from low quantum yields, and thus low OLED performance is often observed (Table 11).

5.6 Other lanthanides

5.6.1 Samarium, dysprosium, praseodymium, holmium, and thulium

Despite relatively low EL efficiency, praseodymium, samarium, dysprosium, holmium, and thulium are interesting due to the possibility to emit simultaneously in the visible and NIR ranges with different intensity ratios.

TABLE 9 Characteristics of some OLEDs based on ytterbium CCs in comparison with OLEDs, based on the emitters of other classes.

Emitter		Heterostructure	Max. irradiance [$\mu W\,cm^{-2}$]	EQE (%)	λ_{EL} (nm)	References
Yb-1	[Yb(dbm)$_3$Bphen]	ITO/TPD/Yb-1/Alq$_3$/Mg,Ag	19.29		985	[219]
Yb-2	[Yb(TPP)(LOEt)]	ITO/PEDOT:PSS/Yb-2:PS/Ca,Al	0.6		977	[220]
Yb-3	[Yb(tta)$_3$(DBSO)]H_2O	ITO/β-NPB/Yb-3(10%):TcTa/ BCP/Alq$_3$/LiF/Al	22.48		980	[221]
Yb-4	[Yb(tta)$_3$(DPSO)]H_2O	ITO/β-NPB/Yb-4(10%):TcTa/ BCP/Alq$_3$/LiF/Al	12.13		980	[221]
Yb-5	[Yb(tta)$_3$(BGA)]H_2O	ITO/β-NPB/Yb-5(10%):TcTa/ BCP/Alq$_3$/LiF/Al	9.60		980	[221]
Yb-6	[Yb(dbm)$_3$(DPEPO)]	ITO/α-NPD/mCP/Yb-6:DPEPO/ TPBi/LiF/Al		0.15	1000–1100	[222]
Yb-7	[Yb(pmbp)Bphen]	ITO/NPB/Yb-7:NPB/Alq$_3$/LiF/Al	0.42	0.0064	980	[223]
Yb-8	[Yb(pmip)TPPO]	ITO/NPB/Yb-8/BCP/Alq$_3$/LiF/Al	0.80		470, 980	[223]
Yb-7,8		ITO/NPB/Yb-7/Yb-8/Alq$_3$/LiF/Al	1.47	0.027	980	[223]
Yb-9	[Yb(K·HOEt)(tbm)$_4$]$_2$	ITO/mCP/Yb-9:mCP/TPBi/LiF/Al	390	0.17	976	[224]
Yb-10	[Yb$_3$q$_9$]	ITO/TPD/Yb-10/Bphen/Yb	50		979	[225]
Yb-11	[Yb(pnd)$_3$]	ITO/NPB/Yb-11:CBP/BCP/Lif/Al	86	0.14	976	[226]
Yb-12	[Yb(hpbo)$_3$]$_2$	ITO/TPD/Yb-13/Bphen/Yb	154	0.053	982	[192]
Yb-13	[Yb(hpbt)$_3$]$_2$	ITO/TPD/Yb-14/Bphen/Yb	**286**	**0.122**	982	[192]

Yb-14	$[Yb(NpOON)_3]_2$	ITO/TPD/Yb-15/Bphen/Yb	**316**	0.6	530, 978, 1028	[227]
Yb-15	$[Yb(NpSON)_3]_2$	ITO/TPD/Yb-16/Bphen/Yb	**889**	1.6	580, 978, 1028	[227]
Yb-16	$[Yb(Np5mbo)_3]_2$	ITO/TPD/Yb-17/Bphen/Yb	**315**	0.082	550, 975	[228]
Yb-17	$[Yb(Np6mbo)_3]_2$	ITO/TPD/Yb-18/Bphen/Yb	**320**	0.085	550, 975	[228]
Yb-18	$[Yb(OC_6F_5)_3phen]$	ITO/TPD/Yb-19/Bphen/Yb	90	**0.24**	979	[229]
Yb-19	$[Yb(OSN)_3]_2$	ITO/TPD/Yb-20/Bphen/Yb	**860**	0.167	984	[230]
Yb-20	$[Yb(SSN)_3]_2$	ITO/TPD/Yb-21/Bphen/Yb	**415**	0.6	992	[230]
Yb-21	$[Yb(ant)_3]$	ITO/PEDOT:PSS/Yb-22/TAZ/Ca	n.a.	**0.21**	1000	[128]
Ru-1	$[Ru(bipy)_2(dpbq)]Cl_2$	ITO/Ru-1/Au	0.4	0.006	900	[231]
Ru-2	$[Ru(bipy)_2(PBIm)]Cl_2$	ITO/Ru-2/Au	0.5	0.030	945	[231]

Key: *dbm*, dibenzoylmethanate; *Bphen*, bathophenanthroline; *TPP*, tetraphenylporphyrin; *LOEt*, Kläui's ligand $\{CoCp[OP(OEt)_2]_3\}$; *tta*, thenoyltrifluoroacetylacetonate; *DBSO*, dibenzyl sulfoxide; *DPSO*, diphenyl sulfoxide; *BGA*, benzoguanamine; *DPEPO*, bis(2-(diphenylphosphino)phenyl)ether oxide; *pmbp*, 1-phenyl-3-methyl-4-(4-tert-butylbenzacyl)-5-pyrazolone; *TPPO*, triphenylphosphine oxide; *pmip*, 1-phenyl-3-methyl-4-isobutyryl-5-pyrazolone; *tbm*, tribenzoylmethide; *q*, 8-hydroxyquinolinate; *pnd*, *N*,*N*,*O*-ligand 6-(pyridin-2-yl)-1,5-naphthyridin-4-ol; *hpbo*, 2-(2-hydroxyphenyl)benzoxazole; *hpbt*, 2-(2-hydroxyphenyl)benzothiazole; *NpOON*, 3-(2-benzoxazol-2-yl)naphtholate; *NpSON*, 3-(2-benzothiazol-2-yl)naphtholate; *Np5mbo*, 3-(5-methylbenzoxazol-2-yl)naphtholate; *Np6mbo*, 3-(6-methylbenzoxazol-2-yl)naphtholate; *OSN*, 2-(2′-mercaptophenyl)benzoxazolate; *SSN*, 2-(2′-mercaptophenyl)benzothiazolate; *ant*, 9-anthracenate; *bipy*, 2,2′-bipyridine; *dpbq*, 2,3-bis(2-pyridin)benzoquinoxaline; *PBIm*, 2-(2-pyridyl)benzimidazole.

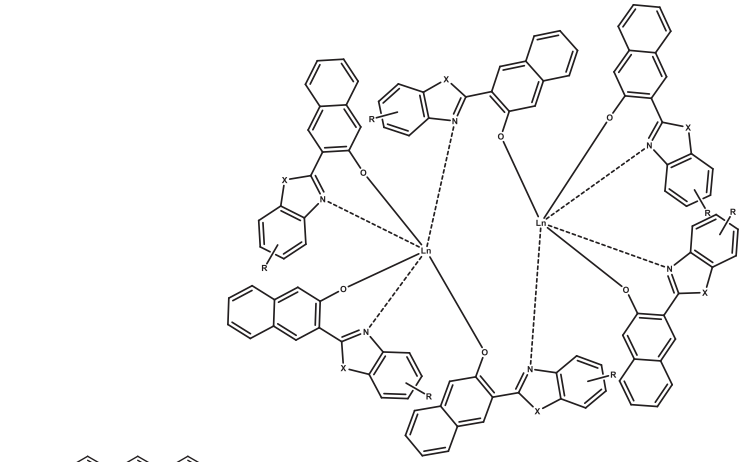

	R = CH_3	R = H	
		O	S
Yb	Yb-16/17	Yb-14	Yb-15
Er	Er-13/14	Er-11	Er-12
Nd	Nd-15/16	Nd-13	Nd-14
Tm	Tm-7/8	Tm-5	Tm-6

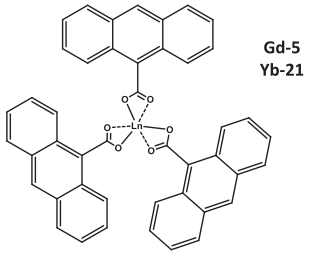

Gd-5
Yb-21

X′ = S	O	S
Yb	Yb-19	Yb-20
Gd	Gd-6	Gd-7
X′ = S	O	S
Yb	Yb-12	Yb-13
Nd	Nd-11	Nd-12

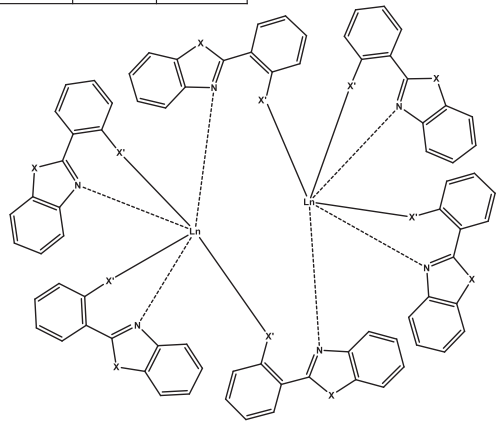

FIG. 30 Lanthanide complexes $Ln(ant)_3$ (Ln = Gd, Yb) [128], $[Ln(hpbo/hpbt)_3]_2$ (Ln = Nd, Yb) [192], $[Ln(NpOON/NpSON)_3]_2$ (Ln = Yb, Er, Nd, Tm) [227], $[Yb(Np5mbo/Np6mbo)_3]_2$ (Ln = Nd, Tm, Er, Yb) [228].

TABLE 10 Characteristics of some OLEDs based on erbium CCs and emitting at around 1.5 μm.

Emitter		Heterostructure	Max. irradiance [$\mu W\,cm^{-2}$]	References
Er-1	[Er(acac)$_3$phen]	ITO/PVK:Er-1/Al:Li/Ag:p-Si	n.a.	[232]
Er-2	[Er(dbm)$_3$phen]	p-Si/SiO$_2$/NPB/Bphen:Er-2/Bphen/Cs$_2$CO$_3$:Bphen/Sm/Au	0.93	[233]
Er-3	[Er(tpm)$_3$(5NO$_2$phen)]	ITO/PEDOT:PSS/Er-3(170 nm)/Ca/Al	n.a.	[234]
Er-4	[Er(tfnb)$_3$bipy]	ITO/PEDOT:PSS/Er-4(97 nm)/Ca/Al	n.a.	[235]
Er-5	[Er(tfa)$_3$(5NO$_2$phen)]	ITO/PEDOT:PSS/Er-5(75 nm)/Ca/Al	n.a.	[236]
Er-6	[Er(tfa)$_3$Bphen]	ITO/PEDOT:PSS/Er-6(70 nm)/Ca/Al	n.a.	[236]
Er-7	[Er(tta)$_3$TPPO]	ITO/β-NPB/Er-7/TPBi/LiF/Al	0.069	[237]
Er-8	[Er(pm)$_3$TPPO]	ITO/β-NPB/Er-8/BCP/Alq$_3$/LiF/Al	0.21	[238]
Er-9	[Er(hfa)$_3$bipy]	ITO/CuPc/Er-9:CBP/BCP/Alq$_3$/LiF/Al	0.5	[239]
Er-10	[Er(pnd)$_3$]	ITO/NPB/Er-10:CBP/BCP/LiF/Al	0.46	[226]
Er-11	[Er(NpOON)$_3$]$_2$	ITO/TPD/Er-11/Bphen/Yb	<0.1	[227]
Er-12	[Er(NpSON)$_3$]$_2$	ITO/TPD/Er-12/Bphen/Yb	<0.1	[227]
Er-13	[Er(Np5mbo)$_3$]$_2$	ITO/TPD/Er-13/Bphen/Yb	EQE = 0.0056%	[228]
Er-14	[Er(Np6mbo)$_3$]$_2$	ITO/TPD/Er-14/Bphen/Yb	EQE = 0.0088%	[228]

Key: *acac*, acetylacetonate; *phen*, phenanthroline; *dbm*, dibenzoylmethanate; *tpm*, 1,1,1-trifluoro-5,5-dimethyl-2,4-hexanedione; *5NO$_2$phen*, 5-nitro-1,10-phenanthroline; *tfnb*, 4,4,4-trifluoro-1-(2-naphthyl)-1,3-butanedione; *bipy*, 2,2′-bipyridine; *tfa*, trifluoroacetate; *Bphen*, bathophenanthroline; *tta*, thenoyltrifluoroacetylacetonate; *TPPO*, triphenylphosphine oxide; *pm*, 1-phenyl-3-methyl-4-isobutyryl-5-pyrazolone; *hfa*, hexafluoroacetylacetonate; *pnd*, *N,N,O*-ligand 6-(pyridin-2-yl)-1,5-naphthyridin-4-ol; *NpOON*, 3-(2-benzoxazol-2-yl)naphtholate; *NpSON*, 3-(2-benzothiazol-2-yl)naphtholate; *Np5mbo*, 3-(5-methylbenzoxazol-2-yl)naphtholate; *Np6mbo*, 3-(6-methylbenzoxazol-2-yl)naphtholate.

TABLE 11 Characteristics of some OLEDs based on neodymium CCs and emitting at around 890, 1060, and 1350 nm.

Emitter		Heterostructure	Max. irradiance [$\mu W cm^{-2}$]	References
Nd-1	[Nd(dbm)$_3$Bphen]	ITO/TPD/Nd-1/Alq$_3$/Mg:Ag (10:1)	0.0001[a]	[240], [241]
Nd-2	[Ndq$_3$]	ITO/TPD/Nd-2/Al	n.a.	[242]
Nd-3	[Nd(9-hpo)$_3$]	ITO/PEDOT:PSS/Nd-3:PVK/Ca/Al	0.85	[243]
Nd-4	[Nd(pnd)$_3$]	ITO/NPB/Nd-4:CBP/BCP/LiF/Al	25	[226]
Ir1-Nd-5	[Ir(dfpp)$_2$pfbim]:[Nd(pmip)$_3$]	ITO/NPB/Ir1:Nd-5 (1:1)/BCP/Alq$_3$/Mg:Ag (9:1)/Ag	6.1	[244]
Nd-6	[Nd(pm)$_3$TPPO]	ITO/NPB/Nd-6/BCP/Alq3/LiF/Al	0.21	[245]
Nd-7	[Nd(hfa)$_3$bipy]	ITO/CuPc/Nd-7:CBP/BCP/Alq$_3$/LiF/Al	28	[239]
Nd-8	[Nd(tta)$_3$phen]	ITO/PEDOT:PSS/Nd-8:mCP/TPBi/LiF/Al	0.022[a]	[246]
Nd-8		ITO/PEDOT:PSS/Nd-8:TcTa:SPPO13 (1:6:3)/TPBi/LiF/Al	0.034[a]	[247]
Nd-9	[Nd(dcq)$_4$]Net$_4$	ITO/PEDOT:PSS/Nd-9:PVK/Ca/Al	0.2	[248]
Nd-11	[Nd(hpbo)$_3$]$_2$	ITO/TPD/Nd-11/Bphen/Yb	74	[192]
Nd-12	[Nd(hpbt)$_3$]$_2$	ITO/TPD/Nd-12/Bphen/Yb	29	[192]
Nd-13	[Nd(NpOON)$_3$]	ITO/TPD/Nd-13/Bphen/Yb	32	[227]
Nd-14	[Nd(NpSON)$_3$]	ITO/TPD/Nd-14/Bphen/Yb	80	[227]
Nd-15	[Nd(Np5mbo)$_3$]	ITO/TPD/Nd-15/Bphen/Yb	80	[228]
Nd-16	[Nd(Np6mbo)$_3$]	ITO/TPD/Nd-16/Bphen/Yb	85	[228]
Nd-17	[Nd(OC$_6$F$_5$)$_3$phen]	ITO/TPD/Nd-17/Yb	18	[229]

Key: *dbm*, dibenzoylmethanate; *Bphen*, bathophenanthroline; *q*, 8-hydroxyquinolinate; *9-hpo*, 9-hydroxyphenalen-1-one; *pnd*, *N,N,O*-ligand 6-(pyridin-2-yl)-1,5-naphthyridin-4-ol; *dfpp*, 2-(2,4-difluorophenyl)pyridine; *pfbim*, 5-fluoro-2-(pyrimidin-2-yl)-1l2-benzo[d]imidazole; *pmip*, 1-phenyl-3-methyl-4-isobutyryl-5-pyrazolone; *TPPO*, triphenylphosphine oxide; *pm*, 1-phenyl-3-methyl-4-isobutyryl-5-pyrazolone; *hfa*, hexafluoroacetylacetonate; *bipy*, 2,2′-bipyridine; *tta*, thenoyltrifluoroacetylacetonate; *phen*, phenanthroline; *dcq*, 5,7-dichloro-8-hydroxyquinolinate; *NpOON*, 3-(2-benzoxazol-2-yl)naphtholate; *NpSON*, 3-(2-benzothiazol-2-yl)naphtholate; *Np5mbo*, 3-(5-methylbenzoxazol-2-yl)naphtholate; *Np6mbo*, 3-(6-methylbenzoxazol-2-yl)naphtholate; *hpbo*, 2-(2-hydroxyphenyl)benzoxazole; *hpbt*, 2-(2-hydroxyphenyl)benzothiazole.
[a]*EQE (%).*

Nonetheless, this interest is limited due to their low PLQY, caused by the ease of the quenching stemming from the high density of excited states and the moderate to small energy gaps (Table 12).

5.6.2 Gadolinium

The $^6P_{7/2}$ resonant level of Gd^{3+} ion, corresponding to the emission at 312 nm, is suitable for UV emission. However, as it is very high in energy (31,940 cm^{-1}), luminescence arising from this level is difficult to sensitize with organic ligands and, moreover, it is easily quenched by their π-conjugated functions. Besides, aliphatic polyaminocarboxylate anions, widely used as in contrast agent for magnetic resonance imaging, cannot provide charge mobility due to the absence of π-conjugated groups, and any conjugated transport host will again quench Gd^{3+}-centered luminescence. As a result, metal-centered electroluminescence of Gd^{3+} has not been studied (Table 13).

However, since Gd^{3+} promotes ligand phosphorescence, several publications, have investigated the use of the ligand luminescence of gadolinium complexes for OLED applications. Brightness up to 1350 cd/m^2 was achieved [230].

5.6.3 Lanthanum and lutetium

Lutetium has a filled f-shell, and lanthanum has an empty f-shell, thus both have no f-f transitions. Due to the ionic nature of the metal-ligand bond, heavy atom effect in La or Lu complexes is not pronounced, and both metals are diamagnetic, so the luminescence of their complexes is represented by the fluorescence of the ligands. This limits interest to them as OLED emitters and only a few examples exist in the literature (Table 14).

5.6.4 Cerium

Trivalent cerium emits due to d-f transitions, similarly to divalent europium, resulting in a broad emission with tunable wavelength. While in common use in LEDs, it is rarely tested in OLEDs, but a few examples exist in the literature (Table 14).

Complexes of non-lanthanide, but rare-earth yttrium and scandium also demonstrate ligand fluorescence. Despite limited interest for their EL, scandium complexes were sometimes considered as host materials [266].

6 Conclusions and perspectives

Organic light-emitting diodes made a long and very fast way from discovery to a widely applied commercial product. Among the main areas of their application are displays, lighting, and sensing. OLED displays are utilized in

TABLE 12 Characteristics of some OLEDs based on praseodymium, samarium, dysprosium, and thulium CCs.

Emitter		Heterostructure	L_{max}, cd/m^2	References
Pr-1	[Pr(dbm)Bphen]	ITO/TPD/Pr-1/Mg:Ag	210	[249]
Pr-1		ITO/TPD/Pr-1:TPD (3:1)/Pr-1/Mg:Ag	50	[249]
Pr-2	[$Pr(hfa)_3(bipy)_2$]	ITO/CuPc/Pr-2/BCP/Alq_3/LiF/Al	183	[250]
Sm-1	[$Sm(tta)_3$TPPO]	ITO/MTCD/Sm-1/Alq_3/Al	~0.5	[251]
Sm-1		ITO/MTCD/Sm-1/Al	~0.5	[251]
Sm-2	[$Sm(hfnh)_3$phen]	ITO/TPD/Sm-2/PBD/Al	9	[252]
Sm-2		ITO/PVK/Sm-2:PVK/PBD/Al	21	[252]
Sm-2		ITO/TPD/Sm-2/BCP/LiF/Al	42	[253]
Sm-3	[$Sm(dbm)_3$Bphen]	ITO/TPD/Sm-3:TPD/Sm-3/Mg:Ag	490	[254]
Sm-4	[Sm(tta)phen]	ITO/TPD/Sm-4/Alq_3/LiF/Al	81	[255]
Sm-5	[$Sm(hfa)_3(phen)_2$MeOH]	ITO/PEDOT:PSS/Sm-5:PVK:PBD/CsF/MgAg/Ag	135	[256]
Sm-6	[$Sm(NO_3)_3(q)_2(phen)]_2$	ITO/PEDOT:PSS/Sm-6:PVK:PBD/Al	507	[257]
Sm-7	[$Sm(cptfbd)_4$]$Nbut_4$	ITO/PEDOT:PSS/Sm-7:CBP:OXD7/BCP/LiF/Al	831	[209]
Dy-1	[$Dy(pm)_3$TPPO]	ITO/CuPc/Dy-1/BCP/Alq_3/LiF/Al	524	[258]
Dy-2	[$Dy(hfa)_3$bipy]	ITO/CuPc/Dy-2/BCP/Alq_3/LiF/Al	1765	[250]

Dy-3	$[Dy(hfa)_3(indazole)_2]$	ITO/CuPc/Dy-3:CBP/BCP/Alq_3/LiF/Al	326	[208]
Tm-1	$[Tm(acac)_3phen]$	ITO/PVK/Tm-1/Al	0.0074[a]	[259]
Tm-1		ITO/2-TNATA:m-MTDATA(2:1)/Tm-1/LiF/Al	47	[260]
Tm-3	$[Tm(OON)_3]_2$	ITO/TPD/Tm-3/Bphen/Yb	232[b]	[192]
Tm-4	$[Tm(SON)_3]_2$	ITO/TPD/Tm-4/Bphen/Yb	279[b]	[192]
Tm-5	$[Tm(NpOON)_3]_2$	ITO/TPD/Tm-5/Bphen/Yb	10 (3.6)[b]	[227]
Tm-6	$[Tm(NpSON)_3]_2$	ITO/TPD/Tm-6/Bphen/Yb	6 (8)[b]	[227]
Tm-7	$[Tm(Np5mbo)_3]$	ITO/TPD/Tm-7/Bphen/Yb	8 (5.8)[b]	[228]
Tm-8	$[Tm(Np6mbo)_3]$	ITO/TPD/Tm-8/Bphen/Yb	10 (7)[b]	[228]

Key: *dbm*, dibenzoylmethanate; *Bphen*, bathophenanthroline; *hfa*, hexafluoroacetylacetonate; *bipy*, 2,2′-bipyridine; *tta*, thenoyltrifluoroacetylacetonate; *TPPO*, triphenylphosphine oxide; *hfnh*, 4,4,5,5,6,6,6-heptafluoro-1-(2-thienyl)hexane-1,3-dione; *phen*, phenanthroline; *q*, 8-hydroxyquinolinate; *cptfbd*, 1-(4-(9H-carbazol-9-yl)phenyl)-4,4,4-trifluorobutane-1,3-dione; *pm*, 1-phenyl-3-methyl-4-isobutyryl-5-pyrazolone; *acac*, acetylacetonate; *NpOON*, 3-(2-benzoxazol-2-yl)naphtholate; *NpSON*, 3-(2-benzothiazol-2-yl)naphtholate; *Np5mbo*, 3-(5-methylbenzoxazol-2-yl)naphtholate; *Np6mbo*, 3-(6-methylbenzoxazol-2-yl)naphtholate; *OSN*, 2-(2′-mercaptophenyl)benzoxazolate; *SSN*, 2-(2′-mercaptophenyl)benzothiazolate.

[a]*Luminous efficacy in lm/W.*

[b]*Max. irradiance in $\mu W/cm^2$.*

TABLE 13 Characteristics of some OLEDs based on gadolinium CCs (ligand luminescence).

Emitter		Heterostructure	λ_{EL} (nm)	L_{max}, cd/m^2	References
Gd-1	[Gd(pmip)$_3$phen]	ITO/TPD/Gd-1/Mg:Ag/Ag	535	126	[146]
Gd-1		ITO/TPD/Gd-1/BCP/Mg:Ag/Ag	535	230 (PE 0.02 lm/W)	[146]
Gd-2	[Gd(pmip)$_3$bipy]	ITO/PVK/Gd-2/Alq$_3$/Mg:Ag/Al		340	[261]
Gd-3	[Gd(mbt)$_3$]	ITO/TPD/Gd-3/Yb	640	n.a.	[144]
Gd-4	[Gd(dbm)$_3$Bphen]	ITO/TPD/Gd-4/Mg:Ag	470 (exciplex)	n.a.	[262]
Gd-4		ITO/TPD/Gd-4:TPD/Gd-4/Mg:Ag	550 (exciplex)	n.a.	[262]
Gd-4		ITO/m-MTDATA/Gd-4/TBP/TPBi/LiF/Al	425–750	n.a.	[263]
Gd-5	[Gd(ant)$_3$]	ITO/PEDOT:PSS/Gd-5/TAZ/Al	500	n.a.	[128]
Gd-6	[Gd(OSN)$_3$]$_2$	ITO/CuPc/2-TNATA/NPB/CBP: Gd-6 or Gd-7 (0.2 wt%)/3TPYMB/LiF/Al		1350 (2.0 cd/A at 100 cd/m^2)	[230]
Gd-7	[Gb(SSN)$_3$]$_2$	ITO/CuPc/2-TNATA/NPB/CBP: Gd-6 or Gd-7 (0.2 wt%)/3TPYMB/LiF/Al		640 (0.4 cd/A at 100 cd/m^2)	[230]

Key: *pmip*, 1-phenyl-3-methyl-4-isobutyryl-5-pyrazolone; *phen*, phenanthroline; *bipy*, 2,2′-bipyridine; *mbt*, 2-mercaptobenzothiazolate; *dbm*, dibenzoylmethanate; *Bphen*, bathophenanthroline; *ant*, 9-anthracenate; *OSN*, 2-(2′-mercaptophenyl)benzoxazolate; *SSN*, 2-(2′-mercaptophenyl)benzothiazolate.

TABLE 14 Characteristics of some OLEDs based on trivalent lanthanum, cerium, and lutetium CCs.

Emitter		Heterostructure	λ_{EL} (nm)	Characteristics	References
La-1	$[La(hhqc)_2(H_2O)_4Cl]$	ITO/La-1/Al	515	FWHM 200 nm	[264]
La-1		ITO/PVK/La-1/Al	515	$L_{max} = 873\,cd/m^2$	[265]
La-2		ITO/TPD/La-2/Yb		No EL	[266]
Ce-1	[Ce(DC-18C6)]	ITO/CuPc/Ce-1:CBP/PBD/LiF/Al	376	$13\,W/cm^2$ at 22 V	[267]
Ce-2	$[Ce(triPrNTB)_2](SO_3CF_3)_3{\cdot}2H_2O$	ITO/NPB/Ce-2:MADN/Alq3/LiF/Al	(0.18, 0.21)[a]	1.5 cd/A 0.52 lm/W	[268]
Lu-1	$[Lu(pmip)_3TPPO]$	ITO/TPD/Lu-1/BCP/Alq3/$Mg_{0.9}Ag_{0.1}$	465	119	[269]

Key: *hhqc*, *N*-hexadecyl-8-hydroxyquinoline-2-carboxamide; *DC-18C6*, dicyclohexano-18-crown-6 complex; *R-NTB*, tri R-substituted (*N*-alkylbenzimidazol-2-ylmethyl)amine (R = *n*Pr); *pmip*, 1-phenyl-3-methyl-4-isobutyryl-5-pyrazolone; *TPPO*, triphenylphosphine oxide.
[a]*CIE coordinates.*

mobile devices and have been often called the best displays ever. OLED TVs have only recently reached the market, but are already widely spread due to their perfect characteristics. OLED lighting, long present in showrooms, also starts to appear as a commercial product, which accelerates the development in this area.

Each OLED achievement raises new demands, among which are the decrease of production costs and the increase of color purity, as well as, as it always will be, the increase in the light intensity and conversion efficiency. Some of these issues can theoretically be easily solved using lanthanide emitters instead of the currently used iridium compounds and fast-developing TADF materials. The advantage of lanthanide-based OLEDs is their use of triplet state in the luminescence process, which is required for efficient electroluminescence; moreover, their quantum yields are at least equal to those of emitters of other classes. Lanthanide complexes exist, emitting in the green (Tb), red (Eu), and NIR (primarily Yb) with high efficiencies. On the other hand, there is still no efficient blue-emitting lanthanide complexes, though d-f emitting complexes or phosphorescent gadolinium complexes with ligand-centered emission (or perhaps thulium complexes, who knows!), may once fill the gap.

Lanthanide complexes are not too expensive both from the point of view of the metal abundance (their reserves are thousands of times higher than of platinum metals) and patent protection. They are typically air-stable, which at least facilitates their handling. The emission bands of the trivalent lanthanides are unprecedently narrow due to f-orbital shielding, making them unsuitable for lighting, but promising for providing very pure colors. Their emission bands have nearly constant wavelengths which are perfectly suitable for display applications: europium emission corresponds to the "perfect red," and terbium emission corresponds to the green of modern color gamuts. Ytterbium luminescence occurs in a biological window, and its relatively narrow band matches well the requirements for bio-applications.

Nonetheless, the intrinsic properties of lanthanide luminescence significantly differ from those of emitters of other classes, which definitively hampers their development as OLED materials. Despite the vast expertise acquired by scientists separately in the fields of OLEDs and lanthanide luminescence, the direct intersection of these fields is difficult. For instance, the widely popular europium and terbium luminescent coordination compounds suffer little from concentration quenching, but feature high excited state energies and large ligand-induced Stokes shifts, compared to the emitters of other classes, which limits (for Eu complexes) or even proscribes (for Tb complexes) the host selection—a basic approach toward the increase of OLED efficiency. This results, in particular, in the necessity to program the mobility of both electrons and holes in the pure emitter layer, in addition to the common requirements of large PLQY, volatility, solubility, chemical, thermal,

and photo stability, etc. Charge carrier mobility can be increased by modification of organic ligands, neutral and anionic, to combine electron-donating and electron-withdrawing groups.

At the same time, lanthanide complexes suffer from a crucial drawback, limiting their EL efficiency by orders of magnitude compared to emitters of other classes: the long lifetime of their excited states. Despite the exact mechanism of the efficiency roll-off in the case of lanthanide complexes is still unknown, a simple decrease of the frequency of the exciton (radiative) relaxation results in the smaller fraction of current flow, generating excitons, and the remaining fraction just flows through the diode and results in OLED degradation. This makes achieving a short lifetime of the excited state the most important issue for lanthanide-based emitters in general and in particular for europium and terbium complexes. This fact is still often overlooked but its taking into account should give a renewed incentive for the development of lanthanide-based luminescent emitters for OLEDs.

In principle, achieving short lifetimes is easier for NIR-emitting lanthanide materials. However, this is clearly to the expense of PLQY, which is often too low for the materials to becomes useful for OLEDs. The only lanthanide that escapes this fate is ytterbium, with short excited states lifetimes in the μs range and reasonable quantum yields reaching now several percent in solid. Besides, despite a quite large ligand-induced Stokes shift, its excited state is lower, and concentration quenching is pronounced, which allows a wide approach of host selection. Altogether, PLQYs of ytterbium complexes exceed those of NIR emitters of other classes in the same wavelength range. This results in the already superior performance of ytterbium-based OLEDs against those based on platinum metal complexes and TADF emitters.

Acknowledgments

U.V. thanks the coworkers from the Laboratory of Chemistry of Coordination Compounds (Chemistry Department, Lomonosov Moscow State University), particularly of the Luminescence group, for their infinite help, and Russian Science Foundation (grant 20-73-10053) and President's grant (MD-2821.2021.1.3) for the financial support.

References

[1] T. Tsujimura, OLED Display Fundamentals and Applications, John Wiley & Sons, Inc, 2017. https://doi.org/10.1002/9781119187493.

[2] M. Koden, OLED Displays and Lighting, John Wiley & Sons, Ltd, Chichester, UK, 2016. https://doi.org/10.1002/9781119040477.

[3] OLED.com, https://oled.com/solutions/solutions-licensing/, 2020.

[4] M. Pope, H.P. Kallmann, P. Magnante, Electroluminescence in organic crystals, J. Chem. Phys. 38 (1963) 2042–2043. https://doi.org/10.1063/1.1733929.

[5] C.W. Tang, S.A. Vanslyke, Organic electroluminescent diodes, Appl. Phys. Lett. 51 (1987) 913–915. https://doi.org/10.1063/1.98799.

[6] P.E. Burrows, V. Bulović, S.R. Forrest, L.S. Sapochak, D.M. McCarty, M.E. Thompson, Reliability and degradation of organic light emitting devices, Appl. Phys. Lett. 65 (1994) 2922–2924. https://doi.org/10.1063/1.112532.

[7] J. Kido, K. Nagai, Y. Okamoto, T. Skotheim, Electroluminescence from polysilane film doped with europium complex, Chem. Lett. 20 (1991) 1267–1270. https://doi.org/10.1246/cl.1991.1267.

[8] M.A. Baldo, M.E. Thompson, S.R. Forrest, Phosphorescent materials for application to organic light emitting devices, Pure Appl. Chem. 71 (1999) 2095–2106. https://doi.org/10.1351/pac199971112095.

[9] A. Endo, M. Ogasawara, A. Takahashi, D. Yokoyama, Y. Kato, C. Adachi, Thermally activated delayed fluorescence from Sn4+-porphyrin complexes and their application to organic light-emitting diodes—a novel mechanism for electroluminescence, Adv. Mater. 21 (2009) 4802–4806. https://doi.org/10.1002/adma.200900983.

[10] C.R. Ronda, Luminescence: From Theory to Applications, Wiley-VCH, 2008.

[11] H. Yersin, Highly Efficient OLEDs With Phosphorescent Materials, Wiley-VCH, 2008. https://doi.org/10.1002/9783527621309.

[12] H. Yersin, A.F. Rausch, R. Czerwieniec, T. Hofbeck, T. Fischer, The triplet state of organo-transition metal compounds. Triplet harvesting and singlet harvesting for efficient OLEDs, Coord. Chem. Rev. 255 (2011) 2622–2652. https://doi.org/10.1016/j.ccr.2011.01.042.

[13] E. Silinsh, V. Capek, Organic molecular crystals: interaction, localization, and transport phenomena, American Institute of Physics (1994). https://books.google.ru/books/about/Organic_Molecular_Crystals.html?id=Wh7wAAAAMAAJ&redir_esc=y.

[14] H. Bässler, Charge transport in disordered organic photoconductors a Monte Carlo simulation study, Phys. Status Solidi B 175 (1993) 15–56. https://doi.org/10.1002/pssb.2221750102.

[15] S.D. Baranovskii, Theoretical description of charge transport in disordered organic semiconductors, Phys. Status Solidi B 251 (2014) 487–525. https://doi.org/10.1002/pssb.201350339.

[16] A. Miller, E. Abrahams, Impurity conduction at low concentrations, Phys. Rev. 120 (1960) 745. https://doi.org/10.1103/PhysRev.120.745.

[17] V. Coropceanu, J. Cornil, D.A. da Silva Filho, Y. Olivier, R. Silbey, J.-L. Bredas, Charge transport in organic semiconductors, Chem. Rev. 107 (2007) 926–952. https://doi.org/10.1007/128_2011_218.

[18] S. Lee, K. Ghaffarzadeh, A. Nathan, J. Robertson, S. Jeon, C. Kim, I.-H. Song, U.-I. Chung, Trap-limited and percolation conduction mechanisms in amorphous oxide semiconductor thin film transistors, Appl. Phys. Lett. 98 (2011) 203508. https://doi.org/10.1063/1.3589371.

[19] R.A. Marcus, Electron transfer reactions in chemistry: theory and experiment, Rev. Mod. Phys. 65 (1993) 599. https://doi.org/10.1002/anie.199311113.

[20] Y.T. Chang, J.K. Chang, Y.T. Lee, P.S. Wang, J.L. Wu, C.C. Hsu, I.W. Wu, W.H. Tseng, T.W. Pi, C.T. Chen, C.I. Wu, High-efficiency small-molecule-based organic light emitting devices with solution processes and oxadiazole-based electron transport materials, ACS Appl. Mater. Interfaces 5 (2013) 10614–10622. https://doi.org/10.1021/am402504g.

[21] M. Aonuma, T. Oyamada, H. Sasabe, T. Miki, C. Adachi, Material design of hole transport materials capable of thick-film formation in organic light emitting diodes, Appl. Phys. Lett. 90 (2007) 183503. https://doi.org/10.1063/1.2733627.

[22] N. Karl, Charge carrier transport in organic semiconductors, Synth. Met. 134 (2003) 649–657.

[23] S. Tiwari, N.C. Greenham, Charge mobility measurement techniques in organic semiconductors, Opt. Quant. Electron. 41 (2009) 69–89. https://doi.org/10.1007/s11082-009-9323-0.

[24] A. Kokil, K. Yang, J. Kumar, Techniques for characterization of charge carrier mobility in organic semiconductors, J. Polym. Sci. B Polym. Phys. 50 (2012) 1130–1144. https://doi.org/10.1002/polb.23103.

[25] N. Thejo Kalyani, S.J. Dhoble, Novel materials for fabrication and encapsulation of OLEDs, Renew. Sustain. Energy Rev. 44 (2015) 319–347. https://doi.org/10.1016/j.rser.2014.11.070.

[26] J. Jayabharathi, K. Jayamoorthy, V. Thanikachalam, Synthesis, photophysical and electroluminescent properties of green organic light emitting devices based on novel iridium complexes containing benzimidazole ligands, J. Organomet. Chem. 761 (2014) 74–83. https://doi.org/10.1016/j.jorganchem.2014.03.002.

[27] D. Hertel, C.D. Müller, K. Meerholz, Bilderzeugung: organische leuchtdioden, Chemie Unserer Zeit 39 (2005) 336–347. https://doi.org/10.1002/ciuz.200400356.

[28] M. Baldo, M. Deutsch, P. Burrows, H. Gossenberger, M. Gerstenberg, V. Ban, S. Forrest, Organic vapor phase deposition, Adv. Mater. 10 (1998) 1505–1514. https://doi.org/10.1002/(SICI)1521-4095(199812)10:18<1505::AID-ADMA1505>3.0.CO;2-G.

[29] Aixtron 2-Gen Deposition System, https://www.oled-info.com/aixtron-commissioned-test-2-gen-ovpd-oled-deposition-system, 2021.

[30] JOLED, https://www.j-oled.com/eng/, 2021.

[31] L. Duan, L. Hou, T.-W. Lee, J. Qiao, D. Zhang, G. Dong, L. Wang, Y. Qiu, Solution processable small molecules for organic light-emitting diodes, J. Mater. Chem. 20 (2010) 6392. https://doi.org/10.1039/b926348a.

[32] T.-W. Lee, T. Noh, H.-W. Shin, O. Kwon, J.-J. Park, B.-K. Choi, M.-S. Kim, D.W. Shin, Y.-R. Kim, Characteristics of solution-processed small-molecule organic films and light-emitting diodes compared with their vacuum-deposited counterparts, Adv. Funct. Mater. 19 (2009) 1625–1630. https://doi.org/10.1002/adfm.200801045.

[33] D. Ma, Y. Qiu, L. Duan, Vacuum-deposited versus spin-coated emissive layers for fabricating high-performance blue–green-emitting diodes, ChemPlusChem 83 (2018) 211–216. https://doi.org/10.1002/cplu.201700382.

[34] L. Deng, W. Li, J. Li, Efficient bluish-green phosphorescent iridium complex for both solution-processed and vacuum-deposited organic light-emitting diodes, Displays 34 (2013) 413–417. https://doi.org/10.1016/j.displa.2013.05.001.

[35] S. Feng, L. Duan, L. Hou, J. Qiao, D. Zhang, G. Dong, L. Wang, Y. Qiu, A comparison study of the organic small molecular thin films prepared by solution process and vacuum deposition: roughness, hydrophilicity, absorption, photoluminescence, density, mobility, and electroluminescence, J. Phys. Chem. C 115 (2011) 14278–14284. https://doi.org/10.1021/jp203674p.

[36] G. Hong, X. Gan, C. Leonhardt, Z. Zhang, J. Seibert, J.M. Busch, S. Bräse, A brief history of OLEDs—emitter development and industry milestones, Adv. Mater. (2021) 2005630. https://doi.org/10.1002/adma.202005630

[37] Samsung Galaxy S20, http://www.displaymate.com/Galaxy_S20_ShootOut_1U.htm, 2021.

[38] Flexible and Rigid LG OLED Light Panels Installed in Baskin Robbins Brown Store, https://www.linkedin.com/pulse/flexible-rigid-lg-oled-light-panels-installed-baskin-robbins-chung, 2021. Accessed 22 November 2020.

[39] OLED Light, http://www.lgdisplay.com/eng/product/oled_light.jsp, 2014. Accessed 22 November 2020.

[40] G. Williams, C. Backhouse, H. Aziz, Integration of organic light emitting diodes and organic photodetectors for lab-on-a-chip bio-detection systems, Electronics 3 (2014) 43–75. https://doi.org/10.3390/electronics3010043.

[41] J. Shinar, R. Shinar, Organic light-emitting devices (OLEDs) and OLED-based chemical and biological sensors: An overview, J. Phys. D Appl. Phys. 41 (2008) 133001. https://doi.org/10.1088/0022-3727/41/13/133001.

[42] E. Kraker, A. Haase, B. Lamprecht, G. Jakopic, C. Konrad, S. Köstler, Integrated organic electronic based optochemical sensors using polarization filters, Appl. Phys. Lett. 92 (2008) 033302. https://doi.org/10.1063/1.2837410.

[43] C.M. Lochner, Y. Khan, A. Pierre, A.C. Arias, All-organic optoelectronic sensor for pulse oximetry, Nat. Commun. 5 (2014) 1–7. https://doi.org/10.1038/ncomms6745.

[44] K.C. Badgujar, A.B. Badgujar, D.V. Dhangar, V.C. Badgujar, Importance and use of pulse oximeter in COVID-19 pandemic: general factors affecting the sensitivity of pulse oximeter, Indian Chem. Eng. 62 (4) (2020) 374–384. https://doi.org/10.1080/00194506.2020.1845988.

[45] J.-C.G. Bünzli, Lanthanide luminescence: from a mystery to rationalization, understanding, and applications, in: J.-C.G. Bünzli, V.K. Pecharsky (Eds.), Handbook on the Physics and Chemistry of Rare Earths, Elsevier, 2016, pp. 141–176. https://doi.org/10.1016/bs.hpcre.2016.08.003.

[46] S. Tobita, M. Arakawa, I. Tanaka, The paramagnetic metal effect on the ligand localized S1-T1 intersystem crossing in the rare-earth-metal complexes with methyl salicylate, J. Phys. Chem. 89 (1985) 5649–5654. https://doi.org/10.1021/j100272a015.

[47] C. Yang, L.M. Fu, Y. Wang, J.P. Zhang, W.T. Wong, X.C. Ai, Y.F. Qiao, B.S. Zou, L.L. Gui, A highly luminescent europium complex showing visible-light-sensitized red emission: direct observation of the singlet pathway, Angew. Chem. Int. Ed. 43 (2004) 5010–5013. https://doi.org/10.1002/anie.200454141.

[48] M. Kleinerman, Energy migration in lanthanide chelates, J. Chem. Phys. 51 (1969) 2370–2381. https://doi.org/10.1063/1.1672355.

[49] O. Malta, Ligand—rare-earth ion energy transfer in coordination compounds. A theoretical approach, J. Lumin. 71 (1997) 229–236. https://doi.org/10.1016/S0022-2313(96)00126-3.

[50] O. Malta, F.G. Silva, A theoretical approach to intramolecular energy transfer and emission quantum yields in coordination compounds of rare earth ions, Spectrochim. Acta A Mol. Biomol. Spectrosc. 54 (1998) 1593–1599.

[51] H. Qi, Z. Zhao, G. Zhan, B. Sun, W. Yan, C. Wang, L. Wang, Z. Liu, Z. Bian, C. Huang, Air stable and efficient rare earth Eu(ii) hydro-tris(pyrazolyl)borate complexes with tunable emission colors, Inorg. Chem. Front. 7 (2020) 4593–4599. https://doi.org/10.1039/d0qi00762e.

[52] P. Dorenbos, F d transition energies of divalent lanthanides in inorganic compounds, J. Phys. Condens. Matter 15 (2003) 575–594. https://doi.org/10.1088/0953-8984/15/3/322.

[53] P. Dorenbos, Anomalous luminescence of Eu 2 and Yb 2 in inorganic compounds, J. Phys. Condens. Matter 15 (2003) 2645–2665. https://doi.org/10.1088/0953-8984/15/17/318.

[54] P. Dorenbos, The 4f ↔4f—15d transitions of the trivalent lanthanides in halogenides and chalcogenides, J. Lumin. 91 (2000) 91–106. https://doi.org/10.1016/S0022-2313(00)00197-6.

[55] K. Van den Eeckhout, P.F. Smet, D. Poelman, Persistent luminescence in Eu2+-doped compounds: a review, Materials (Basel) 3 (2010) 2536–2566. https://doi.org/10.3390/ma3042536.

[56] D. Dutczak, T. Jüstel, C. Ronda, A. Meijerink, Eu2+ luminescence in strontium aluminates, Phys. Chem. Chem. Phys. 17 (2015) 15236–15249. https://doi.org/10.1039/c5cp01095k.

[57] A.J. Freeman, R.E. Watson, Theoretical investigation of some magnetic and spectroscopic properties of rare-earth ions, Phys. Rev. 127 (1962) 2058–2075. https://doi.org/10.1103/PhysRev.127.2058.

[58] H. Ebendorff-Heidepriem, D. Ehrt, Electron spin resonance spectra of Eu2+ and Tb4+ ions in glasses, J. Phys. Condens. Matter 11 (1999) 7627. https://doi.org/10.1088/0953-8984/11/39/317.

[59] A. Diaz, D.A. Keszler, Eu2+ luminescence in the borates X2Z(BO3)2 (X = Ba, Sr; Z = Mg, Ca), Chem. Mater. 9 (1997) 2071–2077. https://doi.org/10.1021/cm9700817.

[60] N. Hirosaki, R.J. Xie, K. Kimoto, T. Sekiguchi, Y. Yamamoto, T. Suehiro, M. Mitomo, Characterization and properties of green-emitting beta—SiAlON: Eu2+ powder phosphors for white light-emitting diodes, Appl. Phys. Lett. 86 (2005) 1–3. https://doi.org/10.1063/1.1935027.

[61] P. Dorenbos, Anomalous luminescence of Eu2+ and Yb2+ in inorganic compounds, J. Phys. Condens. Matter 15 (2003) 2645–2665. https://doi.org/10.1088/0953-8984/15/17/318.

[62] F.D.S. Butement, Absorption and fluorescence spectra of bivalent samarium, europium and ytterbium, Trans. Faraday Soc. 44 (1948) 617–626. https://doi.org/10.1039/tf9484400617.

[63] M.N. Bochkarev, A.A. Fagin, I.L. Fedushkin, A.A. Trifonov, E.N. Kirillov, I.L. Eremenko, S.E. Nefedov, Divalent compounds of thulium, neodymium and dysprosium, Mater. Sci. Forum 315–317 (1999) 144–153. https://doi.org/10.4028/www.scientific.net/msf.315-317.144.

[64] M.N. Bochkarev, I.L. Fedushkin, A.A. Fagin, T.V. Petrovskaya, J.W. Ziller, R.N.R. Broomhall-Dillard, W.J. Evans, Synthesis and structure of the first molecular thulium(II) complex: [TmI2(MeOCH2CH2OMe)2], Angew. Chem. Int. Ed. Engl. 36 (1997) 133–135. https://doi.org/10.1002/anie.199701331.

[65] M.N. Bochkarev, A.A. Fagin, First molecular iodides of neodymium(II) and dysprosium(II), Russ. Chem. Bull. 48 (1999) 1187–1188. https://doi.org/10.1007/BF02496029.

[66] A.A. Fagin, S.V. Salmova, M.N. Bochkarev, Reduction of nitrogen with neodymium(II) and dysprosium(II) diiodides and selected properties of the resulting nitrides, Russ. Chem. Bull. 58 (2009) 230–233. https://doi.org/10.1007/s11172-009-0034-2.

[67] G.V. Khoroshen'kov, A.A. Fag, M.N. Bochkarev, S. Dechert, H. Schumann, Reactions of neodymium(II), dysprosium(II), and thulium(II) diiodides with cyclopentadiene. Molecular structures of complexes CpTmI 2 (THF) 3 and [NdI 2 (THF) 5] + [NdI 4 (THF) 2], Russ. Chem. Bull. 52 (2003) 1715–1719. https://doi.org/10.1023/A:1026132017155.

[68] J. Jiang, N. Higashiyama, K.I. Machida, G.Y. Adachi, The luminescent properties of divalent europium complexes of crown ethers and cryptands, Coord. Chem. Rev. 170 (1998) 1–29. https://doi.org/10.1016/S0010-8545(98)00070-8.

[69] L.A. Ekanger, L.A. Polin, Y. Shen, E.M. Haacke, P.D. Martin, M.J. Allen, A EuII-containing cryptate as a redox sensor in magnetic resonance imaging of living tissue, Angew. Chem. Int. Ed. 54 (2015) 14398–14401. https://doi.org/10.1002/anie.201507227.

[70] R.P. Kelly, T.D.M. Bell, R.P. Cox, D.P. Daniels, G.B. Deacon, F. Jaroschik, P.C. Junk, X.F. Le Goff, G. Lemercier, A. Martinez, J. Wang, D. Werner, Divalent tetra- and penta-phenylcyclopentadienyl europium and samarium sandwich and half-sandwich complexes: synthesis, characterization, and remarkable luminescence properties, Organometallics 34 (2015) 5624–5636. https://doi.org/10.1021/acs.organomet.5b00842.

[71] D.L. Dexter, J.H. Schulman, Theory of concentration quenching in inorganic phosphors, J. Chem. Phys. 22 (1954) 1063. https://doi.org/10.1063/1.1740265.

[72] L.G. Van Uitert, E.F. Dearborn, J.J. Rubin, Mechanisms of energy transfer involving trivalent Er and Tb or tm in sodium rare-earth tungstates, J. Chem. Phys. 47 (1967) 3653–3661. https://doi.org/10.1063/1.1712437.

[73] D. Pi, F. Wang, X. Fan, M. Wang, Y. Zhang, Luminescence behavior of Eu3+ doped LaF3 nanoparticles, Spectrochim. Acta A Mol. Biomol. Spectrosc. 61 (2005) 2455–2459. https://doi.org/10.1016/j.saa.2004.09.009.

[74] L.G. Van Uitert, L.F. Johnson, Energy transfer between rare earth ions, J. Chem. Phys. 44 (1966) 3514–3522.

[75] I. Shoji, S. Kurimura, Y. Sato, T. Taira, A. Ikesue, K. Yoshida, Optical properties and laser characteristics of highly Nd3+-doped Y3Al5O12 ceramics, Appl. Phys. Lett. 77 (2000) 939–941. https://doi.org/10.1063/1.1289039.

[76] G.A. Kumar, R. Riman, E. Snitzer, J. Ballato, Solution synthesis and spectroscopic characterization of high Er3+ content LaF3 for broadband 1.5 mu m amplification, J. Appl. Phys. 95 (2004) 40–47. https://doi.org/10.1063/1.1629772.

[77] Y.C. Li, Y.H. Chang, Y.F. Lin, Y.S. Chang, Y.J. Lin, Synthesis and luminescent properties of Ln3+ (Eu3+, Sm3+, Dy3+)-doped lanthanum aluminum germanate LaAlGe2O7 phosphors, J. Alloys Compd. 439 (2007) 367–375. https://doi.org/10.1016/j.jallcom.2006.08.269.

[78] G. Gao, J. Wei, Y. Shen, M. Peng, L. Wondraczek, Heavily Eu $_2$ O $_3$ -doped yttria-aluminoborate glasses for red photoconversion with a high quantum yield: luminescence quenching and statistics of cluster formation, J. Mater. Chem. C 2 (2014) 8678–8682. https://doi.org/10.1039/C4TC01447B.

[79] S.W. Allison, G.T. Gillies, Remote thermometry with thermographic phosphors: instrumentation and applications, Rev. Sci. Instrum. (1997) 2615. https://doi.org/10.1063/1.1148174.

[80] M.V. Nazarov, J.H. Kang, D.Y. Jeon, S.A. Bukesov, E.-J. Popovici, L. Muresan, Dependency of luminescence properties of Y[sub 2]O[sub 3]:Eu on the activator incorporation degree and lattice parameter, J. Soc. Inf. Disp. 13 (2005) 309. https://doi.org/10.1889/1.1904932.

[81] V. Khudoleeva, L. Tcelykh, A. Kovalenko, A. Kalyakina, A. Goloveshkin, L. Lepnev, V. Utochnikova, Terbium-europium fluorides surface modified with benzoate and terephthalate anions for temperature sensing: does sensitivity depend on the ligand?, J. Lumin. 201 (2018) 500–508. https://doi.org/10.1016/j.jlumin.2018.05.002.

[82] V.Y. Khudoleeva, V.V. Utochnikova, A.S. Kalyakina, I.M. Deygen, A.A. Shiryaev, Ł. Marciniak, V.A. Lebedev, I.V. Roslyakov, A.V. Garshev, L.S. Lepnev, U. Schepers, S. Bräse, N.P. Kuzmina, Surface modified EuxLa1-xF3 nanoparticles as luminescent biomarkers: still plenty of room at the bottom, Dyes Pigments 143 (2017) 348–355. https://doi.org/10.1016/j.dyepig.2017.04.058.

[83] V.Y. Khudoleeva, V.V. Utochnikova, A.S. Goloveshkin, Ł. Marciniak, A.V. Knotko, L.S. Lepnev, N.P. Kuzmina, Surface modified LnxLa1-xF3 (Ln = Dy, Yb) nanoparticles: toward bright NIR luminescence, Dyes Pigments 160 (2019) 21–27. https://doi.org/10.1016/j.dyepig.2018.04.046.

[84] C.Y. Sun, X.J. Zheng, X.B. Chen, L.C. Li, L.P. Jin, Assembly and upconversion luminescence of lanthanide-organic frameworks with mixed acid ligands, Inorg. Chim. Acta Lett. 362 (2009) 325–330. https://doi.org/10.1016/j.ica.2008.03.115.

[85] S.K. Singh, K. Kumar, S.B. Rai, Multifunctional Er3+-Yb3+ codoped Gd 2O3 nanocrystalline phosphor synthesized through optimized combustion route, Appl. Phys. B Lasers Opt. 94 (2009) 165–173. https://doi.org/10.1007/s00340-008-3261-6.

[86] F. Lahoz, C. Pérez-Rodríguez, S.E. Hernández, I.R. Martín, V. Lavín, U.R. Rodríguez-Mendoza, Upconversion mechanisms in rare-earth doped glasses to improve the efficiency of silicon solar cells, Sol. Energy Mater. Sol. Cells 95 (2011) 1671–1677. https://doi.org/10.1016/j.solmat.2011.01.027.

[87] E. Mathieu, A. Sipos, E. Demeyere, D. Phipps, D. Sakaveli, K.E. Borbas, Lanthanide-based tools for the investigation of cellular environments, Chem. Commun. 54 (2018) 10021–10035. https://doi.org/10.1039/C8CC05271A.

[88] E. Hemmer, N. Venkatachalam, H. Hyodo, A. Hattori, Y. Ebina, H. Kishimoto, K. Soga, Upconverting and NIR emitting rare earth based nanostructures for NIR-bioimaging, Nanoscale 5 (2013) 11339–11361. https://doi.org/10.1039/c3nr02286b.

[89] A.D. Sontakke, K. Biswas, A.K. Mandal, K. Annapurna, Time resolved fluorescence and energy transfer analysis of Nd 3+-Yb 3+-Er 3+ triply-doped Ba-Al-metaphosphate glasses for an eye safe emission (1.54 μm), J. Fluoresc. 20 (2010) 425–434. https://doi.org/10.1007/s10895-009-0562-z.

[90] W.J. Miniscalco, Erbium-doped glasses for fiber amplifiers at 1500 nm, J. Lightwave Technol. 9 (1991) 234–250. https://doi.org/10.1109/50.65882.

[91] P. Hänninen, H. Härmä (Eds.), Lanthanide Luminescence, Springer, Berlin Heidelberg, 2011. https://doi.org/10.1007/978-3-642-21023-5.

[92] S. Biju, Y.K. Eom, J.-C.G. Bünzli, H.K. Kim, A new tetrakis β-diketone ligand for NIR emitting LnIII ions: luminescent doped PMMA films and flexible resins for advanced photonic applications, J. Mater. Chem. C. 1 (2013) 6935. https://doi.org/10.1039/c3tc31181c.

[93] L.N. Puntus, K.J. Schenk, J.C.G. Bünzli, Intense near-infrared luminescence of a mesomorphic ionic liquid doped with lanthanide β-diketonate ternary complexes, Eur. J. Inorg. Chem. (2005) 4739–4744. https://doi.org/10.1002/ejic.200500593.

[94] E.R. Trivedi, S.V. Eliseeva, J. Jankolovits, M.M. Olmstead, S. Petoud, V.L. Pecoraro, Highly emitting near-infrared lanthanide "encapsulated sandwich" metallacrown complexes with excitation shifted toward lower energy, J. Am. Chem. Soc. 136 (2014) 1526–1534. https://doi.org/10.1021/ja4113337.

[95] J.C. Lutter, S.V. Eliseeva, G. Collet, I. Martinić, J.W. Kampf, B.L. Schneider, A. Carichner, J. Sobilo, S. Lerondel, S. Petoud, V.L. Pecoraro, Iodinated metallacrowns: toward combined bimodal near-infrared and X-ray contrast imaging agents, Chem. A Eur. J. 26 (2020) 1274–1277. https://doi.org/10.1002/chem.201905241.

[96] H. Cañibano, Y. Guyot, C. Goutaudier, L. Laversenne, G. Boulon, Spectroscopic properties and quenching mechanisms of Yb3+-doped garnet crystals, J. Phys. IV 119 (2004) 143–144. https://doi.org/10.1051/jp4:2004119028.

[97] O. Meza, L.A. Diaz-Torres, P. Salas, E. De la Rosa, C. Angeles-Chavez, D. Solis, Cooperative pair driven quenching of Yb3+ emission in nanocrystalline ZrO2:Yb3+, J. Nano Res. 5 (2009) 121–134. https://doi.org/10.4028/www.scientific.net/JNanoR.5.121.

[98] A.V. Orlova, V.Y. Kozhevnikova, L.S. Lepnev, A.S. Goloveshkin, I.M. Le-Deigen, V.V. Utochnikova, NIR emitting terephthalates (SmxDyyGd1-x-y)2(tph)3(H2O)4 for luminescence thermometry in the physiological range, J. Rare Earths 38 (2020) 492–497. https://doi.org/10.1016/j.jre.2020.01.010.

[99] A.Y. Grishko, V.V. Utochnikova, A.A. Averin, A.V. Mironov, N.P. Kuzmina, Unusual luminescence properties of heterometallic REE terephthalates, Eur. J. Inorg. Chem. 2015 (2015) 1660–1664. https://doi.org/10.1002/ejic.201403071.

[100] V.V. Utochnikova, A.Y. Grishko, D.S. Koshelev, A.A. Averin, L.S. Lepnev, N.P. Kuzmina, Lanthanide heterometallic terephthalates: concentration quenching and the principles of the "multiphotonic emission", Opt. Mater. (Amsterdam) 74 (2017) 201–208. https://doi.org/10.1016/j.optmat.2017.02.052.

[101] OLED Introduction and Basic OLED Information | LED-Info, (n.d.). https://www.oled-info.com/oled-introduction (Accessed 22 November 2020).

[102] J. Karl, A. Gschneidner, V. Pecharsky, Rare-Earth Element | Uses, Properties, & Facts | Britannica, https://www.britannica.com/science/rare-earth-element, 2020. Accessed 20 November 2020.

[103] Lanthanum Oxide Price Globally 2009–2025, https://www.statista.com/statistics/450139/global-reo-lanthanum-oxide-price-forecast/, 2021. Accessed 20 November 2020.

[104] Rare Earth Mine Production by Country, https://www.statista.com/statistics/268011/top-countries-in-rare-earth-mine-production/, 2021. Accessed 20 November 2020.
[105] Chinese Rare Earth Prices, https://www.statista.com/statistics/280038/chinese-domestic-and-export-prices-for-rare-earth-oxides/, 2021. Accessed 20 November 2020.
[106] Rare Earth Deposits Wordwide and by Country, https://www.statista.com/statistics/277268/rare-earth-reserves-by-country/, 2021. Accessed 20 November 2020.
[107] Platinum Metal Reserves Worldwide by Country 2019, https://www.statista.com/statistics/273624/platinum-metal-reserves-by-country/, 2021. Accessed 20 November 2020.
[108] J.-C.G. Bünzli, A.-S. Chauvin, Lanthanides in solar energy conversion, in: J.C.G. Bunzli, V.K. Pecharsky (Eds.), Handbook on the Physics and Chemistry of Rare Earths, 2014, pp. 169–281. https://doi.org/10.1016/B978-0-444-62711-7.00261-9.
[109] S.K. Gupta, T. Rajeshkumar, G. Rajaraman, R. Murugavel, An air-stable Dy(III) single-ion magnet with high anisotropy barrier and blocking temperature, Chem. Sci. 7 (2016) 5181–5191. https://doi.org/10.1039/c6sc00279j.
[110] A.S. Gajarushi, M. Wasim, R. Nabi, S. Kancharlapalli, V.R. Rao, G. Rajaraman, C. Subramaniam, M. Shanmugam, Lanthanide complexes as molecular dopants for realizing air-stable n-type graphene logic inverters with symmetric transconductance, Mater. Horiz. 6 (2019) 743–750. https://doi.org/10.1039/c8mh01241e.
[111] G.G. Condorelli, G. Malandrino, I.L. Fragala, Engineering of molecular architectures of β-diketonate precursors toward new advanced materials, Coord. Chem. Rev. 251 (2007) 1931–1950. https://doi.org/10.1016/j.ccr.2007.04.016.
[112] A. Drozdov, N. Kuzmina, Volatile compounds of lanthanides, in: J. Reedijk, K. Poeppelmeier (Eds.), Comprehensive Inorganic Chemistry II, Elsevier, 2013, pp. 511–534. https://doi.org/10.1016/B978-0-08-097774-4.00223-0.
[113] R.E. Sievers, S.B. Turnipseed, L. Huang, A.F. Lagalante, Volatile barium β-diketonates for use as MOCVD precursors, Coord. Chem. Rev. 128 (1993) 285–291. https://doi.org/10.1016/0010-8545(93)80035-4.
[114] V.V. Utochnikova, N.P. Kuzmina, Photoluminescence of lanthanide aromatic carboxylates, Russ. J. Coord. Chem. Khimiya. 42 (2016) 679–694. https://doi.org/10.1134/S1070328416090074.
[115] M. Bredol, U. Kynast, C. Ronda, Designing luminescent materials, Adv. Mater. (Weinheim, Ger.) 3 (1991) 361–367. https://doi.org/10.1002/adma.19910030707.
[116] J. Rocha, C.D.S. Brites, L.D. Carlos, Lanthanide organic framework luminescent thermometers, Chem. Eur. J. 22 (2016) 14782–14795. https://doi.org/10.1002/chem.201600860.
[117] Y. Cui, B. Chen, G. Qian, Lanthanide metal-organic frameworks for luminescent sensing and light-emitting applications, Coord. Chem. Rev. 273–274 (2014) 76–86. https://doi.org/10.1016/j.ccr.2013.10.023.
[118] V.V. Utochnikova, A.S. Kalyakina, L.S. Lepnev, N.P. Kuzmina, Luminescence enhancement of nanosized ytterbium and europium fluorides by surface complex formation with aromatic carboxylates, J. Lumin. 170 (2016) 633–640. https://doi.org/10.1016/j.jlumin.2015.03.033.
[119] V.V. Utochnikova, O.V. Kotova, A.A. Vaschenko, L.S. Lepnev, A.G. Vitukhnovsky, N.P. Kuzmina, Reactive chemical vapor deposition method as new approach for obtaining electroluminescent thin film materials, Adv. Mater. Sci. Eng. 2012 (2012) 1–9. https://doi.org/10.1155/2012/809028.
[120] K.K. Gangu, S. Maddila, S.B. Jonnalagadda, A review on synthesis, crystal structure and functionality of naphthalenedicarboxylate ligated metal-organic frameworks, Inorg. Chim. Acta 466 (2017) 308–323. https://doi.org/10.1016/J.ICA.2017.06.038.

[121] G.A. Hebbink, S.I. Klink, L. Grave, P.G.B. Oude Alink, F.C.J.M. van Veggel, Singlet energy transfer as the main pathway in the sensitization of near-infrared Nd3+ luminescence by Dansyl and Lissamine dyes, ChemPhysChem 3 (2002) 1014–1018. https://doi.org/10.1002/cphc.200290002.

[122] L.Y. Mironov, E.B. Sveshnikova, V.L. Ermolaev, Direct evidence of energy transfer from a singlet ligand level to lanthanide ions in their diketonate complexes, Opt. Spektrosk. 119 (2015) 77–83. https://doi.org/10.1134/S0030400X15070188.

[123] Y.J. Huang, C. Ke, L.M. Fu, Y. Li, S.F. Wang, Y.C. Ma, J.P. Zhang, Y. Wang, Excitation energy-transfer processes in the sensitization luminescence of europium in a highly luminescent complex, ChemistryOpen 8 (2019) 388–392. https://doi.org/10.1002/open.201900012.

[124] B. You, H.J. Kim, N.G. Park, Y.S. Kim, Design of efficient electroluminescent lanthanide(III) complexes, Bull. Kor. Chem. Soc. 22 (2001) 1005–1008. https://www.researchgate.net/publication/279574346_Design_of_efficient_electroluminescent_lanthanideIII_complexes. Accessed 19 November 2020.

[125] S. Shuvaev, V. Utochnikova, Ł. Marciniak, A. Freidzon, I. Sinev, R. Van Deun, R.O. Freire, Y. Zubavichus, W. Grünert, N. Kuzmina, Lanthanide complexes with aromatic o-phosphorylated ligands: synthesis, structure elucidation and photophysical properties, Dalton Trans. 43 (2014) 3121–3136. https://doi.org/10.1039/c3dt52600c.

[126] J.Y. Hu, Y. Ning, Y.S. Meng, J. Zhang, Z.Y. Wu, S. Gao, J.L. Zhang, Highly near-IR emissive ytterbium(iii) complexes with unprecedented quantum yields, Chem. Sci. 8 (2017) 2702–2709. https://doi.org/10.1039/C6SC05021B.

[127] V.V. Utochnikova, A.D. Kovalenko, A.S. Burlov, L. Marciniak, I.V. Ananyev, A.S. Kalyakina, N.A. Kurchavov, N.P. Kuzmina, Lanthanide complexes with 2-(tosylamino)benzylidene-N-benzoylhydrazone, which exhibit high NIR emission, Dalton Trans. 44 (2015) 12660–12669. https://doi.org/10.1039/C5DT01161B.

[128] V.V. Utochnikova, A.S. Kalyakina, I.S. Bushmarinov, A.A. Vashchenko, L. Marciniak, A.M. Kaczmarek, R. Van Deun, S. Bräse, N.P. Kuzmina, Lanthanide 9-anthracenate: solution processable emitters for efficient purely NIR emitting host-free OLED, J. Mater. Chem. C 4 (2016) 9848–9855.

[129] N.M. Shavaleev, R. Scopelliti, F. Gumy, J.-C.G. Bünzli, Surprisingly bright near-infrared luminescence and short radiative lifetimes of ytterbium in hetero-binuclear Yb−Na chelates, Inorg. Chem. 48 (2009) 7937–7946. https://doi.org/10.1021/ic900888m.

[130] A.N. Aslandukov, V.V. Utochnikova, D.O. Goriachiy, A.A. Vashchenko, D.M. Tsymbarenko, M. Hoffmann, M. Pietraszkiewicz, N.P. Kuzmina, E.S. Information, The development of a new approach toward lanthanide-based OLED fabrication: new host materials for Tb-based emitters, Dalton Trans. 47 (2018) 16350–16357. https://doi.org/10.1039/C8DT02911C.

[131] A.S. Kalyakina, V.V. Utochnikova, E.Y. Sokolova, A.A. Vaschenko, L.S. Lepnev, R. Van Deun, A.L.A.L. Trigub, Y.V.Y.V. Zubavichus, M. Hoffmann, S. Mühl, N.P. Kuzmina, OLED thin film fabrication from poorly soluble terbium o-phenoxybenzoate through soluble mixed-ligand complexes, Org. Electron. Phys. Mater. Appl. 28 (2016) 319–329. https://doi.org/10.1016/j.orgel.2015.11.006.

[132] V.V. Utochnikova, E.V. Latipov, A.I. Dalinger, Y.V. Nelyubina, A.A. Vashchenko, M. Hoffmann, A.S. Kalyakina, S.Z. Vatsadze, U. Schepers, S. Bräse, N.P. Kuzmina, Lanthanide pyrazolecarboxylates for OLEDs and bioimaging, J. Lumin. 202 (2018) 38–46. https://doi.org/10.1016/j.jlumin.2018.05.022.

[133] A.S. Kalyakina, V.V. Utochnikova, M. Zimmer, F. Dietrich, A.M. Kaczmarek, R. Van Deun, A.A. Vashchenko, A.S. Goloveshkin, M. Nieger, M. Gerhards, U. Schepers, S. Bräse, Remarkable high efficiency of red emitters using Eu(iii) ternary complexes, Chem. Commun. 54 (2018) 5221–5224. https://doi.org/10.1039/C8CC02930J.

[134] V. Utochnikova, A. Aslandukov, Jean-Claude G. Bunzli, Tracking Down the Key Parameter Responsible for Low Brightness of Lanthanide-Based OLEDs, (n.d.).
[135] O. Moudam, B.C. Rowan, M. Alamiry, P. Richardson, B.S. Richards, A.C. Jones, N. Robertson, Europium complexes with high total photoluminescence quantum yields in solution and in PMMA, Chem. Commun. (43) (2009) 6649–6651. https://doi.org/10.1039/b914978c.
[136] M. Montalti, A. Credi, L. Prodi, M.T. Gandolfi, Handbook of Photochemistry, third ed., CRC Press, New York, 2006. https://doi.org/10.1201/9781420015195.
[137] A.S. Kalyakina, V.V. Utochnikova, I.S. Bushmarinov, I.V. Ananyev, I.L. Eremenko, D. Volz, F. Rönicke, U. Schepers, R. Van Deun, A.L. Trigub, Y.V. Zubavichus, N.P. Kuzmina, S. Bräse, Highly luminescent, water-soluble lanthanide fluorobenzoates: syntheses, structures and photophysics, part I: lanthanide pentafluorobenzoates, Chem. A Eur. J. 21 (2016) 17921–17932. https://doi.org/10.1002/chem.201501816.
[138] V.V. Utochnikova, N.N. Solodukhin, A.A. Aslandukov, K.V. Zaitsev, A.S. Kalyakina, A.A. Averin, I.A. Ananyev, A.V. Churakov, N.P. Kuzmina, Luminescence enhancement by p-substituent variation, Eur. J. Inorg. Chem. 2017 (2017) 107–114. https://doi.org/10.1002/ejic.201600843.
[139] A.S. Kalyakina, V.V. Utochnikova, I.S. Bushmarinov, I.M. Le-Deygen, D. Volz, P. Weis, U. Schepers, N.P. Kuzmina, S. Bräse, Lanthanide fluorobenzoates as bio-probes: a quest for the optimal ligand fluorination degree, Chem. Eur. J. 23 (2017) 14944–14953. https://doi.org/10.1002/chem.201703543.
[140] B. Sun, C. Wei, H. Wei, Z. Cai, H. Liu, Z. Zang, W. Yan, Z. Liu, Z. Bian, C. Huang, Highly efficient roomerature phosphorescence achieved by gadolinium complexes, Dalton Trans. 48 (2019) 14958–14961. https://doi.org/10.1039/c9dt03050f.
[141] Z. Gong, Z. Zhang, Room temperature phosphorescence optosensing for gadolinium, Mikrochim. Acta 126 (1997) 117–121. https://doi.org/10.1007/bf01242672.
[142] L. Zang, H. Zhao, Y. Zheng, F. Qin, J. Yao, Y. Tian, Z. Zhang, W. Cao, Twenty-fold enhancement of gadolinium-porphyrin phosphorescence at room temperature by free gadolinium ion in liquid phase, J. Phys. Chem. C 119 (2015) 2811–28116. https://doi.org/10.1021/acs.jpcc.5b08783.
[143] Valentina Utochnikova, Andrey Vaschenko, I. Dalinger, I. Vatsadze, S. Vatsadze, N. Kuzmina, Pyrazolo [1,5-a] Gadolinium Pyrimidinecarboxylates and Organic LEDs Based on Them, RURU2671964C1, n.d. https://yandex.ru/patents/doc/RU2671964C1_20181108. (Accessed 24 January 2021).
[144] M.A. Katkova, V.A. Ilichev, A.N. Konev, I.I. Pestova, G.K. Fukin, M.N. Bochkarev, 2-Mercaptobenzothiazolate complexes of rare earth metals and their electroluminescent properties, Org. Electron. 10 (2009) 623–630. https://doi.org/10.1016/j.orgel.2009.02.020.
[145] V.V. Utochnikova, A.S. Kalyakina, I.S. Bushmarinov, A.A. Vashchenko, L. Marciniak, A.M. Kaczmarek, R. Van Deun, S. Bräse, N.P. Kuzmina, Lanthanide 9-anthracenate: solution processable emitters for efficient purely NIR emitting host-free OLEDs, J. Mater. Chem. C 4 (2016) 9848–9855. https://doi.org/10.1039/c6tc03586h.
[146] D.Q. Gao, C.H. Huang, K. Ibrahim, F.Q. Liu, An organic electroluminescent device made from a gadolinium complex, Solid State Commun. 121 (2002) 145–147. https://doi.org/10.1016/S0038-1098(01)00467-7.
[147] C.P. Shipley, S. Capecchi, O.V. Salata, M. Etchells, P.J. Dobson, V. Christou, Orange electroluminescence from a divalent europium complex, Adv. Mater. 11 (1999) 533–536. https://doi.org/10.1002/(SICI)1521-4095(199905)11:7<533::AID-ADMA533>3.0.CO;2-U.

[148] G. Zhan, L. Wang, Z. Zhao, P. Fang, Z. Bian, Z. Liu, Highly efficient and air-stable lanthanide Eu II complex: new emitter in organic light emitting diodes, Angew. Chem. 132 (2020) 19173–19177. https://doi.org/10.1002/ange.202008423.

[149] LG NanoCell, https://www.lg.com/uk/lgnanocell/color.jsp, 2021.

[150] D.Y. Chen, W. Liu, C.J. Zheng, K. Wang, F. Li, S.L. Tao, X.M. Ou, X.H. Zhang, Isomeric thermally activated delayed fluorescence emitters for color purity-improved emission in organic light-emitting devices, ACS Appl. Mater. Interfaces 8 (2016) 16791–16798. https://doi.org/10.1021/acsami.6b03954.

[151] J.G. Kim, Y. Hwang, H. Hwang, J.H. Choi, Y.W. Park, B.K. Ju, Enhanced optical efficiency and color purity for organic light-emitting diodes by finely optimizing parameters of nanoscale low-refractive index grid, Sci. Rep. 10 (2020) 5631. https://doi.org/10.1038/s41598-020-62470-5.

[152] W.C. Tien, L.Y. Chen, Y.W. Zeng, K.W. Chang, A.K. Chu, Narrow-band emitting microcavity OLED with ITO DBR electrode for sensing applications, Electron. Lett. 51 (2015) 2034–2035. https://doi.org/10.1049/el.2015.2464.

[153] K. Klimes, Z.Q. Zhu, J. Li, Efficient blue phosphorescent OLEDs with improved stability and color purity through judicious triplet exciton management, Adv. Funct. Mater. 29 (2019) 1903068. https://doi.org/10.1002/adfm.201903068.

[154] J.C.G. Bünzli, S. Comby, A.S. Chauvin, C.D.B. Vandevyver, New opportunities for lanthanide luminescence, J. Rare Earths 25 (2007) 257–274. https://doi.org/10.1016/S1002-0721(07)60420-7.

[155] J.C.G. Bünzli, A.S. Chauvin, C.D.B. Vandevyver, S. Bo, S. Comby, Lanthanide bimetallic helicates for in vitro imaging and sensing, Ann. N. Y. Acad. Sci. 1130 (2008) 97–105. https://doi.org/10.1196/annals.1430.010.

[156] X.D. Wang, O.S. Wolfbeis, R.J. Meier, Luminescent probes and sensors for temperature, Chem. Soc. Rev. 42 (2013) 7834–7869. https://doi.org/10.1039/c3cs60102a.

[157] L. Pereira, Organic Light Emitting Diodes: The Use of Rare Earth and Transition Metals, CRC Press, 2012.

[158] H. Gallardo, G. Conte, A.J. Bortoluzzi, I.H. Bechtold, A. Pereira, W.G. Quirino, C. Legnani, M. Cremona, Synthesis, structural characterization, and photo and electroluminescence of a novel terbium(III) complex: {Tris(acetylacetonate) [1,2,5]thiadiazolo[3,4-f][1,10]phenanthroline}terbium(III), Inorg. Chim. Acta 365 (2011) 152–158. https://doi.org/10.1016/j.ica.2010.09.003.

[159] I.V. Taydakov, A.A. Akkuzina, R.I. Avetisov, A.V. Khomyakov, R.R. Saifutyarov, I.C. Avetissov, Effective electroluminescent materials for OLED applications based on lanthanide 1.3-diketonates bearing pyrazole moiety, J. Lumin. 177 (2016) 31–39. https://doi.org/10.1016/j.jlumin.2016.04.017.

[160] C. Adachi, M.A. Baldo, S.R. Forrest, Electroluminescence mechanisms in organic light emitting devices employing a europium chelate doped in a wide energy gap bipolar conducting host, J. Appl. Phys. 87 (2000) 8049. https://doi.org/10.1063/1.373496.

[161] L. Bergmann, D.M. Zink, S. Bräse, T. Baumann, D. Volz, Metal–organic and organic TADF-materials: status, challenges and characterization, Top. Curr. Chem. 374 (2016) 22. https://doi.org/10.1007/s41061-016-0022-6.

[162] Z. Yang, Z. Mao, Z. Xie, Y. Zhang, S. Liu, J. Zhao, J. Xu, Z. Chi, M.P. Aldred, Recent advances in organic thermally activated delayed fluorescence materials, Chem. Soc. Rev. 46 (2017) 915–1016. https://doi.org/10.1039/c6cs00368k.

[163] J.M. Busch, D.S. Koshelev, A.A. Vashchenko, O. Fuhr, M. Nieger, V.V. Utochnikova, S. Bräse, Various structural design modifications: para-substituted diphenylphosphinopyridine bridged Cu(I) complexes in organic light-emitting diodes, Inorg. Chem. 60 (2021) 2315–2332. https://doi.org/10.1021/acs.inorgchem.0c03187.

[164] W.M. Faustino, O.L. Malta, G.F. de Sá, Theoretical modeling of thermally activated luminescence quenching through charge transfer states in lanthanide complexes, Chem. Phys. Lett. 429 (2006) 595–599. https://doi.org/10.1016/j.cplett.2006.08.059.

[165] H. Xu, Q. Sun, Z. An, Y. Wei, X. Liu, Electroluminescence from europium(III) complexes, Coord. Chem. Rev. 293–294 (2015) 228–249. https://doi.org/10.1016/j.ccr.2015.02.018.

[166] V.V. Utochnikova, D.S. Koshelev, A.V. Medvedko, A.S. Kalyakina, I.S. Bushmarinov, A.Y. Grishko, U. Schepers, S. Bräse, S.Z. Vatsadze, Europium 2-benzofuranoate: synthesis and use for bioimaging, Opt. Mater. (Amst). 74 (2017) 191–196. https://doi.org/10.1016/j.optmat.2017.05.038.

[167] D.S. Koshelev, T.Y. Chikineva, V.Y. Kozhevnikova (Khudoleeva), A.V. Medvedko, A.A. Vashchenko, A.S. Goloveshkin, D.M. Tsymbarenko, A.A. Averin, A. Meschkov, U. Schepers, S.Z. Vatsadze, V.V. Utochnikova, On the design of new europium heteroaromatic carboxylates for OLED application, Dyes Pigments 170 (2019) 107604. https://www.sciencedirect.com/science/article/abs/pii/S0143720819307090?via%3Dihub Accessed 4 June 2019.

[168] R. Guerrero-Lemus, J. Sanchiz, M. Sierra-Ramos, I.R. Martín, C. Hernández-Rodríguez, D. Borchert, Downshifting maximization procedure applied to [Eu(bphen)(tta)3] at different concentrations applied to a photovoltaic device and covered with a hemispherical reflector, Sensors Actuators A Phys. 271 (2018) 60–65. https://doi.org/10.1016/j.sna.2018.01.010.

[169] M. Pietraszkiewicz, O. Pietraszkiewicz, J. Karpiuk, A. Majka, G. Dutkiewicz, T. Borowiak, A.M. Kaczmarek, R. Van Deun, Highly photoluminescent europium tetraphenylimidodiphosphinate ternary complexes with heteroaromatic co-ligands. Solution and solid state studies, J. Lumin. 170 (2016) 411–419. https://doi.org/10.1016/j.jlumin.2015.10.033.

[170] J.P. Martins, P. Martín-Ramos, C. Coya, M.R. Silva, M.E.S. Eusebio, A. De Andrés, Á.L. -Álvarez, J. Martín-Gil, Highly luminescent pure-red-emitting fluorinated β-diketonate europium(III) complex for full solution-processed OLEDs, J. Lumin. 159 (2015) 17–25. https://doi.org/10.1016/j.jlumin.2014.10.020.

[171] I.G. Fomina, A.B. Ilyukhin, Y.S. Zavorotny, V.I. Gerasimova, I.V. Taidakov, N.P. Datskevich, A.G. Vitukhnovskii, Z.V. Dobrokhotova, I.L. Eremenko, Binuclear europium(III) pivalates with 4,7-diphenyl-1,10-phenanthroline: controllable synthesis, unique structural transitions, and remarkable luminescence, Polyhedron 129 (2017) 105–113. https://doi.org/10.1016/j.poly.2017.03.034.

[172] V.V. Utochnikova, N.N. Solodukhin, A.N.A.N. Aslandukov, L. Marciniak, I.S. Bushmarinov, A.A. Vashchenko, N.P. Kuzmina, Lanthanide tetrafluorobenzoates as emitters for OLEDs: new approach for host selection, Org. Electron. 44 (2017) 85–93. https://doi.org/10.1016/j.orgel.2017.01.026.

[173] M.I. Kozlov, A.N. Aslandukov, A.A. Vashchenko, A.V. Medvedko, A.E. Aleksandrov, R. Grzibovskis, A.S. Goloveshkin, L.S. Lepnev, A.R. Tameev, A. Vembris, V.V. Utochnikova, On the development of a new approach to the design of lanthanide-based materials for solution-processed OLEDs, Dalton Trans. 48 (2019) 17298–17309. https://doi.org/10.1039/c9dt03823j.

[174] S.H. Rhee, K.B. Nam, C.S. Kim, M. Song, M. Cho, S.H. Jin, S.Y. Ryu, Effect of electron mobility of the electron transport layer on fluorescent organic light-emitting diodes, ECS Solid State Lett. 3 (2014) R19. https://doi.org/10.1149/2.011404ssl.

[175] A. Kovalenko, P.O. Rublev, L.O. Tcelykh, A.S. Goloveshkin, L.S. Lepnev, A.S. Burlov, A.A. Vashchenko, L. Marciniak, A.M. Magerramov, N.G. Shikhaliyev, S.Z. Vatsadze, V. Utochnikova, Lanthanide complexes with 2-(tosylamino)-benzylidene- N-(aryloyl) hydrazones: universal luminescent materials, Chem. Mater. 31 (2019) 759–773. https://doi.org/10.1021/acs.chemmater.8b03675.

[176] X. Sen Zhao, Z.F. Zhao, L. Zhou, Q. Zhu, Z.W. Liu, Z.Q. Bian, C.H. Huang, H.J. Zhang, Highly efficient green organic light-emitting devices based on terbium complex by employing hole block material as host, Sci. China Technol. Sci. 61 (2018) 1334–1339. https://doi.org/10.1007/s11431-018-9276-7.

[177] H. Xin, F.Y. Li, M. Shi, Z.Q. Bian, C.H. Huang, Efficient electroluminescence from a new terbium complex, J. Am. Chem. Soc. 125 (2003) 7166–7167. https://doi.org/10.1021/ja034087a.

[178] G. Yu, F. Ding, H. Wei, Z. Zhao, Z. Liu, Z. Bian, L. Xiao, C. Huang, Highly efficient terbium(III)-based organic light-emitting diodes obtained by exciton confinement, J. Mater. Chem. C 4 (2015) 121–125. https://doi.org/10.1039/c5tc02944a.

[179] Z. Chen, F. Ding, F. Hao, Z. Bian, B. Ding, Y. Zhu, F. Chen, C. Huang, A highly efficient OLED based on terbium complexes, Org. Electron. 10 (2009) 939–947. https://doi.org/10.1016/j.orgel.2009.04.023.

[180] C. Murawski, K. Leo, M.C. Gather, Efficiency roll-off in organic light-emitting diodes, Adv. Mater. 25 (2013) 6801–6827. https://doi.org/10.1002/adma.201301603.

[181] M.A. Baldo, D.F. O'Brien, Y. You, A. Shoustikov, S. Sibley, M.E. Thompson, S.R. Forrest, Highly efficient phosphorescent emission from organic electroluminescent devices, Nature 395 (1998) 151–154. https://doi.org/10.1038/25954.

[182] S.Y. Ni, X.R. Wang, Y.Z. Wu, H.Y. Chen, W.Q. Zhu, X.Y. Jiang, Z.L. Zhang, R.G. Sun, Decay mechanisms of a blue organic light emitting diode, Appl. Phys. Lett. 85 (2004) 878–880. https://doi.org/10.1063/1.1777819.

[183] M. Deussen, M. Scheidler, H. Bässler, Electric field-induced photoluminescence quenching in thin-film light-emitting diodes based on poly(phenyl-p-phenylene vinylene), Synth. Met. 73 (1995) 123–129. https://doi.org/10.1016/0379-6779(95)03307-6.

[184] C. Adachi, M.A. Baldo, S.R. Forrest, S. Lamansky, M.E. Thompson, R.C. Kwong, High-efficiency red electrophosphorescence devices, Appl. Phys. Lett. 78 (2001) 1622. https://doi.org/10.1063/1.1355007.

[185] L. Zhang, B. Li, L. Zhang, Z. Su, Reduced efficiency roll-off in organic light-emitting diodes by a novel short-lived organoeuropium emitter, ACS Appl. Mater. Interfaces 1 (2009) 1852–1855. https://doi.org/10.1021/am900408h.

[186] P.P. Sun, J.P. Duan, J.J. Lih, C.H. Cheng, Synthesis of new europium complexes and their application in electroluminescent devices, Adv. Funct. Mater. 13 (2003) 683–691. https://doi.org/10.1002/adfm.200304378.

[187] Y. Liu, Y. Wang, J. He, Q. Mei, K. Chen, J. Cui, C. Li, M. Zhu, J. Peng, W. Zhu, Y. Cao, High-efficiency red electroluminescence from europium complex containing a neutral dipyrido(3,2-a:2′,3′-c)phenazine ligand in PLEDs, Org. Electron. 13 (2012) 1038–1043. https://doi.org/10.1016/j.orgel.2012.02.024.

[188] J. Kido, H. Hayase, K. Hongawa, K. Nagai, K. Okuyama, Bright red light-emitting organic electroluminescent devices having a europium complex as an emitter, Appl. Phys. Lett. 65 (1994) 2124–2126. https://doi.org/10.1063/1.112810.

[189] L. Zhang, B. Li, S. Yue, M. Li, Z. Hong, W. Li, A terbium (III) complex with triphenylamine-functionalized ligand for organic electroluminescent device, J. Lumin. 128 (2008) 620–624. https://doi.org/10.1016/j.jlumin.2007.10.008.

[190] V. Bulach, F. Sguerra, M.W. Hosseini, Porphyrin lanthanide complexes for NIR emission, Coord. Chem. Rev. 256 (2012) 1468–1478. https://doi.org/10.1016/j.ccr.2012.02.027.

[191] S. Comby, J.-C.G. Bünzli, Chapter 235: Lanthanide near-infrared luminescence in molecular probes and devices, in: K. Gschneidner Jr., J.-C. Bünzli, V. Pecharsky (Eds.), Handbook on the Physics and Chemistry of Rare Earths, Elsevier B.V, Amsterdam, 2007, pp. 217–470. https://doi.org/10.1016/S0168-1273(07)37035-9.

[192] M.A. Katkova, A.P. Pushkarev, T.V. Balashova, A.N. Konev, G.K. Fukin, S.Y. Ketkov, M.N. Bochkarev, Near-infrared electroluminescent lanthanide [Pr(iii), Nd(iii), Ho(iii), Er(iii), Tm(iii), and Yb(iii)] N,O-chelated complexes for organic light-emitting devices, J. Mater. Chem. 21 (2011) 16611. https://doi.org/10.1039/c1jm13023d.

[193] T.W. Canzler, J. Kido, Exciton quenching in highly efficient europium-complex based organic light-emitting diodes, Org. Electron. 7 (2006) 29–37. https://doi.org/10.1016/j.orgel.2005.10.004.

[194] H. Xu, K. Yin, W. Huang, Highly improved electroluminescence from a series of novel Eu complexes with functional single-coordinate phosphine oxide ligands: tuning the intramolecular energy transfer, morphology, and carrier injection ability of the complexes, Chem. Eur. J. 13 (2007) 10281–10293. https://doi.org/10.1002/chem.200700678.

[195] N.A.H. Male, O.V. Salata, V. Christou, Enhanced electroluminescent efficiency from spin-coated europium(III) organic light-emitting device, Synth. Met. 126 (2002) 7–10. https://doi.org/10.1016/S0379-6779(01)00373-3.

[196] C. Adachi, M.A. Baldo, M.E. Thompson, S.R. Forrest, Nearly 100% internal phosphorescence efficiency in an organic light emitting device, J. Appl. Phys. 90 (2001) 5048–5051. https://doi.org/10.1063/1.1409582.

[197] M. Pietraszkiewicz, M. Maciejczyk, I.D.W. Samuel, S. Zhang, Highly photo- and electroluminescent 1,3-diketonate Eu(iii) complexes with spiro-fluorene-xantphos dioxide ligands: synthesis and properties, J. Mater. Chem. C 1 (2013) 8028–8032. https://doi.org/10.1039/c3tc30783b.

[198] S. Wang, B. Zhang, Y. Hou, C. Du, Y. Wu, A highly pure red luminescent europium(iii) complex with a Schiff base zinc(ii) complex as a neutral ligand, J. Mater. Chem. C 1 (2013) 406–409. https://doi.org/10.1039/c2tc00279e.

[199] Y. Liu, K. Chen, K. Xing, Y. Wang, H. Jiang, X. Deng, M. Zhu, W. Zhu, Conjugated and nonconjugated bipolar-transporting dinuclear europium(III) complexes involving triphenylamine and oxadiazole units: synthesis, photophysical and electroluminescent properties, Tetrahedron 69 (2013) 4679–4686. https://doi.org/10.1016/j.tet.2013.03.092.

[200] H. Xu, L.H. Wang, X.H. Zhu, K. Yin, G.Y. Zhong, X.Y. Hou, W. Huang, Application of chelate phosphine oxide ligand in Eu(III) complex with mezzo triplet energy level, highly efficient photoluminescent, and electroluminescent performances, J. Phys. Chem. B 110 (2006) 3023–3029. https://doi.org/10.1021/jp055355p.

[201] J. Fang, D. Ma, Efficient red organic light-emitting devices based on a europium complex, Appl. Phys. Lett. 83 (2003) 4041–4043. https://doi.org/10.1063/1.1626022.

[202] H. You, H. Li, J. Fang, Q. Wang, L. Wang, D. Ma, Improved efficiency by doping blue iridium (III) complex in europium complex-based light-emitting diodes, J. Phys. D Appl. Phys. 40 (2007) 1363–1367. https://doi.org/10.1088/0022-3727/40/5/009.

[203] B. Zhao, H. Zhang, Y. Miao, Z. Wang, L. Gao, H. Wang, Y. Hao, B. Xu, W. Li, Low turn-on voltage and low roll-off rare earth europium complex-based organic light-emitting diodes with exciplex as the host, J. Mater. Chem. C 5 (2017) 12182–12188. https://doi.org/10.1039/c7tc03694a.

[204] H. You, J. Fang, J. Gao, D. Ma, Improved efficiency of organic light-emitting diodes based on a europium complex by fluorescent dye, J. Lumin. 122–123 (2007) 687–689. https://doi.org/10.1016/j.jlumin.2006.01.260.

[205] L. Huang, K.Z. Wang, C.H. Huang, F.Y. Li, Y.Y. Huang, Bright red electroluminescent devices using novel second-ligand-contained europium complexes as emitting layers, J. Mater. Chem. 11 (2001) 790–793. https://doi.org/10.1039/b006919l.

[206] Y. Liu, Y. Wang, C. Li, Y. Huang, D. Dang, M. Zhu, W. Zhu, Y. Cao, Red polymer light-emitting devices based on an oxadiazole-functionalized europium(III) complex, Mater. Chem. Phys. 143 (2014) 1265–1270. https://doi.org/10.1016/j.matchemphys.2013.11.032.

[207] T. Oyamada, Y. Kawamura, T. Koyama, H. Sasabe, C. Adachi, Formation of europium chelate complexes by vacuum co-deposition and their application in organic light-emitting diodes, Adv. Mater. 16 (2004) 1082–1086. https://doi.org/10.1002/adma.200400090.

[208] Z. Ahmed, K. Iftikhar, Efficient layers of emitting ternary lanthanide complexes for fabricating red, green, and yellow OLEDs, Inorg. Chem. 54 (2015) 11209–11225. https://doi.org/10.1021/acs.inorgchem.5b01630.

[209] S. Biju, L.J. Xu, M.A. Hora Alves, R.O. Freire, Z.N. Chen, Bright orange and red light-emitting diodes of new visible light excitable tetrakis-Ln-β-diketonate (Ln = Sm3+, Eu3+) complexes, New J. Chem. 41 (2017) 1687–1695. https://doi.org/10.1039/c6nj03450k.

[210] M. Shi, F. Li, T. Yi, D. Zhang, H. Hu, C. Huang, Tuning the triplet energy levels of pyrazolone ligands to match the 5D0 level of europium(III), Inorg. Chem. 44 (2005) 8929–8936. https://doi.org/10.1021/ic050844p.

[211] D. Guo, Z. Deng, C. Liang, P. Lin, Y. Li, Y. Xu, The photoluminescent and electroluminescent properties of a new Europium complex, J. Lumin. 122–123 (2007) 683–686. https://doi.org/10.1016/j.jlumin.2006.01.259.

[212] L. Liu, Z. Xu, Z. Lou, F. Zhang, B. Sun, J. Pei, Photoluminescence and electroluminescence mechanism on a novel complex Eu(o-BBA)3(phen), J. Lumin. 122–123 (2007) 961–963. https://doi.org/10.1016/j.jlumin.2006.01.338.

[213] A. Pereira, H. Gallardo, G. Conte, W.G. Quirino, C. Legnani, M. Cremona, I.H. Bechtold, Investigation of the energy transfer mechanism in OLEDs based on a new terbium β-diketonate complex, Org. Electron. 13 (2012) 90–97. https://doi.org/10.1016/j.orgel.2011.10.007.

[214] X. Li, Z. Deng, Y. Zhang, Y. Shi, R. Wang, Emission mechanism in the terbium complex doped PVK system, Front. Optoelectron. China 1 (2008) 130–133. https://doi.org/10.1007/s12200-008-0010-8.

[215] E. Girotto, A. Pereira, C. Arantes, M. Cremona, A.J. Bortoluzzi, C.A.M. Salla, I.H. Bechtold, H. Gallardo, Efficient terbium complex based on a novel pyrazolone derivative ligand used in solution-processed OLEDs, J. Lumin. 208 (2019) 57–62. https://doi.org/10.1016/j.jlumin.2018.12.027.

[216] Y. Shi, Z. Deng, J. Xiao, D. Xu, Z. Chen, R. Wang, Electroluminescence characteristics of a new kind of rare-earth complex: TbY(o-MOBA)6(phen)2*2H2O, J. Lumin. 122–123 (2007) 272–274. https://doi.org/10.1016/j.jlumin.2006.01.138.

[217] D. Chubich, G. Dovbeshko, O. Fesenko, R. Fedorovich, T. Gavrilko, V. Cherepanov, A. Marchenko, A. Naumovets, V. Nechitaylo, G. Puchkovska, L. Viduta, A. Vitukhnovskii, Light-emitting diode of planar type based on nanocomposites consisting of island au film and organic luminofore Tb(thd)3, Mol. Cryst. Liq. Cryst. 497 (2008) 186–195. https://doi.org/10.1080/15421400802462656.

[218] M. Kamimura, S. Takahiro, M. Yoshida, Y. Hashimoto, R. Fukushima, K. Soga, Over-1000 nm near-infrared fluorescent biodegradable polymer nanoparticles for deep tissue in vivo imaging in the second biological window, Polym. J. 49 (2017) 799–803. https://doi.org/10.1038/pj.2017.59.

[219] Y. Kawamura, Y. Wada, M. Iwamuro, T. Kitamura, S. Yanagida, Near-infrared electroluminescence from ytterbium(III) complex, Chem. Lett. 29 (2000) 280–281. https://doi.org/10.1246/cl.2000.280.

[220] T.S. Kang, B.S. Harrison, T.J. Foley, A.S. Knefely, J.M. Boncella, J.R. Reynolds, K.S. Schanze, Near-infrared electroluminescence from lanthanide tetraphenylporphyrin: polystyrene blends, Adv. Mater. 15 (2003) 1093–1097. https://doi.org/10.1002/adma.200304692.

[221] Z. Ahmed, R.E. Aderne, J. Kai, H.I.P. Chavarria, M. Cremona, Ytterbium β-diketonate complexes for near infra-red organic light-emitting devices, Thin Solid Films 620 (2016) 34–42. https://doi.org/10.1016/j.tsf.2016.07.076.

[222] K. Jinnai, R. Kabe, C. Adachi, A near-infrared organic light-emitting diode based on an Yb(III) complex synthesized by vacuum co-deposition, Chem. Commun. 53 (2017) 5457–5460. https://doi.org/10.1039/c7cc01580a.

[223] Z. Li, H. Zhang, J. Yu, Near-infrared electroluminescence from double-emission-layers devices based on ytterbium (III) complexes, Thin Solid Films 520 (2012) 3663–3667. https://doi.org/10.1016/j.tsf.2011.12.052.

[224] B.L. Reid, S. Stagni, J.M. Malicka, M. Cocchi, G.S. Hanan, M.I. Ogden, M. Massi, Lanthanoid β-triketonates: a new class of highly efficient NIR emitters for bright NIR-OLEDs, Chem. Commun. 50 (2014) 11580–11582. https://doi.org/10.1039/c4cc04961f.

[225] E.V. Baranov, G.K. Fukin, T.V. Balashova, A.P. Pushkarev, I.D. Grishin, M.N. Bochkarev, 8-Quinolinolate complexes of yttrium and ytterbium: Molecular arrangement and fragmentation under laser impact, Dalton Trans. 42 (2013) 15699–15705. https://doi.org/10.1039/c3dt51706c.

[226] H. Wei, G. Yu, Z. Zhao, Z. Liu, Z. Bian, C. Huang, Constructing lanthanide [Nd(iii), Er(iii) and Yb(iii)] complexes using a tridentate N,N,O-ligand for near-infrared organic light-emitting diodes, Dalton Trans. 42 (2013) 8951. https://doi.org/10.1039/c3dt50778e.

[227] A.P. Pushkarev, V.A. Ilichev, T.V. Balashova, D.L. Vorozhtsov, M.E. Burin, D.M. Kuzyaev, G.K. Fukin, B.A. Andreev, D.I. Kryzhkov, A.N. Yablonskiy, M.N. Bochkarev, Lanthanide complexes with substituted naphtholate ligands: extraordinary bright near-infrared luminescence of ytterbium, Russ. Chem. Bull. 62 (2013) 392–397. https://doi.org/10.1007/s11172-013-0051-z.

[228] T.V. Balashova, N.A. Belova, M.E. Burin, D.M. Kuzyaev, R.V. Rumyantcev, G.K. Fukin, A.P. Pushkarev, V.A. Ilichev, A.F. Shestakov, I.D. Grishin, M.N. Bochkarev, Substituted naphtholates of rare earth metals as emissive materials, RSC Adv. 4 (2014) 35505–35510. https://doi.org/10.1039/c4ra03915g.

[229] A.P. Pushkarev, V.A. Ilichev, A.A. Maleev, A.A. Fagin, A.N. Konev, A.F. Shestakov, R.V. Rumyantzev, G.K. Fukin, M.N. Bochkarev, Electroluminescent properties of lanthanide pentafluorophenolates, J. Mater. Chem. C 2 (2014) 1532–1538. https://doi.org/10.1039/c3tc32054e.

[230] V.A. Ilichev, A.V. Rozhkov, R.V. Rumyantcev, G.K. Fukin, I.D. Grishin, A.V. Dmitriev, D.A. Lypenko, E.I. Maltsev, A.N. Yablonskiy, B.A. Andreev, M.N. Bochkarev, LMCT facilitated room temperature phosphorescence and energy transfer in substituted thiophenolates of Gd and Yb, Dalton Trans. 46 (2017) 3041–3050. https://doi.org/10.1039/C6DT04519G.

[231] S. Xun, J. Zhang, X. Li, D. Ma, Z.Y. Wang, Synthesis and near-infrared luminescent properties of some ruthenium complexes, Synth. Met. 158 (2008) 484–488. https://doi.org/10.1016/j.synthmet.2008.03.018.

[232] R.G. Sun, Y.Z. Wang, Q.B. Zheng, H.J. Zhang, A.J. Epstein, 1.54 μm infrared photoluminescence and electroluminescence from an erbium organic compound, J. Appl. Phys. 85 (2000) 7589. https://doi.org/10.1063/1.373027.

[233] F. Wei, Y.Z. Li, G.Z. Ran, G.G. Qin, 1.54 μm electroluminescence from p-Si anode organic light emitting diode with Bphen: Er(DBM)3phen as emitter and Bphen as electron transport material, Opt. Express 18 (2010) 13542–13546. https://doi.org/10.1364/oe.18.013542.

[234] P. Martín-Ramos, M.R. Silva, C. Coya, C. Zaldo, Á.L. Álvarez, S. Álvarez-García, A.M. Matos Beja, J. Martín-Gil, Novel erbium(iii) fluorinated β-diketonate complexes with N,N-donors for optoelectronics: from synthesis to solution-processed devices, J. Mater. Chem. C 1 (2013) 2725–2734. https://doi.org/10.1039/c3tc00649b.

[235] P. Martín-Ramos, C. Coya, Á.L. Álvarez, M. Ramos Silva, C. Zaldo, J.A. Paixão, P. Chamorro-Posada, J. Martín-Gil, Charge transport and sensitized 1.5 μm electroluminescence properties of full solution-processed NIR-OLED based on novel Er(III) fluorinated β-diketonate ternary complex, J. Phys. Chem. C 117 (2013) 10020–10030. https://doi.org/10.1021/jp402174s.

[236] P. Martín-Ramos, C. Coya, V. Lavín, I.R. Martín, M.R. Silva, P.S.P. Silva, M. García-Vélez, A.L. Alvarez, J. Martín-Gil, Active layer solution-processed NIR-OLEDs based on ternary erbium(III) complexes with 1,1,1-trifluoro-2,4-pentanedione and different N, N-donors, Dalton Trans. 43 (2014) 18087–18096. https://doi.org/10.1039/c4dt01694g.

[237] Z. Ahmed, R.E. Aderne, J. Kai, J.A.L.C. Resende, H.I. Padilla-Chavarría, M. Cremona, Near infrared organic light emitting devices based on a new erbium(iii) β-diketonate complex: synthesis and optoelectronic investigations, RSC Adv. 7 (2017) 18239–18251. https://doi.org/10.1039/c6ra27473k.

[238] Z. Li, J. Yu, L. Zhou, H. Zhang, R. Deng, Z. Guo, 1.54 μm near-infrared photoluminescent and electroluminescent properties of a new erbium (III) organic complex, Org. Electron. Phys. Mater. Appl. 9 (2008) 487–494. https://doi.org/10.1016/j.orgel.2008.02.010.

[239] Z. Ahmed, K. Iftikhar, Variant coordination sphere, for efficient photo- and electroluminescence of 0.4-1.8 μm, of lanthanide(III) complexes containing a β-diketone ligand with low vibrational frequency C-F bonds and a flexible 2,2′-bipyridine ligand, Polyhedron 85 (2015) 570–592. https://doi.org/10.1016/j.poly.2014.08.064.

[240] Y. Kawamura, Y. Wada, Y. Hasegawa, M. Iwamuro, T. Kitamura, S. Yanagida, Observation of neodymium electroluminescence, Appl. Phys. Lett. 74 (1999) 3245. https://doi.org/10.1063/1.123357.

[241] Y. Kawamura, Y. Wada, S. Yanagida, Near-infrared photoluminescence and electroluminescence of neodymium(III), erbium(III), and ytterbium(III) complexes, Jpn. J. Appl. Phys. 40 (2001) 350. https://doi.org/10.1143/JJAP.40.350.

[242] O.M. Khreis, R.J. Curry, M. Somerton, W.P. Gillin, Infrared organic light emitting diodes using neodymium tris-(8-hydroxyquinoline), J. Appl. Phys. 88 (2000) 777. https://doi.org/10.1063/1.373803.

[243] A. O'Riordan, E. O'Connor, S. Moynihan, P. Nockemann, P. Fias, R. Van Deun, D. Cupertino, P. Mackie, G. Redmond, Near infrared electroluminescence from neodymium complex–doped polymer light emitting diodes, Thin Solid Films 497 (2006) 299–303. https://doi.org/10.1016/j.tsf.2005.10.071.

[244] Z.Q. Chen, F. Ding, Z.Q. Bian, C.H. Huang, Efficient near-infrared organic light-emitting diodes based on multimetallic assemblies of lanthanides and iridium complexes, Org. Electron. Phys. Mater. Appl. 11 (2010) 369–376. https://doi.org/10.1016/j.orgel.2009.11.015.

[245] Z. Li, J. Yu, L. Zhou, R. Deng, H. Zhang, The near-infrared optical properties of an Nd (III) complex and its potential application in electroluminescence, Inorg. Chem. Commun. 12 (2009) 151–153. https://doi.org/10.1016/j.inoche.2008.12.001.

[246] A. Shahalizad, A. D'Aléo, C. Andraud, M.H. Sazzad, D.H. Kim, Y. Tsuchiya, J.C. Ribierre, J.M. Nunzi, C. Adachi, Near infrared electroluminescence from Nd(TTA)3phen in solution-processed small molecule organic light-emitting diodes, Org. Electron. 44 (2017) 50–58. https://doi.org/10.1016/j.orgel.2017.01.044.

[247] A. Shahalizad, D.H. Kim, S. Rao Bobbara, Y. Tsuchiya, A. D'Aléo, C. Andraud, J.C. Ribierre, J.M. Nunzi, C. Adachi, Enhanced near-infrared electroluminescence from a neodymium complex in organic light-emitting diodes with a solution-processed exciplex host, Appl. Phys. Lett. 114 (2019) 033301. https://doi.org/10.1063/1.5054721.

[248] A. O'Riordan, R. Van Deun, E. Mairiaux, S. Moynihan, P. Fias, P. Nockemann, K. Binnemans, G. Redmond, Synthesis of a neodymium-quinolate complex for near-infrared electroluminescence applications, Thin Solid Films 516 (2008) 5098–5102. https://doi.org/10.1016/j.tsf.2007.11.112.

[249] Z.R. Hong, C.J. Liang, R.G. Li, F.X. Zang, D. Fan, W.L. Li, L.S. Hung, S.T. Lee, Infrared and visible emission from organic electroluminescent devices based on praseodymium complex, Appl. Phys. Lett. 79 (2001) 1942–1944. https://doi.org/10.1063/1.1391239.

[250] Z. Ahmed, K. Iftikhar, Efficient photoluminescent complexes of 400-1800 nm wavelength emitting lanthanides containing organic sensitizers for optoelectronic devices, RSC Adv. 4 (2014) 63696–63711. https://doi.org/10.1039/c4ra11330f.

[251] R. Reyes, E.N. Hering, M. Cremona, C.F.B. Da Silva, H.F. Brito, C.A. Achete, Growth and characterization of OLED with samarium complex as emitting and electron transporting layer, Thin Solid Films 420–421 (2002) 23–29. https://doi.org/10.1016/S0040-6090(02)00651-X.

[252] Y. Zheng, L. Fu, Y. Zhou, J. Yu, Y. Yu, S. Wang, H. Zhang, Electroluminescence based on a β-diketonate ternary samarium complex, J. Mater. Chem. 12 (2002) 919–923. https://doi.org/10.1039/b110373c.

[253] J. Yu, L. Zhou, H. Zhang, Y. Zheng, H. Li, R. Deng, Z. Peng, Z. Li, Efficient electroluminescence from new lanthanide (Eu3+, Sm 3+) complexes, Inorg. Chem. 44 (2005) 1611–1618. https://doi.org/10.1021/ic0485561.

[254] B. Chu, W.L. Li, Z.R. Hong, F.X. Zang, H.Z. Wei, D.Y. Wang, M.T. Li, C.S. Lee, S.T. Lee, Observation of near infrared and enhanced visible emissions from electroluminescent devices with organo samarium(III) complex, J. Phys. D Appl. Phys. 39 (2006) 4549. https://doi.org/10.1088/0022-3727/39/21/006.

[255] R. Deng, J. Yu, H. Zhang, L. Zhou, Z. Peng, Z. Li, Z. Guo, Photoluminescence and electroluminescence properties of a samarium complex Sm(TTA)3phen, Chem. Phys. Lett. 443 (2007) 258–263. https://doi.org/10.1016/j.cplett.2007.06.080.

[256] Z. Kin, H. Kajii, Y. Hasegawa, T. Kawai, Y. Ohmori, Optical and electroluminescent properties of samarium complex-based organic light-emitting diodes, Thin Solid Films 516 (2008) 2735–2738. https://doi.org/10.1016/j.tsf.2007.04.060.

[257] S.K. Behzad, E. Najafi, M.M. Amini, M. Janghouri, E. Mohajerani, S.W. Ng, Yellow-green electroluminescence of samarium complexes of 8-hydroxyquinoline, J. Lumin. 156 (2014) 219–228. https://doi.org/10.1016/j.jlumin.2014.08.013.

[258] Z.F. Li, L. Zhou, J.B. Yu, H.J. Zhang, R.P. Deng, Z.P. Peng, Z.Y. Guo, Synthesis, structure, photoluminescence, and electroluminescence properties of a new dysprosium complex, J. Phys. Chem. C 111 (2007) 2295–2300. https://doi.org/10.1021/jp064749t.

[259] Z. Hong, W. Li, D. Zhao, C. Liang, X. Liu, J. Peng, D. Zhao, Spectrally-narrow blue light-emitting organic electroluminescent devices utilizing thulium complexes, Synth. Met. 104 (1999) 165–168. https://doi.org/10.1016/S0379-6779(99)00060-0.

[260] H. He, W. Li, Z. Su, B. Chu, D. Bi, Y. Chen, D. Wang, W. Su, B. Li, Interfacial exciplex electroluminescence between diamine derivatives with starburst molecular structure and tris(acetylacetonato)-(mono-phenothroline) thulium, J. Alloys Compd. 470 (2009) 448–451. https://doi.org/10.1016/j.jallcom.2008.02.100.

[261] F.L.D. Gao, C. Huang, I. Kui, Fabrication of green electroluminescent devices, J. Rare Earths 20 (2002) 16.

[262] C.J. Liang, D. Zhao, Z.R. Hong, R.G. Li, W.L. Li, J.Q. Yu, Exciplex emissions in bilayer and doped thin films containing a non-fluorescent gadolinium complex, Thin Solid Films 371 (2000) 207–210. https://doi.org/10.1016/S0040-6090(00)01017-8.

[263] M. Li, W. Li, L. Chen, Z. Kong, B. Chu, B. Li, Z. Hu, Z. Zhang, Tuning emission color of electroluminescence from two organic interfacial exciplexes by modulating the thickness of middle gadolinium complex layer, Appl. Phys. Lett. 88 (2006) 091108. https://doi.org/10.1063/1.2181194.

[264] J. Ouyang, L. Li, Z. Tai, Z. Lu, G. Wang, Organic electroluminescent devices with Langmuir-Blodgett films of an amphiphilic complex with an 8-hydroxyquinoline as an emitter, Chem. Commun. (1997) 815–816. https://doi.org/10.1039/a700742f.

[265] J.M. Ouyang, W.H. Ling, C. Yang, Y. Li, G. Yu, Double-layer electroluminescent devices with Langmuir-Blodgett films of amphiphilic 8-hydroxyquinoline lanthanum as emitter, Mater. Sci. Eng. B 85 (2001) 247–250. https://doi.org/10.1016/S0921-5107(01)00596-7.

[266] M.A. Katkova, V.A. Ilichev, A.N. Konev, M.N. Bochkarev, Rare-earth metal 8-hydroxyquinolinate complexes as materials for organic light-emitting diodes, Russ. Chem. Bull. 57 (2008) 2281–2284. https://doi.org/10.1007/s11172-008-0321-3.

[267] T. Yu, W. Su, W. Li, R. Hua, B. Chu, B. Li, Ultraviolet electroluminescence from organic light-emitting diode with cerium(III)–crown ether complex, Solid State Electron. 51 (2007) 894–899. https://doi.org/10.1016/j.sse.2007.05.003.

[268] X.L. Zheng, Y. Liu, M. Pan, X.Q. Lü, J.Y. Zhang, C.Y. Zhao, Y.X. Tong, C.Y. Su, Bright blue-emitting Ce3+ complexes with encapsulating polybenzimidazole tripodal ligands as potential electroluminescent devices, Angew. Chem. Int. Ed. 46 (2007) 7399–7403. https://doi.org/10.1002/anie.200702401.

[269] H. Xin, M. Shi, F.Y. Li, M. Guan, D.Q. Gao, C.H. Huang, K. Ibrahim, F.Q. Liu, Photoluminescence and electroluminescence properties of three ternary lutetium complexes, New J. Chem. 27 (2003) 1485–1489. https://doi.org/10.1039/b304451c.

Further reading

[270] V.V. Utochnikova, N.N. Solodukhin, A.A. Aslandukov, K.V. Zaitsev, A.S. Kalyakina, A.A. Averin, I.A. Ananyev, A.V. Churakov, N.P. Kuzmina, Highly luminescent, water-soluble lanthanide fluorobenzoates: syntheses, structures and photophysics. Part II: luminescence enhancement by p-substituent variation, Eur. J. Inorg. Chem. 2017 (2016) 107–114.

[271] A. Zampetti, A. Minotto, F. Cacialli, Near-infrared (NIR) organic light-emitting diodes (OLEDs): challenges and opportunities, Adv. Funct. Mater. 29 (2019) 1807623. https://doi.org/10.1002/adfm.201807623.

[272] D.D. Ramteke, R.S. Gedam, Luminescence properties of Gd3+ containing glasses for ultra-violet (UV) light, J. Rare Earths 32 (2014) 389–393. https://doi.org/10.1016/S1002-0721(14)60082-X.